



**Silja
Frankenbach**

**OS ESTUÁRIOS COMO SUMIDOUROS DE
CARBONO: FOTOSSÍNTESE, FOTOINHIBIÇÃO
E RESILIÊNCIA DA PRODUTIVIDADE PRIMÁRIA
PELÁGICA E BÊNICA**

**ESTUARIES AS CARBON SINKS:
PHOTOSYNTHETIC ACTIVITY, PHOTOINHIBITION
AND RESILIENCE IN PELAGIC-BENTHIC PRIMARY
PRODUCTION**



Silja
Frankenbach

OS ESTUÁRIOS COMO SUMIDOUROS DE CARBONO: FOTOSÍNTESE, FOTOINHIBIÇÃO E RESILIÊNCIA DA PRODUTIVIDADE PRIMÁRIA PELÁGICA E BÊNICA

ESTUARIES AS CARBON SINKS: PHOTOSYNTHETIC ACTIVITY, PHOTOINHIBITION AND RESILIENCE IN PELAGIC-BENTHIC PRIMARY PRODUCTION

Tese apresentada à Universidade de Aveiro para cumprimento dos requisitos necessários à obtenção do grau de Doutor em Biologia, realizada sob a orientação científica do Doutor João António de Almeida Serôdio, Professor Auxiliar com Agregação do Departamento de Biologia da Universidade de Aveiro.



UNIÃO EUROPEIA
Fundo Social Europeu



PROGRAMA OPERACIONAL POTENCIAL HUMANO

Apoio financeiro da Fundação para a
Ciência e Tecnologia e do Fundo Social
Europeu no âmbito do III Quadro
Comunitário de Apoio, através da
Bolsa de Doutoramento
SFRH/BD/86788/2012

For Xael and Jörg

“forty-two”
Deep Thought

O júri

Presidente

Prof. Doutor Eduardo Anselmo Ferreira da Silva
Professor Catedrático, Universidade de Aveiro

Vogais

Prof. Doutor Jorge Miguel Luz Marques da Silva
Professor Auxiliar, Departamento de Biologia Vegetal, Faculdade de Ciências da Universidade de Lisboa

Prof. Doutor João Miguel Sousa da Silva
Investigador Auxiliar, CCMAR-Centro de Ciências do Mar, Universidade do Algarve

Prof. Doutor Ana Cristina Gomes da Cunha
Professora Auxiliar, Departamento de Biologia, Universidade do Minho

Prof. Doutor António José Arsénia Nogueira
Professor Catedrático, Departamento de Biologia, Universidade de Aveiro

Prof. Doutor João António de Almeida Serôdio
Professor Auxiliar com Agregação, Departamento de Biologia, Universidade de Aveiro (Orientador)

Acknowledgements

Living in Portugal and receiving a PhD fellowship in marine ecophysiology full filled one of my big dreams in life and I am grateful that I got the chance to live it. I knew it would not be easy, but I never expected that so many challenges would occur at the same time. When life challenges us, it is of high importance to have a supportive environment and therefore I would like to take the chance and thank all the people who have supported me in one or the other way along the last years:

First of all, I would like to say “thank you” to my supervisor, Prof. João Serôdio for all his patience and extensive support! He never seemed to get tired of answering to all of my “stupid question”, at least he didn’t show it to me. Moreover, whenever I heard other PhD students talking about their supervisors, it reminded me of how lucky I am for having him as my boss. Thank you!

Thanks to my (ex-) lab members and/ or colleges and co-authors for the pleasant work atmosphere, helping hands and minds. It was a pleasure to work with you: Andreina Azevedo * Cláudia Bártolo * Cláudio Brandão * Sandra Craveiro * Gregor Christa * Diana Dias * João Dias * Gisela Dionísio * Carmen Elias * Cristina Esteves * João Ezequiel * Violeta Ferreira * Cátia Fidalgo * Jörg Frommlet * Johannes Gössling * Bárbara Guimarães * Miguel Leal * Filipa Leandro * Ana Luís * Pedro Monteiro * Anthony Moreira * Mariana Pandeirada * Ana Pedro * Sandra Plecha * Vanessa Reis * William Schmidt * Carla Santos * Inês Silva * João Simões * Ana Sousa * Lígia Sousa * Rui Rocha * Leandro Vaz * Nuno Vaz *

Thanks to the staff members of the University of Aveiro, especially to: Luís Carvalheiro * Fernando Cozinheiro * Paula Curveira * Abel Ferreira * Lísia Lopes * Ivo Mateus * Carlos Nascimento * Aida Oliveria * Inês Rosa * Amélia Ribeiro * Fátima Serafim * Clarisse Soares * Miguel Rocha*

A special “thank you” goes out to Alexandra Elbakyan for providing a lot of the scientific literature, which was essential for this work.

Agradeço também aos moradores e trabalhadores de Aveiro por me fazerem sentir bem-vinda, nomeadamente: À Amélia Almeida, à Eneida Cardoso, ao Luís Damas, Rafael Furlan, à Catarina Marques, à Sandra Oliveira, à Isabel Ribeiro, educadoras e pais da Creche e Pré-Escola da Vera Cruz, aos farmacêuticos da Farmácia Saúde, aos funcionários e médicos do Centro de Saúde da Gafanha da Nazaré, aos funcionários, aos trabalhadores das padarias ‘Venepão’ e ‘Santo Grão’, e aos funcionários de AFUAv aos trabalhadores do Mercado de Santiago.

Thank you to the people I am grateful to be present at some time during this time. I don’t want to miss any of you: *Marta Alves * Nivas Babu * Juliane Bettig * Katrin Broetz * Tony Coe * Amin Dvrpnh * Carina Felix *Horst Buchholz * Elisa Cazzola * Ana Genua * Maria Glockzin * Irina Gorodetskaya * Ensieh Hosseini * Somya Joshi * Paula Maia * Maruxa Malvar * Mariana Morgado * Farzin Mohseni * Bridgida Matos * Catarina Matzen da Silva * Vinu Nivas * Manu Piater * Sérgio Prats * Lapo Ragionieri * Gwen Renard * Rajesh Surendran * Saeed Tamimi * Marcela Vaz

**Acknowledgements
(cont.)**

Thank you to Jörg Römbke for never giving up on me and the unlimited support and guidance through out of my whole life!

Thanks to my son, Xael who unconsciously gave my life a counterbalance with loads of love, laughter and different points of view. Please forgive me for all those days I didn't play with you just because I was too tired or had to work. Your presence however constantly reminded me of what is truly important in life. Thank you for being the child you are!

palavras-chave

Diatomáceas, Estuários, Fitoplâncton, Fluorescência da clorofila *a*, Fotoinibição, Fotoproteção, Microfitobentos, Migração Vertical, Produtividade Primária, Variabilidade Espaço-Temporal

Resumo

Os estuários são reconhecidos como um dos tipos de ecossistemas mais produtivos na Terra. A sua elevada produtividade primária é devida em larga medida à fixação fotossintética de carbono pelo fitoplâncton e microfitobentos, as comunidades de microalgas e cianobactérias que habitam a coluna de água e os sedimentos subtidais e intertidais, respetivamente. Em comparação com o fitoplâncton, o microfitobentos tem sido muito menos estudado relativamente aos processos fotofisiológicos que controlam a sua produtividade, bem como à sua contribuição para a produção primária global do estuário.

Um destes processos é a fotoinibição, a diminuição da atividade fotossintética causada pela luz, considerada como um importante fator limitante da produtividade primária no ambiente estuarino. O impacto negativo da fotoinibição na fotossíntese depende do balanço entre a fotoinativação e a reparação do fotossistema II (PSII). Baseado num recente método de imagiologia multi-actínica de fluorescência da clorofila, este trabalho avaliou a fotoaclimação e capacidade de fotoproteção contra a fotoinibição, medida pela redução da fotoinativação do PSII. A fotoinativação e reparação do PSII variou entre diferentes tipos de comunidades, indicando a existência de um balanço entre a fotoproteção baseada na motilidade celular e em mecanismos fisiológicos. Espécies epipélicas (móveis) mostraram uma menor capacidade fisiológica de prevenir danos, enquanto as formas epipsâmicas (imóveis) aparentaram ser menos suscetíveis à fotoinibição e mais dependentes de fotoproteção fisiológica.

Este trabalho investigou ainda um aspeto pouco estudado, relacionado com a presença de quantidades substanciais de biomassa de microalgas em sedimentos subsuperficiais. Pela análise de sedimentos intertidais da Ria de Aveiro (Portugal), foi descoberto que as células enterradas conseguem recuperar rapidamente a sua atividade fotossintética quando expostas a condições da superfície. Foi também concluído que a biomassa subsuperficial (0.5-10 cm) potencialmente viável representa 2-3 vezes a biomassa presente nas camadas superficiais (0.0-0.5 cm). Estes resultados suportam a hipótese de que a biomassa subsuperficial desempenha um papel ecológico importante enquanto fonte de células fotossinteticamente competentes capazes de 're-inocular' a superfície, contribuindo para a elevada produtividade das áreas intertidais.

A importância relativa da contribuição do fitoplâncton e do microfitobentos para a produtividade primária ao nível do ecossistema foi avaliada para a Ria de Aveiro, comparando a variabilidade espaço-temporal da biomassa e produtividade de diferentes comunidades. Este estudo baseou-se na medição de taxas absolutas de transporte de electrões no PSII e a estimação de taxas de fixação de carbono. Por unidade de biomassa, estas atingiram 68,0 e 19,1 mg C mg Chl $a^{-1} d^{-1}$, para o fitoplâncton e o microfitobentos, respectivamente. Por unidade de área, a produtividade anual foi mais elevada no caso do microfitobentos, atingindo 105,2 g C $m^{-2} yr^{-1}$, por oposição a 49,9 g C $m^{-2} yr^{-1}$, para o fitoplâncton. Considerando a totalidade da área da Ria de Aveiro, os resultados salientam a importância das áreas intertidais enquanto sumidouros de carbono e reservatórios de "carbono azul", e locais de elevada produtividade primária, contribuindo com mais de 60% do total anual de 12428,3 t C yr^{-1} .

Keywords

Chlorophyll *a* Fluorescence, Diatoms Estuaries, Microphytobenthos, Photoinhibition, Photoprotection, Phytoplankton, Primary Productivity, Spatio-temporal Variability, Vertical Migration

Abstract

Estuaries are recognized amongst the most productive ecosystems on Earth. Their high primary productivity is largely due to the photosynthetic carbon fixation by phytoplankton and microphytobenthos, the communities of microalgae and cyanobacteria that inhabit the water column and subtidal or intertidal sediments, respectively. In comparison with the phytoplankton, the microphytobenthos has been much less studied regarding the photophysiological processes affecting primary productivity, and their relative role as contributors to estuarine-level production.

One of these processes is photoinhibition, the high light-induced decrease in photosynthetic activity, considered a major limiting factor of growth and primary productivity in the variable and extreme estuarine environment. The detrimental impact of photoinhibition on photosynthesis depends on the balance between the photoinactivation and repair of photosystem II (PSII). By successfully adapting to microphytobenthos a recently-developed methodology based on multi-actinic imaging of chlorophyll fluorescence, this work evaluated their photoacclimation and photoprotective capacity, as measured by the reduction in PSII photoinactivation. PSII photoinactivation and repair was found to vary between different communities, pointing to a trade-off between cellular motility-based and physiological photoprotective mechanisms. Epipellic (motile) species showed a reduced physiological capacity for preventing photodamage, while epipsammic (non-motile) forms appeared less susceptible to photoinactivation and more dependent on physiological photoprotection.

This work further investigated an overlooked aspect of microphytobenthos ecology, related to the presence of substantial amounts of microalgal biomass in subsurface sediments. By studying samples from intertidal areas of the Ria de Aveiro (Portugal), this work found that buried cells can quickly regain photosynthetic activity when exposed to surface conditions. Potential viable subsurface (0.5-10 cm) microalgal biomass was found to represent 2-3 times the amount of biomass present at the surface layers (0.0-0.5 cm). These results support the hypothesis that subsurface biomass may play an important ecological role as a source of photosynthetically competent cells capable of 're-inoculating' the surface, contributing to the high productivity of intertidal areas.

The relative importance of phytoplankton and microphytobenthos as contributors to ecosystem-level primary productivity was evaluated in the Ria de Aveiro, by comparing the spatio-temporal variability of biomass and productivity of different communities. This study made use of a new type of fluorometer allowing the measurement of absolute rates of PSII electron transport rates and the estimation of carbon fixation rates. Biomass-specific productivity rates for phytoplankton and microphytobenthos were found to reach 68.0 and 19.1 mg C mg Chl $a^{-1} d^{-1}$, respectively. Annual areal production rates were higher for the microphytobenthos, reaching 105.2 g C $m^{-2} yr^{-1}$, as opposed to 49.9 g C $m^{-2} yr^{-1}$ for the phytoplankton. The annual rates upscaled for the whole Ria de Aveiro highlight the importance of the intertidal areas as significant carbon sinks and reservoirs of active 'blue carbon', and as main sites of primary productivity, found to contribute with more than 60% of the total ecosystem-level budget 12428.3 t C yr^{-1} .

CONTENTS

Contents.....	III
List of Figures.....	V
List of Tables.....	IX
Notation.....	X
Chapter 1.....	1
Estuaries as carbon sinks: productivity of phytoplankton and microphytobenthos.....	3
Photoinhibition, photoprotection and productivity.....	5
General objectives and thesis outline.....	7
References.....	9
Chapter 2.....	15
Key index words.....	17
Abstract.....	17
Introduction.....	18
Material and procedures.....	20
Rationale of experiments.....	20
Sampling and sample preparation.....	20
Experimental setup.....	21
Actinic light mask design and control.....	22
Image analysis.....	23
Chlorophyll fluorescence measurement.....	23
Surface biomass measurement.....	23
Light-response curves of fluorescence.....	24
Determination of actinic light level.....	25
Exposure time for reaching steady state.....	26
Light-induced vertical migration.....	27
Dependence on initial light conditions.....	27
Statistical analysis.....	27
Assessment.....	28
Light curve design: determination of actinic light levels.....	28
Exposure time for reaching steady state.....	28
Light-induced vertical migration.....	30
Dependence on initial light conditions.....	31
Discussion.....	32
Approaching steady state while minimizing vertical migration.....	33

Independency of initial conditions	33
Additional advantages	35
Comments and recommendations	36
Acknowledgements	37
References	38
Chapter 3	43
Key index words.....	45
Abstract	45
Introduction	46
Materials and methods.....	49
Sampling and sample preparation	49
Photoacclimation state and photoprotection capacity	50
Photoinactivation and repair	50
Multi-actinic imaging of chlorophyll fluorescence	52
Image analysis and determination of fluorescence parameters	53
Chlorophyll <i>a</i> concentration	53
Taxonomic composition.....	53
Statistical analyses.....	54
Results.....	54
Sample taxonomic composition and chlorophyll content.....	54
Photoacclimation state and photoprotection capacity	55
Photoinactivation and repair	58
Discussion	62
Light response and induction kinetics of <i>rETR</i> and NPQ	62
Susceptibility to photoinactivation.....	65
Photoprotective role of NPQ	66
Photoinactivation versus repair.....	67
Photoprotective capacity: NPQ versus ϕ_{PI}	69
Acknowledgements.....	70
References	71
Chapter 4	79
Keywords.....	81
Abstract	81
Introduction	82
Material and methods	84

Sampling sites	84
Recovery of photosynthetic activity.....	84
Subsurface vertical migration	86
Vertical distribution of subsurface biomass.....	86
Ecosystem-level subsurface biomass fraction	87
Chlorophyll <i>a</i> quantification.....	88
Statistical analysis	88
Results.....	88
Recovery of photosynthetic activity.....	88
Subsurface vertical migration	92
Vertical distribution of MPB biomass	93
Ecosystem-level subsurface biomass fraction	94
Discussion	96
Photosynthetic resilience.....	96
Subsurface vertical migration	98
Vertical distribution of subsurface biomass.....	99
Ecosystem-level subsurface biomass and 'blue carbon' budgets.....	100
Acknowledgements	102
References	103
Chapter 5	113
Key index words.....	115
Abstract	115
Introduction	116
Material and Methods	117
Study area, sampling and sample processing.....	117
Physical parameters.....	120
Biomass	120
Chlorophyll <i>a</i> fluorescence	121
Absorption cross section of PS II.....	121
Effective quantum yield and relative electron transport rate of PSII	122
Light-response curves of <i>rETR</i>	122
Absolute ETR and carbon fixation rates.....	122
Areal rates of carbon fixation	123
Light attenuation coefficients	124
Estimation of ecosystem-level annual primary productivity	125

Statistical analysis	126
Results.....	126
Hourly variability in physical conditions, photophysiology, and biomass-specific productivity	126
Spatio-temporal variability: fortnight and seasonal time scales	132
Biomass-specific productivity.....	136
Light attenuation coefficients	136
Areal production rates	137
Discussion	139
Abiotic factors.....	139
Biomass	140
Photophysiology and photoacclimation state	142
Biomass-specific, areal and ecosystem-level productivity.....	144
Assumptions and limitations of chlorophyll fluorescence-based productivity estimates.....	145
Acknowledgments.....	148
References	149
Chapter 6	157
References.....	163

LIST OF FIGURES

Chapter 2

Figure 1. Illustration of the measurement of single-pulse light-response curves (SPLC) of chlorophyll fluorescence on MPB samples. A. Light mask comprising eight areas of actinic light (AAL), and three replicates for each light level ('3 × 8' light mask), designed to fit a well plate containing 24 replicated MPB samples. Numbers indicate the irradiance levels ($\mu\text{mol quanta m}^{-2} \text{ s}^{-1}$) applied in each group of three AALs. B. Effective quantum yield of PSII, $\Delta F/F_m'$ (false color scale), as measured for each AAL by applying a single saturating pulse after exposure to the actinic light mask for 120. Numbers indicate the average $\Delta F/F_m'$ values determined for each sample, used for calculating the $rETR$ values plotted in Fig. 2.

26

Figure 2. Single-pulse light-response curves of $rETR$ as measured on microphytobenthos samples after 120 s of actinic light mask exposure. Comparison of typical quasi-continuous light curve (generated by a light mask with 24 different light levels) and one light curve based on eight light levels (generated by using a 3 × 8 light mask). Lines represent the fit of the Eilers and Peeters (1988) model (Eq. 4). Vertical bars: one standard error.....28

Figure 3. Variation over time of $rETR$ light curve parameters α , $rETR_m$ and E_k upon exposure to actinic light of microphytobenthos samples treated with diatom motility inhibitor Lat A as compared to untreated (control) samples. Lines represent a 3-point moving average of each parameter.29

Figure 4. Short-term light-induced changes in microalgal surface biomass under different irradiance levels, as measured by the microalgal biomass reflectance index NDVI (Eq. 3).

30

Figure 5. Effects of initial light conditions (LL and HL: 50 and 1000 $\mu\text{mol quanta m}^{-2} \text{ s}^{-1}$, respectively) on the parameters of $rETR$ light-response curves α , $rETR_m$ and E_k as measured using different experimental protocols: RLC (10 s light step), SSLC (60 s light step) and SPLC generated after 10, 30 and 60 s of light mask exposure. Mean values of three independent measurements. Vertical bars: one standard error.....31

Chapter 3

Figure 1. Variation over time of light-response curves of fluorescence parameters F_s and F_m' (normalized to F_o) for samples collected at VA-EPL (A) and GE-EPM (B) sampling sites. Light curves measured at 3.75, 15 and 30 min after the start of light exposure. Data points are mean values of 9 replicated measurements. Error bars represent ± 1 standard error.....55

Figure 2. Variation over time of light-response curves of relative electron transport rate at PSII ($rETR$) for samples collected at VA-EPL (A) and GE-EPM (B) sampling sites. Light curves measured at 3.75, 15 and 30 min after the start of light exposure. Data points are mean values of 9 independent measurements. Error bars represent ± 1 standard error. Lines represent the model of Eilers & Peeters (1988) fitted to mean values at each time. Model parameters (α , $rETR_m$ and E_k) at the end of light exposure (30 min).57

Figure 3. Variation over time of light-response curves of non-photochemical quenching (NPQ) for samples collected at VA-EPL (A) and GE-EPM (B) sampling sites. Light curves measured at 3.75, 15 and 30 min after the start of light exposure. Data points are mean values of 9 independent measurements. Error bars represent ± 1 standard error.

Lines represent the model of Serôdio & Lavaud (2011) fitted to mean values at each time. Model parameters (NPQ_m , n and E_{50}) at the end of light exposure (30 min).....58

Figure 4. Example of the variation with time of exposure of the fraction of functional PSII (A) under different irradiance levels (numbers at the top), for controls (C), samples treated with lincomycin (L) and samples treated with lincomycin and nigericin (L+N). Results for samples collected at VA-EPL (A) and GE-EPM (B) (8 And 10 August 2016, respectively). Lines represent fitted models (Eqs. 3 and 4 for controls and lincomycin-treated samples, respectively) and numbers are the estimated rate constants (k_{REC} and k_{PI} for controls and lincomycin-treated samples, respectively).....60

Figure 5. Variation of the rate constants of photoinactivation (k_{PI}) with irradiance (E), as measured on samples treated with lincomycin (L) and with lincomycin and nigericin (L+N), for samples collected at VA-EPL (A) and GE-EPM (B). Lines represent linear regression equations fitted to k_{PI} values. Data points are mean values of 9 replicated measurements. Error bars represent ± 1 standard error.61

Figure 6. Rate constants of photoinactivation (k_{PI}) and repair (k_{REC}) measured for the highest irradiance applied at each experiment ($1120 \mu\text{mol quanta m}^{-2} \text{s}^{-1}$), for samples collected at VA-EPL and GE-EPM. Data points are mean values of 9 replicated measurements. Error bars represent ± 1 standard error.62

Chapter 4

Figure 1. Recovery of PSII effective quantum yield (Φ_{PSII}) of samples collected at VA following exposure to surface conditions, for different depths. (A) Variation of Φ_{PSII} over time for four different depths. Lines represent the fitting of Eq. (1) to data collected for each depth. (B) Φ_{PSII} plotted against depths for three time points. Average of three independent measurements. Error bars indicate one standard error.89

Figure 2. Recovery of PSII effective quantum yield (Φ_{PSII}) of samples collected at GE following exposure to surface conditions, for different depths. (A) Variation of Φ_{PSII} over time for four different depths. Lines represent the fitting of Eq. (1) to data collected for each depth. (B) Φ_{PSII} plotted against depths for three time points. Average of three independent measurements. Error bars indicate one standard error.90

Figure 3. Variation with depth of the rate constant of Φ_{PSII} recovery (k_t) for samples collected at VA and GE.....90

Figure 4. Variation with depth of the relative abundance of three main taxonomical groups (diatoms, cyanobacteria and euglenoids) in sampling sites VA (A) and GE (B). Cells categorized as 'other' were in most cases unidentified.91

Figure 5. Variation of sub-millimeter scale Chl *a* vertical profiles over the time course of a diurnal low tide exposure. Panels A and B refer to two independent experiments. Average of three independent samples.....92

Figure 6. Depth-integrated Chl *a* content over the time course of a diurnal low tide exposure, during two independent experiments (from data shown in Fig. 5). Arrow indicates the low tide peak at the corresponding sampling side.93

Figure 7. Depth profiles of Chl *a* content in the three sampling sites VA (A), TO (B) and GE (C). Line represents the fitting of Eq. (2). The estimated values of the parameters of Eq. (2) C_0 , k_C , and C_d are shown. Average Chl *a* concentration of nine sediment cores. Error bars indicate one standard error.94

Figure 8. Classification of the intertidal areas Ria de Aveiro regarding the ratios of total biomass and of total viable biomass to surface biomass ($C_{sub,total}$ and $C_{sub,viable}$, respectively). Values of $C_{sub,total}$ and $C_{sub,viable}$ determined for each intertidal habitat were applied to the total intertidal area. Numbers identify the main channels: Mira Channel (1) Ílhavo Channel (2), São Jacinto Channel (3), Espinheiro Channel (4). .95Figure 1. Ria de Aveiro, Portugal. The different habitats are highlighted in green, for intertidal areas, blue for subtidal areas, and grey for other. Sampling sites are marked with a black dot: Vista Alegre (VA), Gafanha da Encarnação (GE), and Torreira (TO)..... 119

Chapter 5

Figure 2. Schematic describing the modelling workflow followed in this study. Biomass-specific productivity rates (P^B , $mg\ C\ mg\ Chl\ a^{-1}\ h^{-1}$) were calculated from irradiance (E) and fluorescence-based parameters (F_v/F_m , $\Delta F/F_m'$, σ_{II}). Productivity per unit area was calculated by depth-integrating PB using light-response curves of PB, chlorophyll a content, and light attenuation. Depth-integration was carried out differently for phytoplankton and microphytobenthos, using light attenuation coefficient for the water column (k_w) and the sediment (k_s), respectively. Parameters in green were measured in this study. Parameters in blue were taken from published sources. Numbers represent the equations describing each step. 125

Figure 3. Hourly variation of abiotic (A-D) and photophysiological (E-J) parameters along one day in Torreira (TO) during neap (A, C, E, G, I) and spring tide (B, D, F, H, J) in July 2013. Blue areas represent high tide; vertical bars demonstrate the beginning/end of the high tide. Mean values of three replicates. Error bars represent one standard error. ... 127

Figure 4. Hourly variation of abiotic (A-D) and photophysiological (E-J) parameters along one day in Gafanha de Encarnação (GE) during neap (A, C, E, G, I) and spring tide (B, D, F, H, J) in July 2013. Blue areas represent high tide; vertical bars demonstrate the beginning/end of the high tide. Mean values of three replicates. Error bars represent one standard error. 128

Figure 5. Hourly variation of abiotic (A-D) and photophysiological (E-J) parameters along one day in Vista Alegre (VA) during neap (A, C, E, G, I) and spring tide (B, D, F, H, J) in July 2013. Blue areas represent high tide; vertical bars demonstrate the beginning/end of the high tide. Mean values of three replicates. Error bars represent one standard error..... 129

Figure 6. Seasonal variation of abiotic (A-F) and photophysiological (G-X) parameters in sampling sites Torreira (TO; A, D, G, J, M, P, S, V), Gafanha da Encarnação (GE; B, E, H, K, N, Q, T, W) and Vista Alegre (VA; C, F, I, L, O, R, U, X). PP in blue and MPB yellow. Spring tide (full circles) and Neap tide (empty circles). Mean values of three replicates. Error bars represent one standard error. 133

Figure 7. Vertical profile of spectrally-averaged irradiance (percentage of incident irradiance) in intertidal sediments of the three sampling sites Vista Alegre (VA), Gafanha da Encarnação (GE) and Torreira (TO). Number are the downwelling light attenuation coefficients (K_s) for each type of sediment. Mean values of three replicates. Error bars represent one standard error. 136

Figure 8. Hourly rates of biomass-specific primary production of phytoplankton (PP) and microphytobenthos (MPB) along two days in July 2013, on tides (A, C, E) and spring tides (B, D, F), at the three sampling sites, Torreira (TO; A, B), Gafanha da Encarnação (GE; C, D) and Vista Alegre (VA; E, F). 137

Figure 9. Seasonal variation of daily rates of primary production of phytoplankton (PP) and microphytobenthos (MPB) during spring (S) and neap (N) tide in sampling sites Torreira (A), Gafanha da Encarnação (B) and Vista Alegre (C)..... 138

LIST OF TABLES

Chapter 5

Table 1. Summary of the data used for the upscaling of local areal primary production rates ($\text{g C m}^{-2} \text{ yr}^{-1}$) to ecosystem-level carbon fixation budget (t C yr^{-1}). Percentages refer to the proportion of primary production of phytoplankton or microphytobenthos relatively to the total..... 139

Table 2. Daily and annual primary productivity rates of phytoplankton and microphytobenthos as measured in this study and in published studies. Average values unless stated otherwise. ^a maximum daily values. ^b range of compiled values..... 145

NOTATION

A	Initial slope of a $rETR$ vs E curve [$\mu\text{mol quanta}^{-1} \text{m}^2 \text{s}$]
σ_{II}	Absorption cross-section of PSII [nm^2]
ϕ_{PI}	Relative quantum yield of photoinactivation [$\text{m}^2 \mu\text{mol quanta s}^{-1}$]
ϕ_{PII}	Effective quantum yield of PSII [dimensionless]
A	Fraction of functional PSII
a, b, c	Parameters of the Eilers and Peeters (1988) model (arbitrary units)
AAL	Areas of Actinic Light
AOI	Areas of Interest
ATP	Adenosine triphosphate
Chl a	Chlorophyll a concentration [$\text{mg Chl } a \text{ m}^{-3}$ or $\text{mg Chl } a \text{ m}^{-2}$]
Css	Concentration of cohesive sediments [mg L^{-1}]
D1	Protein subunit of the PSII reaction centre
DDx	Xanthophyll cycle pigment Diadinoxanthin
Deg	Degradation of periplasmic proteins Protease
DTx	Xanthophyll cycle pigment Diatoxanthin
E	PAR irradiance [$\mu\text{mol quanta m}^{-2} \text{s}^{-1}$]
E_{50}	Irradiance level corresponding to 50% of NPQ_m in a NPQ vs E curve [$\mu\text{mol quanta m}^{-2} \text{s}^{-1}$]
E_k	Light-saturation parameter of a $rETR$ vs E curve [$\mu\text{mol quanta m}^{-2} \text{s}^{-1}$]
EPL	Epipelon
EPM	Epipsammon
$E(z)$	PAR irradiance [$\mu\text{mol quanta m}^{-2} \text{s}^{-1}$] at depth z
ETR	Absolute rates of electron transport of PSII [electrons $\text{PSII}^{-1} \text{s}^{-1}$]
$rETR$	Relative electron transport rate of PSII [dimensionless]
$rETR_m$	Maximum $rETR$ in a $rETR$ vs E curve [dimensionless]
F_o, F_m	Minimum and maximum fluorescence of a dark-adapted sample [arbitrary units]
F_s, F'_m	Steady-state and maximum fluorescence of a light-adapted sample [arbitrary units]
$F_{m'm}$	Maximum fluorescence level measured during the construction of the light- response or induction curve
F_v/F_m	Maximum quantum yield of PSII [dimensionless]
$\Delta F/F'_m$	Effective quantum yield of PSII [dimensionless]

FRRF	Fast repetition rate fluorometry
FtsH	Protease
GE	Gafanha da Encarnação
k_s	Light extinction coefficient in the sediment [mm^{-1}]
k_w	Light extinction coefficient in the water column [m^{-1}]
k_{PI}	Rate constant of photoinactivation of PSII [s^{-1}]
k_{REC}	Rate constant of repair of PSII [s^{-1}]
L	Lincomycin
L+N	Lincomycin and Nigericin
Lat A	Latrunculin A
LC	Light-response curve
LHC	Light harvesting complex
MPB	Microphytobenthos
MT	Multi-turnover
N	Sigmoidicity coefficient of a NPQ vs E curve
NADPH	Nicotinamide adenine dinucleotide phosphate
NDVI	Normalized Difference Reflectance Index
$ne(\text{O}_2)$	Number of electrons required for evolution of 1 molecule of O_2
NPQ	Non-photochemical quenching index [dimensionless]
NPQ_m	Maximum NPQ value reached in a NPQ vs E curve
NT	Neap tides
P	Depth-integrated photosynthetic rate [$\text{mg C m}^{-2} \text{h}^{-1}$]
P^B	Biomass-specific photosynthetic rate [$\text{mg C mg Chl a}^{-1} \text{d}^{-1}$]
PAR	Photosynthetic active radiation
PQ	Plastoquinone
PSII	Photosystem II
PSII(A)	Fraction of functional PSII
PSU	Number of chlorophyll a molecules per photosynthetic unit
QA	Quinone
q_E	energy-dependent quenching
RLC	Rapid light-response curve
ROS	Reactive oxygen species
r_{O_2}	Rates of O_2 evolution [$\text{mmol O}_2 \text{ mg Chl a}^{-1} \text{s}^{-1}$]

SP	Saturation pulse
SPLC	Single-Pulse Light Curve
SSLC	Steady-State Light Curve
ST	Spring tides
TO	Torreira
VA	Vista alegre
VM	Vertical migration
XC	Xantophyll cycle
Z	Depth [μm , mm or m]

Chapter 1

GENERAL INTRODUCTION

Estuaries as carbon sinks: productivity of phytoplankton and microphytobenthos

Estuaries are recognized as one of the most productive ecosystems on the planet (Costanza et al., 1997; Underwood and Kromkamp, 1999), being estimated to contribute to up to 10% of world primary production (McLusky and Elliott, 2007). The high productivity of estuaries is based on the high photosynthetic activity of several stress tolerant groups of primary producers that include phytoplankton and microphytobenthos but also others, such as sea grasses, macroalgae, and if considering the salt marshes, halophyte plants. These microalgal communities display key ecological roles in the estuarine ecosystem, representing an essential food source for grazers (Middelburg et al., 2000), and mediating nutrient cycling (Hochard et al., 2010). The microphytobenthos is further involved in the control of oxygen and nutrient fluxes across the sediment–water interface (Eyre et al., 2011), and in promoting sediment biostabilization, acting as bioengineers (Passarelli et al., 2014). The high productivity of phytoplankton and microphytobenthos is based on high rates of carbon fixation, contributing to making the estuarine habitats major sinks of CO₂ (Falkowski and Raven, 1997; Middelburg et al., 2000). However, because of the large inputs of organic carbon originating from land, decomposition and remineralization may prevail over carbon fixation and estuaries may act as net respirers (Cloern et al., 2014). The balance between gross and net productivity is difficult to untangle, also because of methodological issues (Cloern et al., 2014; Underwood and Kromkamp, 1999).

The phytoplankton and the microphytobenthos are the communities of phototrophic microalgae and cyanobacteria that inhabit the water column and the benthos, respectively. In estuaries, the phytoplankton is often dominated by eukaryotic single-cell microalgae. The most abundant groups are the Bacillariophyceae (diatoms) and Dinophyceae (dinoflagellates), although species of the Chlorophyceae, Haptophyceae Cryptophyceae, and Euglenophyceae, as well as prokaryotic Cyanobacteria, are also commonly present (Gameiro et al., 2007; Kromkamp et al., 1998; Underwood and Kromkamp, 1999; Vidal et al., 2017). The microphytobenthos colonize intertidal or shallow subtidal benthic habitats, and is particularly abundant in unvegetated, sedimentary habitats (MacIntyre et al., 1996; Underwood and Kromkamp, 1999). The microphytobenthos is typically dominated by diatoms, but members of the Cyanobacteria, Euglenophyceae, Chlorophyceae and Dinophyceae may also be found (Benoiston et al., 2017; MacIntyre et al., 1996; Underwood and Kromkamp, 1999). In contrast with the planktonic diatoms, that are mostly centric, benthic diatoms are almost exclusively pennate species, comprised of cells that typically

have a well-defined main axis and often bilateral symmetry (Round 1990). The species of diatoms of the microphytobenthos are classified into two groups, corresponding to two main life forms (Admiraal, 1984; Round, 1990; Taylor and Paterson, 1998): the epipelon, comprising biraphid motile species, that are dominant in fine muddy sediments, where they move freely between the sediment particles; and the epipsammon, comprising predominantly non-motile or partially motile species that colonize coarser, sandier sediments, where they tend to attach to the sediment particles. Epipellic and epipsammonic species are taxonomically closely related and can occur sympatrically, but differ markedly in motility, ecology and preferred sedimentary habitat.

The phytoplankton and the microphytobenthos are not mutually exclusive. Particularly in tidal estuaries, sediment resuspension and deposition events frequently cause the transport of cells from the sediment to the water column and vice-versa, and some species are commonly found in both habitats. These are as referred to as tytoplanktonic, an ill-defined group that comprise both centric and pennate forms that can inhabit both the water column and the sediment (Barnett et al., 2015).

The relative importance of phytoplankton and microphytobenthos as contributors to global, estuarine-level productivity has been a motive of interest for decades (Underwood and Kromkamp, 1999), but has been hampered by difficulties in the application of methods to the two types of communities yielding results that can be directly comparable. The measurement of the primary production of phytoplankton, based on ^{14}C uptake, although not free from problems, has been standardized and used routinely in many estuaries (Cloern et al., 2014). In the case of microphytobenthos, the situation is more complex. Firstly, a variety of method has been used, including ^{14}C fixation (e.g. Hartig et al., 1998), oxygen exchange (using benthic chambers; e.g. Brotas and Catarino, 1995) and oxygen production (using oxygen microelectrodes; Revsbech et al., 1983). Secondly, the very thin photic zone of the sediment poses significant problems not only in obtaining vertically resolved measurements, but also in the extrapolation of biomass-specific to area productivity rates (e.g. Laviale et al., 2016; Serôdio et al., 2001).

Since the introduction of *in vivo* chlorophyll fluorometry, major efforts have been put in place to develop protocols to estimate rates of photosynthesis of phytoplankton (e.g. Kolber and Falkowski, 1993; Lawrenz et al., 2013; Morris et al., 2008; Silsbe et al., 2015). Because of the optically thin nature of sediment samples, the protocols used for dilute phytoplankton samples cannot be directly applied to the microphytobenthos. As such, the attempts of using chlorophyll fluorescence to estimate photosynthetic rates of sediment samples have been based on empirical indices and not, as for the phytoplankton, on the

measurement of absolute rates of PSII electron transport (Du and Chung, 2009; Serôdio, 2003). More recently, a new type of fluorometer (Multi-Color PAM, Walz) has been introduced that allows the measurement of absolute rates of PSII electron transport rates (Schreiber et al., 2012). This new instrument, and associated protocols, open promising possibilities for the application of fluorescence-based estimates of primary productivity both in optically thin and, to some extent, in optically-thick samples (Klughammer and Schreiber, 2015).

Photoinhibition, photoprotection and productivity

Photoinhibition consists in the light-induced decrease in photosynthetic activity. It results from the photoinactivation of the D1 protein of PSII (Kyle et al., 1984), and is an inevitable side effect of oxygenic photosynthesis, being ubiquitous across all photosynthetic taxa (Campbell et al., 2003; Falkowski et al., 2008). Under ecologically relevant conditions, photoinhibition ('net photoinhibition') results from the outcome of the balance between PSII photoinactivation and processes of PSII repair, having a negative impact on primary productivity.

The mechanism of PSII photoinactivation *in vivo* has been explained by two main hypotheses: i) the 'Mn-cluster' paradigm, stating that photoinhibition originates from the direct excitation and inactivation of the Mn_4CaO_5 cluster of the PSII Oxygen Evolving Complex; ii) the 'photosynthetic pigment' paradigm, stating that PSII photoinactivation is due to the absorption of excess light through the photosynthetic antenna, and consequent accumulation of reactive oxygen species (ROS) (Tyystjärvi, 2013; Zavafer et al., 2015). From extensive experimentation, a 'hybrid' paradigm has recently emerged, acknowledging that both processes can occur concurrently (Murphy et al., 2017; Oguchi et al., 2011; Tyystjärvi, 2013; Zavafer et al., 2015). On the other hand, PSII repair is a complex process that involves multiple steps, including the proteolytic degradation of the D1 protein by FtsH and Deg proteases, the ribosomal synthesis of the precursor to the D1 and its insertion into the thylakoid membrane, the maturation of the D1 protein and the assembly of the oxygen-evolving machinery (Takahashi and Murata, 2008; Tyystjärvi, 2013). There is currently the growing belief that the light stress acts predominantly by inhibiting repair and not by promoting inactivation (Murata et al., 2012; Nishiyama et al., 2006). This new paradigm of photoinhibition is still under debate, calling for more detailed experimental evidence, namely regarding the including the impact of environmental stressor factors (Murata et al., 2007).

Under natural conditions, the detrimental impact of photoinhibition on photosynthetic performance and productivity depends on the balance between PSII photoinactivation and repair but also on the effectiveness of several photoprotective mechanisms that limit the extent of light-induced damages (Takahashi and Badger, 2011). These photoprotective processes can be of two main types (Raven, 2011): processes that restrict the rate of photons incident on the photosynthetic apparatus, that include chloroplast light avoidance movements (e.g. in centric planktonic diatoms; Furukawa et al., 1998) and whole cell phototactic responses within steep light gradients (e.g. in pennate benthic diatoms; Laviale et al., 2016), and processes that limit the photodamage caused by absorbed photons, such as those based on the dissipation of absorbed light energy, the main being the non-photochemical quenching (NPQ) of chlorophyll fluorescence and associated xanthophyll cycle (Müller, 2001; Ruban, 2016).

Photoinhibition can have substantial metabolic costs for the cell and be a major limiting factor of growth and primary productivity and downstream ecological consequences (Adams et al., 2013; Murchie and Niyogi, 2011; Raven, 2011). This is because PSII photoinactivation lowers the number of functional PSII, affecting the production of ATP and NADPH, and decreasing carbon fixation rates. On the other hand, PSII repair is a relatively slow process that relies on the removal and replacement of protein subunits, an energetically expensive process, critically dependent on ATP (Murata et al., 2012; Nath et al., 2013). Also the operation of photoprotective mechanisms have a negative impact on photosynthetic efficiency, growth and productivity. Downregulation by dissipation of absorbed energy by NPQ lowers photosynthetic rates to levels below their potential maximum and consumes additional cellular resources (Raven, 2011).

Photoprotection and photoinhibition have been studied in much more detail for phytoplankton, although in many cases data originates from isolated species grown in culture, than for microphytobenthos (Campbell and Tyystjärvi, 2012). Possible reasons include the historically larger interest on phytoplankton, but also the challenging methodological issues of the study of sedimentary biofilms, especially when dominated by motile cells. For the microphytobenthos, the functioning of photoprotection mechanisms have been reasonably studied (e.g. Laviale et al., 2015; Serôdio et al., 2005), but the photoinactivation versus repair balance has only been addressed marginally (Cartaxana et al., 2013; Serôdio et al., 2012).

General objectives and thesis outline

Considering the current gaps in knowledge regarding microphytobenthos photophysiology and productivity, this work aimed to address the following general objectives:

- i) optimize the application to microphytobenthos of a recently-developed method for the characterization of the photoacclimation state of undisturbed samples, based on non-sequential light-response curves of chlorophyll fluorescence indices ('single-pulse light curves', SPLC);
- ii) evaluate the inherent photoprotective capacity of microphytobenthos communities, as measured by the reduction in photoinactivation of photosystem II (PSII) caused by light stress;
- iii) assess the role of subsurface microalgal biomass as a potential source of photosynthetically active cells for microphytobenthos biofilms at the surface;
- iv) estimate areal and ecosystem-level primary productivity of phytoplankton and intertidal microphytobenthos in a tidal estuarine system, the Ria de Aveiro (Portugal), based on synoptic *in situ* measurements of absolute rates of electron transport rate of photosystem II, using a novel type of PAM fluorometer.

These general objectives were pursued in the following four chapters, each corresponding to an article published (or in preparation, in the case of chapter 5) in peer-reviewed scientific journals.

Chapter 2 addresses the establishment of a novel methodological approach, based on non-sequential light response curves of chlorophyll fluorescence indices ('single-pulse light curves'), to improve photophysiological studies on microphytobenthos, and the characterization of photoacclimation state of undisturbed sedimentary biofilm samples.

Chapter 3 evaluates the photoprotective capacity against photoinhibition of microphytobenthos communities inhabiting contrasting sedimentary habitats and relying on distinct light responses: epipelagic communities, using motility (vertical migration) to regulate light exposure, and epipsammic communities, relying solely on physiological photoprotective mechanisms. The capacity for photoprotective was quantified in terms of the reduction in PSII photoinactivation conferred by the inherent physiological mechanisms in operation.

Chapter 4 addresses an overlooked aspect of microphytobenthos ecology, key for understanding their role as a carbon sink, namely the importance of subsurface microalgal

biomass as a potential source of photosynthetically active cells for surface biofilms. This was approached by investigating if buried cells can regain photosynthetic activity following resurfacing, evaluating the role of vertical migration in facilitating the resurfacing processes, and estimating the fraction of microalgal present below the surface, in different intertidal sediment types of the Ria de Aveiro, a tidal estuary located in central Portugal.

Chapter 5 describes a synoptic study carried out in the Ria de Aveiro, aiming to characterize comparatively the spatio-temporal variability of the biomass, photosynthetic activity and productivity of phytoplankton and microphytobenthos, and the obtention of an integrated budget of carbon fixation by planktonic and benthic microalgal communities.

References

- Adams, W. W., Müller, O., Cohu, C. M., and Demmig-Adams, B. (2013). May photoinhibition be a consequence, rather than a cause, of limited plant productivity? *Photosynth. Res.* 117, 31–44.
- Admiraal, W. (1984). The ecology of estuarine sediment-inhabiting diatoms. *Prog. Phycol. Res.* 3, 269–322.
- Barnett, A., Méléder, V., Blommaert, L., Lepetit, B., Gaudin, P., Vyverman, W., et al. (2015). Growth form defines physiological photoprotective capacity in intertidal benthic diatoms. *ISME J.* 9, 32–45.
- Benoiston, A., Ibarbalz, F. M., Bittner, L., Guidi, L., Jahn, O., Dutkiewicz, S., et al. (2017). The evolution of diatoms and their biogeochemical functions. *Philos. Trans. R. Soc. B Biol. Sci.* 372, 20160397.
- Brotas, V., and Catarino, F. (1995). Microphytobenthos primary production of Tagus estuary intertidal flats (Portugal). *Neth. J. Aquat. Ecol.* 29, 333–339.
- Campbell, D. A., Cockshutt, A. M., and Porankiewicz-Asplund, J. (2003). Analysing photosynthetic complexes in uncharacterized species or mixed microalgal communities using global antibodies. *Physiol. Plant.* 119, 322–327.
- Campbell, D. A., and Tyystjärvi, E. (2012). Parameterization of photosystem II photoinactivation and repair. *Biochim. Biophys. Acta - Bioenerg.* 1817, 258–265.
- Cartaxana, P., Domingues, N., Cruz, S., Jesus, B., Laviale, M., Serôdio, J., et al. (2013). Photoinhibition in benthic diatom assemblages under light stress. *Aquat. Microb. Ecol.* 70, 87–92.
- Cloern, J. E., Foster, S. Q., and Kleckner, A. E. (2014). Phytoplankton primary production in the world's estuarine-coastal ecosystems. *Biogeosciences*, 11, 2477–2501.
- Costanza, R., D'Agre, R., de Groot, R., Farber, S., Grasso, M., Hannon, B., et al. (1997). The value of the world's ecosystem services and natural capital. *Nature* 387, 253–260.
- Du, G. Y., and Chung, I. K. (2009). Estimating areal production of intertidal microphytobenthos based on spatio-temporal community dynamics and laboratory measurements. *Ocean Sci. J.* 44, 189–197.
- Eyre, B. D., Ferguson, A. J. P., Webb, A., Maher, D., and Oakes, J. M. (2011). Denitrification, N-fixation and nitrogen and phosphorus fluxes in different benthic habitats and their contribution to the nitrogen and phosphorus budgets of a shallow

- oligotrophic sub-tropical coastal system (southern Moreton Bay, Australia). *Biogeochemistry* 102, 111–133.
- Falkowski, P. G., Fenchel, T., and Delong, E. F. (2008). The microbial engines that drive earth's biogeochemical cycles. *Science*. 320, 1034–1039.
- Falkowski and Raven (1997), *Aquatic Photosynthesis* (Blackwell, Oxford, UK)
- Furukawa, T., Watanabe, M., and Shihira-Ishikawa, I. (1998). Green- and blue-light-mediated chloroplast migration in the centric diatom *Pleurosira laevis*. *Protoplasma* 203, 214–220.
- Gameiro, C., Cartaxana, P., and Brotas, V. (2007). Environmental drivers of phytoplankton distribution and composition in Tagus Estuary, Portugal. *Estuar. Coast. Shelf Sci.* 75, 21–34.
- Hartig, P., Wolfstein, K., Lippemeier, S., and Colijn, F. (1998). Photosynthetic activity of natural microphytobenthos populations measured by fluorescence (PAM) and ¹⁴C-tracer methods: A comparison. *Mar. Ecol. Prog. Ser.* 166, 53–62.
- Hochard, S., Pinazo, C., Grenz, C., Evans, J. L. B., and Pringault, O. (2010). Impact of microphytobenthos on the sediment biogeochemical cycles: A modeling approach. *Ecol. Modell.* 221, 1687–1701.
- Klughammer, C., and Schreiber, U. (2015). Apparent PS II absorption cross-section and estimation of mean PAR in optically thin and dense suspensions of *Chlorella*. *Photosynth. Res.* 123, 77–92.
- Kolber, Z., and Falkowski, P. G. (1993). Use of active fluorescence to estimate phytoplankton photosynthesis in situ. *Limnol. Oceanogr.* 38, 1646–1665.
- Kromkamp, J., Barranguet, C., and Peene, J. (1998). Determination of microphytobenthos PSII quantum efficiency and photosynthetic activity by means of variable chlorophyll fluorescence. *Mar. Ecol. Prog. Ser.* 162, 45–55.
- Kyle, D. J., Ohad, I., and Arntzen, C. J. (1984). Membrane protein damage and repair: Selective loss of a quinone-protein function in chloroplast membranes. *Proc. Natl. Acad. Sci.* 81, 4070–4074.
- Laviale, M., Ezequiel, J., Pais, C., Cartaxana, P., and Serôdio, J. (2015). The “crème brûlée” sampler: A new high-resolution method for the fast vertical sampling of intertidal fine sediments. *J. Exp. Mar. Bio. Ecol.* 468, 37–44.
- Laviale, M., Frankenbach, S., and Serôdio, J., (2016). The importance of being fast: comparative kinetics of vertical migration and non-photochemical quenching of benthic diatoms under light stress. *Mar. Biol.* 163, 1–12.

- Lawrenz, E., Silsbe, G. M., Capuzzo, E., Ylöstalo, P., Forster, R. M., Simis, S. G. H., et al. (2013). Predicting the Electron Requirement for Carbon Fixation in Seas and Oceans. *PLoS One* 8.
- MacIntyre, H. L., Geider, R. J., and Miller, D. C. (1996). Microphytobenthos: The Ecological Role of the “Secret Garden” of Unvegetated, Shallow-Water Marine Habitats. I. Distribution, Abundance and Primary Production. *Estuaries* 19, 186.
- McLusky, D.S., Elliott, M. (2007) Transitional waters: A new approach, semantics or just muddying the waters? *Estuar. Coast. Shelf Sci.* 71(3-4), 359-363
- Middelburg, J. J., Barranguet, C., Boschker, H. T. S., Herman, P. M. J., Moens, T., and Heip, C. H. R. (2000). The fate of intertidal microphytobenthos carbon: An in situ ¹³C-labeling study. *Limnol. Oceanogr.* 45, 1224–1234.
- Morris, E. P., Forster, R. M., Peene, J., and Kromkamp, J. C. (2008). Coupling between Photosystem II electron transport and carbon fixation in microphytobenthos. *Aquat. Microb. Ecol.* 50, 301–311.
- Müller, P. (2001). Non-photochemical quenching. a response to excess light energy. *Plant Physiol.* 125, 1558–1566.
- Murata, N., Allakhverdiev, S. I., and Nishiyama, Y. (2012). The mechanism of photoinhibition in vivo: Re-evaluation of the roles of catalase, α -tocopherol, non-photochemical quenching, and electron transport. *Biochim. Biophys. Acta - Bioenerg.* 1127–1133.
- Murata, N., Takahashi, S., Nishiyama, Y., and Allakhverdiev, S. I. (2007). Photoinhibition of photosystem II under environmental stress. *Biochim. Biophys. Acta - Bioenerg.* 1767, 414–421.
- Murchie, E. H., and Niyogi, K. K. (2011). Manipulation of photoprotection to improve plant photosynthesis. *Plant Physiol.* 155, 86–92.
- Murphy, C. D., Roodvoets, M. S., Austen, E. J., Dolan, A., Barnett, A., and Campbell, D. A. (2017). Photoinactivation of photosystem II in *Prochlorococcus* and *Synechococcus*. *PLoS One* 12, 1–24.
- Nath, K., Jajoo, A., Poudyal, R. S., Timilsina, R., Park, Y. S., Aro, E. M., et al. (2013). Towards a critical understanding of the photosystem II repair mechanism and its regulation during stress conditions. *FEBS Lett.* 587, 3372–3381.
- Nishiyama, Y., Allakhverdiev, S. I., and Murata, N. (2006). A new paradigm for the action of reactive oxygen species in the photoinhibition of photosystem II. *Biochim. Biophys. Acta - Bioenerg.* 1757, 742–749.

- Oguchi, R., Terashima, I., Kou, J., and Chow, W. S. (2011). Operation of dual mechanisms that both lead to photoinactivation of Photosystem II in leaves by visible light. *Physiol. Plant.* 142, 47–55.
- Passarelli, C., Olivier, F., Paterson, D. M., Meziane, T., and Hubas, C. (2014). Organisms as cooperative ecosystem engineers in intertidal flats. *J. Sea Res.* 92, 92–101.
- Raven, J. A. (2011). The cost of photoinhibition. *Physiol. Plant.* 142, 87–104.
- Revsbech, N. P., Jørgensen, B. B., Blackburn, T. H., and Cohen, Y. (1983). Microelectrode studies of the photosynthesis and O₂, H₂S, and pH profiles of a microbial mat. *Limnol. Oceanogr.* 28, 1062–1074.
- Round, F.E.; Crawford, R.M.; and Mann, D. (1990) *The Diatoms - Biology & Morphology of the genera*. Cambridge: Cambridge University Press.
- Ruban, A. V. (2016). Nonphotochemical chlorophyll fluorescence quenching: mechanism and effectiveness in protecting plants from photodamage. *Plant Physiol.* 170, 1903–16.
- Schreiber, U., Klughammer, C., and Kolbowski, J. J. (2012). Assessment of wavelength-dependent parameters of photosynthetic electron transport with a new type of multi-color PAM chlorophyll fluorometer. *Photosynth Res.* 113, 127–144.
- Serôdio, J., Ezequiel, J., Barnett, A., Mouget, J-L., Méléder, V., Laviale, M. and Lavaud J. (2012). Efficiency of photoprotection in microphytobenthos: Role of vertical migration and the xanthophyll cycle against photoinhibition. *Aquat. Microb. Ecol.* 67, 161–175.
- Serôdio, J. (2003). A chlorophyll fluorescence index to estimate short-term rates of photosynthesis by intertidal microphytobenthos. *J. Phycol.* 39, 33–46.
- Serôdio, J., Cruz, S., Vieira, S., and Brotas, V. (2005). Non-photochemical quenching of chlorophyll fluorescence and operation of the xanthophyll cycle in estuarine microphytobenthos. *J. Exp. Mar. Bio. Ecol.* 326, 157–169.
- Serôdio, J., Da Silva, J. M., and Catarino, F. (2001). Use of in vivo chlorophyll a fluorescence to quantify short-term variations in the productive biomass of intertidal microphytobenthos. *Mar. Ecol. Prog. Ser.* 218, 45–61.
- Silsbe, G. M., Oxborough, K., Suggett, D. J., Forster, R. M., Ihnken, S., Lawrenz, E. (2015). Toward autonomous measurements of photosynthetic electron transport rates : An evaluation of active fluorescence-based measurements of photochemistry. *oceanography: Methods* 138–155.
- Takahashi, S., and Badger, M. R. (2011). Photoprotection in plants: A new light on photosystem II damage. *Trends Plant Sci.* 16, 53–60.

- Takahashi, S., and Murata, N. (2008). How do environmental stresses accelerate photoinhibition? *Trends Plant Sci.* 13, 178–182. doi:10.1016/j.tplants.2008.01.005.
- Taylor, I. S., and Paterson, D. M. (1998). Microspatial variation in carbohydrate concentrations with depth in the upper millimetres of intertidal cohesive sediments. *Estuar. Coast. Shelf Sci.* 46, 359–370.
- Tyystjärvi, E. (2013). Photoinhibition of Photosystem II. *Int. Rev. Cell Mol. Biol.* 300, 243–303.
- Underwood, G. J. C., and Kromkamp, J. (1999). Primary production by phytoplankton and microphytobenthos in estuaries. *Adv. Ecol. Res.* 29, 93–153.
- Vidal, T. T., Calado, A. J., Moita, M. T., and Cunha, M. R. (2017). Phytoplankton dynamics in relation to seasonal variability and upwelling and relaxation patterns at the mouth of Ria de Aveiro (West Iberian Margin) over a four-year Period. *PLoS One* 12, 1–25.
- Zavafer, A., Cheah, M. H., Hillier, W., Chow, W. S., and Takahashi, S. (2015). Photodamage to the oxygen evolving complex of photosystem II by visible light. *Sci. Rep.* 5, 16363.

Chapter 2

ONE PULSE, ONE LIGHT CURVE: FAST CHARACTERIZATION OF THE LIGHT RESPONSE OF MICROPHYTOBENTHOS BIOFILMS USING CHLOROPHYLL FLUORESCENCE

Published:

Frankenbach S., Serôdio J. (2017) One pulse, one light curve: Fast characterization of the light response of microphytobenthos biofilms using chlorophyll fluorescence. *Limnology and Oceanography: Methods*. 15 554-566.

DOI: 10.1002/lom3.10180

Key index words

Chlorophyll fluorescence, diatoms, microphytobenthos, rapid light curves, steady state light curves, single-pulse light curves, vertical migration

Abstract

Research on microphytobenthos photosynthesis has increasingly relied on Pulse Amplitude Modulation (PAM) fluorometry, often through the generation of light response curves of the relative electron transport of PSII (*rETR*), generated through the sequential exposure to a range of actinic irradiances. However, fast, vertical phototactic responses by the motile diatoms that dominate these biofilms occur during the generation of sequential light curves. Light-induced vertical migration is known to confound the characterization of the inherent physiological response of the cells forming the biofilm. The alternative approach of shortening the duration of the light curve protocol prevents the reaching of a physiological steady state and results in light curves heavily dependent on initial light conditions. This study tested the application to microphytobenthos of a recently introduced method allowing for the fast generation of non-sequential light curves, based on steady-state and temporally independent measurements ('single-pulse light curves', SPLC). This method was compared to the commonly used sequential protocols regarding its ability to (i) measure a steady-state light response, (ii) minimize the effects of vertical migration and (iii) minimize the effects of photoacclimation state induced by initial conditions. The results indicate that the SPLC method can be optimized by applying one light exposure period of just 60 s prior to the generation of the light curve, resulting in a clearly advantageous alternative to the sequential protocols. It effectively allows characterizing the steady-state light response of microphytobenthos samples while avoiding the effects of light-induced vertical migration and of the initial light conditions on light curve parameters.

Introduction

Since its introduction to the study of microphytobenthos (MPB), Pulse Amplitude Modulated fluorometry (PAM; Schreiber et al., 1986) has become an ubiquitous method for assessing the photosynthetic performance of these diatom-dominated microbial biofilms (e.g., Kromkamp et al. 1998; Serôdio et al. 2008; Perkins et al. 2010; Laviale et al. 2015). Besides its exceptional potentialities for the in-depth study of photosynthetic processes in photoautotrophs in general, this technique provides a number of specific advantages for studies on MPB: (i) it allows for fast and non-invasive measurements, especially relevant to avoid disrupting the sediment-water/air interface, and (ii) to quantitatively monitor changes in the surface biomass of the biofilm associated to vertical migration by motile diatoms ('productive biomass'; Kelly et al., 2001; Serôdio et al., 2001; Jesus et al., 2006), opening the possibility to calculate biomass-weighted fluorescence proxies for MPB photosynthetic rates (Barranguet and Kromkamp, 2000; Serôdio et al., 2007).

One of the main uses of PAM fluorometry is to characterize the photosynthetic response to light, through the generation of light-response curves of various chlorophyll fluorescence indices, such as the effective quantum yield of PSII ($\Delta F/F_m'$), the relative electron transport rate ($rETR$) or the non-photochemical quenching index (NPQ). In most cases, light-response curves of fluorescence measured on MPB are based on the sequential exposure of the same sample to a range of actinic irradiances (Serôdio et al. 2005; Waring et al. 2007; Chevalier et al. 2010; Lefebvre et al. 2011; Ubertini et al. 2015). However, because the photosynthetic activity of a sample depends not only on the irradiance to which it is exposed at the moment of measurement but also on the recent light history, sequential light-response curves are bound to be affected by the lack of independency between measurements (Perkins et al. 2006; Herlory et al. 2007; Ihnken et al. 2010). This problem is aggravated in the case of MPB, because the motile diatoms that dominate these biofilms respond phototactically to changes in irradiance (Serôdio et al. 2006a; Mclachlan et al. 2009; Ezequiel et al. 2015; Cohn et al. 2015), which may induce substantial vertical migration during the construction of the light curve (Perkins et al. 2006; Jesus et al. 2006b; Herlory et al. 2007). Light-induced vertical migration is expected to cause changes in fluorescence parameters and indices affecting the apparent light response independently of the physiological state of the microalgae that form the biofilm. This is due to changes in species composition (Perkins et al. 2001) in the photic zone, and in the vertical distribution of cells and the resulting relative contribution of sub-surface fluorescence (Forster and Kromkamp 2004; Serôdio 2004).

To minimize the undesired confounding effects of vertical migration, the light response of MPB biofilms has been characterized by light-response curves based on Rapid Light Curve (RLC) protocols. RLCs are generated by applying short periods (10-30 s) of exposure to each irradiance level (Schreiber et al. 1997; White and Critchley 1999) that, as opposed to conventional light-response curves (often termed 'steady-state light curves', or SSLC), do not allow for the sample to reach a steady state (Serôdio et al. 2005; Herlory et al. 2007; Lefebvre et al. 2011). RLCs are thus heavily dependent on initial conditions (light exposure and photoacclimation state at the beginning of the curve) as well as light history during the generation of the curve (Perkins et al. 2006; Serôdio et al. 2006b; Ihnken et al. 2010). In recent years, a number of studies have compared the different protocols used to generate light-response curves in MPB biofilms, the general conclusion being that RLCs cannot be used as unambiguous proxies for steady-state light curves (Perkins et al. 2006; Serôdio et al. 2006b; Herlory et al. 2007; Lefebvre et al. 2011), although they may provide valuable information on short-term photoacclimation, not possible to obtain otherwise (Cruz and Serôdio 2008).

Recently, a new method was introduced that allows for the generation of non-sequential light-response curves of chlorophyll fluorescence based on steady-state and temporally independent measurements ('single-pulse light curves', SPLC; Serôdio et al. 2013). The method is based on the projection of a set of spatially-separated beams of actinic light of different intensities ('light mask') on a group of replicated samples and on the simultaneous detection of the fluorescence response to the various actinic light levels using a chlorophyll fluorescence imaging system. This approach appears particularly promising for the case of MPB, as it allows to dramatically reduce the time required for completing a full light-response curve (to the time required for a single measurement), minimizing both the induction of vertical phototactic migration, and the issues associated to non-steady-state measurements of RLC protocols. In this study, we tested the application of this method to generate light-response curves on undisturbed MPB samples, by determining the optimal protocol conditions for samples dominated by motile microalgae, and comparing it with the commonly used protocols of sequential light-response curves.

Material and procedures

Rationale of experiments

The ideal protocol for generating light-response curves of fluorescence in MPB samples should observe the following criteria: (i) allow to describe the steady-state light response of the studied samples, (ii) yield results not significantly affected by vertical migration occurring during the generation of the light curves, and (iii) provide measurements independent from short-term photoacclimation state induced by initial light conditions. This study tested the verification of these conditions by the method based on SPLCs. In a first set of experiments, the time necessary to reach a physiological steady state was determined using a diatom motility inhibitor to prevent the confounding effects of vertical migration. In a second step, the extent of light-induced vertical migration occurring for the period of light exposure required to reach a steady state, determined in the previous experiments, was evaluated. A third set of experiments compared the effects of different initial light conditions on the light-response curves generated by SPLCs and by the conventional sequential protocols used to generate SSLCs or RLCs.

Before these tests were performed, a preliminary experiment was carried out to determine the light levels to be used to generate the light-response curves. This experiment also served to illustrate one of the most valuable aspects of the new method, which is the possibility to freely define the light values used to generate the light curves, including their number and distribution along the light range, as well as the number of replicates for each level.

Sampling and sample preparation

Sediment samples were collected during low tide on an intertidal mudflat near Vista Alegre (40°35'14.1"N 8°41'15.8"W), Ria de Aveiro, Portugal. The sediment was composed of fine particles (97% < 63 µm) and known to support microalgal biofilms dominated by motile diatoms throughout the year (Serôdio et al. 2006b; Frankenbach et al. 2014). The top 1 cm was collected using a spatula and transported to the laboratory where it was sieved (1 mm mesh) and thoroughly mixed. The homogenized sediment was deposited into plastic trays to form a layer of 3-4 cm thick slurry, and was covered by natural seawater and at a constant temperature (17 °C). The experiments were carried out on the day following sampling, during periods coinciding with the low tide in the sampling site. Before the start of the low tide period, the overlying water was carefully removed, and the superficial (ca. 0.5 cm) layer of sediment was collected using a spatula. After being thoroughly mixed, the

sediment was transferred to 24-well plates (Tissue Culture Plate, Sarstedt, Nümbrecht, Germany) filling the wells completely (ca. 3 mL), thus creating 24 true replicates. To promote the upward migration of microalgae and the formation of the biofilm, the plates were placed in a growth chamber (Biotronette, LAB-LINE Instruments, India) where they were exposed to light provided by fluorescence lamps ($120 \mu\text{mol quanta m}^{-2} \text{s}^{-1}$; FL40SS w/37, Sanyo, Osaka, Japan).

Experimental setup

The setup consisted of a Pulse Amplitude Modulation (PAM) imaging chlorophyll fluorometer and a digital projector, used as a source of actinic light, as described in Serôdio et al. (2013) and Laviale et al. (2016). The imaging chlorophyll fluorometer (Open FluorCAM 800-O/1010, Photon Systems Instruments; Brno, Czech Republic) comprised four 13×13 cm LED panels emitting red light (emission peak at 621 nm, 40 nm bandwidth), two providing modulated measuring light ($< 0.1 \mu\text{mol quanta m}^{-2} \text{s}^{-1}$), and the other two providing saturating pulses ($> 7000 \mu\text{mol quanta m}^{-2} \text{s}^{-1}$, 0.8 s), and a 2/3" CCD camera (CCD381) with a F1.2 (2.8-6 mm) objective. Chlorophyll fluorescence images (512×512 pixels, 695-780 nm spectral range) were captured and processed using the FluorCam7 software (Photon Systems Instruments, PSI).

A LCD digital projector (EB-X14; Seiko Epson, Suwa, Japan) comprising a mercury arc lamp providing a light output of 3,000 lumens, was used as an actinic light source. The projector was positioned in a way that the projected light incident on the center of the area monitored by the CCD camera. Projector settings were set to provide the widest range of light intensities at the sample level. The projector was used to project a 'light mask', i.e. a set of 24 circular spatially separated areas of actinic light (AAL), arranged in a 4×6 matrix. The light masks were designed so that the 24 AALs matched and covered the whole surface (16 mm diameter) of the 24 samples in the well plate.

This setup was also used to measure fast changes in microalgal biomass present at the surface of the sediment samples, based on a physiology-independent spectral reflectance index, as described by Laviale et al. (2016). Surface biomass was measured by acquiring images of diffusive reflectance in the red and infrared regions of all samples contained in the well plate. The red and infrared reflectance images were captured by illuminating the samples with four halogen lamps (50 W, Auchan JD 230V/GU 10), providing a light intensity of $250 \mu\text{mol quanta m}^{-2} \text{s}^{-1}$ and a light spectrum with a strong emission in the red and infrared regions, by sequentially use one red (FF01-676/29-25; Semrock, Rochester, NY, USA; transmission peak at 676 nm, 29-nm bandwidth) and one infrared

(FF01-747/33-25, Semrock; transmission peak at 747 nm; 33-nm bandwidth) bandpass filters. The filters were positioned between the camera lenses and the CCD and were switched using a computer-controlled filter wheel. The switching of the filters and the capture of the red and infrared images was carried out in less than 30 s using the FluorCam7 software (PSI), by running a user-defined protocol.

Actinic light mask design and control

The light masks were designed in Microsoft PowerPoint, using a code written in Microsoft Visual Basic defining the number, position, size, shape, light intensity and spectrum (R:G:B ratios; see below) of each AAL (Serôdio et al. 2013). The light level of the various areas of actinic light (AAL) composing the light mask were measured and controlled through a custom-made multi-sensor platform. This consisted of 24 flat light sensors (log-scale analog sensors, model GA1A12S202, Sharp, Osaka, Japan) mounted on a perfboard so that their positions matched the ones of the samples in the 24-well plate. The light sensors were placed at same height as the samples in relation to the camera and the projector. The plate was painted matte black to minimize light scattering. The spectral sensitivity of the sensors allowed for measurements in the PAR range (sensitivity >10% in the 400-700 nm range; peaking at 555 nm). The light sensors were connected to a microcontroller (Arduino UNO R3; www.arduino.cc) using a multiplexer shield (MuxShield II, Mayhew Labs, Greenville, SC, USA). The multiplexer shield allowed reading the 24 sensors simultaneously through just one analog pin of the microcontroller. The sensors were calibrated individually against a recently-calibrated PAR sensor (LS-C, connected to a ULM-500 reading unit; Walz, Effeltrich, Germany). Each sensor was calibrated using its readings when placed in its position in the plate, to account for the distance from the projector and the angle of incident light, for a light intensity range from 5 to 1600 $\mu\text{mol quanta m}^{-2} \text{ s}^{-1}$. The linear correlation between the sensor readings and the PAR sensor measurements was in all cases very high ($r^2 > 0.999$). A set of macros written in MS Visual Basic allowed setting the target PAR values for each AAL and read the incident levels in all AALs in real time in a MS Excel file. This information was then sent to MS PowerPoint in order to change the projected light intensity accordingly. This process was based on a relationship previously established between MS PowerPoint RGB code and projected PAR levels (R:G:B ratio maintained constant; Serôdio et al. 2013). The procedure was repeated iteratively until the incident levels matched the desired values, which typically was achieved in a small number of iterations. The MS Visual Basic code was adapted from the source code of the Arduino Excel Commander ([---

22](http://sites.google.com/site/robertovalgolio/sistemi-</p></div><div data-bbox=)

programmi/arduino-excel-commander). The use of this multi-sensor platform allowed the designing of light masks much more time-efficient, because all 24 AAL could be set and measured simultaneously, taking into account any eventual light spillover between adjacent AALs.

Image analysis

Chlorophyll fluorescence and red/infrared data were extracted by defining Areas of Interest (AOIs) for each well, using the FluorCam7 software. The AOIs were centered on the AALs but to avoid border effects the size of AOIs were defined as smaller than the actual surface of the sample (ca. 450 pixels). For each fluorescence measurement (saturating pulse, see below), the kinetics of the fluorescence signal of each AOI was analyzed individually to exclude possible flickering events caused by the projector light.

Chlorophyll fluorescence measurement

Chlorophyll fluorescence indices were measured by applying a single saturating pulse and determining the fluorescence parameters F_o and F_m (for dark-adapted samples) or F_s and F_m' (for samples exposed to actinic light) for each AOI. Fluorescence parameters were measured by averaging all pixel values of each AOI and by averaging the fluorescence intensity during the 2 s immediately before the saturating pulse (determining F_o or F_s), and during 0.6 s during the application of the saturating pulse (determining F_m or F_m' ; total duration of 800 ms). For each AOI, the maximum and the effective PSII quantum yield were calculated as $F_v/F_m = (F_m - F_o)/F_m$ and $\Delta F/F_m' = (F_m' - F_s)/F_m'$, respectively. Fluorescence measurements on light-acclimated samples were used to calculate the relative electron transport rate ($rETR$) index, given by:

$$rETR = E \frac{F_m' - F_s}{F_m'} = E \Delta F / F_m' \quad (1)$$

Surface biomass measurement

Surface biomass was measured by computing the index NDVI (Normalized Difference Reflectance Index; Rouse et al. 1973), based on red and infrared reflectance images:

$$NDVI = \frac{R_r - R_{ir}}{R_{ir} + R_r} \quad (2)$$

where R_r and R_{ir} represent the red and infrared reflectance, respectively (Laviale et al. 2016). For each sample, NDVI was calculated by averaging all pixels of each AOI. R_r and R_{ir} were calculated from the normalization to the reflectance of a reference 18% grey

standard (Kaavie GC-1 A4 Size Grey Card), measured for the same AOIs. Images were also captured in the dark and were subtracted from images of both the sample and the grey reference to account for the dark current noise.

Light-response curves of fluorescence

Sequential light-response curves (SSLC and RLC) were generated by applying a light mask consisting of AALs ($n = 3$) with the same irradiance level. The light curve was generated by incrementally increasing the light intensity applying the following PAR values in all AALs: 87, 178, 282, 410, 587, 858, 1126, 1406 $\mu\text{mol quanta m}^{-2} \text{s}^{-1}$. This set of irradiance values was defined from the results of the preliminary experiment on the optimization of the distribution of eight E levels along the full range of applicable irradiance (see below). $rETR$ light curves were generated by applying a saturating pulse and determining F_s and F_m' after exposing the samples to each actinic light intensity for 30 s or 60 s, in the case of the sequential RLCs or SSLCs, respectively. Single Pulse Light Curves (SPLC) were generated by applying a single saturating pulse yielding $rETR$ measurements for all 24 samples simultaneously, after applying a light mask consisting of 3×8 light levels (same PAR levels as indicated above) for a pre-determined period of exposure (Fig. 1). For the preliminary experiment designed to determine the light levels to use (see below), a light mask consisting of 24 light levels, equally spaced along the range of PAR levels (0 to 1300 $\mu\text{mol quanta m}^{-2} \text{s}^{-1}$), was applied.

$rETR$ vs E curves were described by fitting the model of Eilers and Peeters (1988), and by estimating the parameters α (the initial slope of the curve), $rETR_m$ (maximum $rETR$) and E_k (the light-saturation parameter):

$$rETR(E) = \frac{E}{aE^2 + bE + c} \quad (3)$$

where

$$\alpha = \frac{1}{c}, \quad rETR_m = \frac{1}{b + \sqrt{ac}} \quad \text{and} \quad E_k = \frac{c}{b + \sqrt{ac}} \quad (4)$$

All models were fitted using Microsoft Excel Solver. Model parameters were estimated iteratively by minimizing a least-square function, forward differencing, and the default quasi-Newton search method.

Determination of actinic light level

Most commercially-available PAM fluorometers allow to apply only a small number of actinic light intensities, selected from a fixed, pre-defined set of values ('PAR list', e.g., Heinz Walz, 2009). The method here tested, based on a digitally-controlled actinic light source, opens the possibility to freely define the light values, both in terms of number and intensity, used for generating light curves. Therefore, a preliminary test was carried out in order to select the E levels to use for generating SPLCs and sequential light-response curves (SSLC and RLC) in the following experiments of the study. This is of importance because the number and distribution of the E levels along the range of physiological response affect the values of the model parameters used to describe the light curves (Henley 1993; MacIntyre et al. 2002; Jones et al. 2014). Firstly, a light mask consisting of 24 AAL of light levels equally spaced along the range of applicable light intensities (0 to $1400 \mu\text{mol quanta m}^{-2} \text{s}^{-1}$) was applied to a set of replicated samples to generate a quasi-continuous set of $rETR$ measurements. This enabled to characterize in detail the shape of the light-response curve, which was used to design a light mask consisting of 3×8 light levels, considered as a good compromise between detailing the light response and replication. Additionally, the use of eight light levels allowed to better compare the results of the presented method and of standard protocols, as it is the number of light levels used in many studies (e.g., White and Critchley 1999; Ralph and Gademann 2005; Serôdio et al. 2005; Perkins et al. 2007; Morris et al. 2008; Mouget et al. 2008; Lefebvre et al. 2011).

The 3×8 light mask was designed by determining eight irradiance values such that the corresponding $rETR$ values were equally spaced along the light curve, optimizing the description of the light response both when changes in $rETR$ with E are steeper (light-limited region of the curve) or occur at slower rates (light-saturated region of the curve). The eight light levels were determined by minimizing the linear distance between their corresponding $rETR$ values, as predicted from the light curve parameters of the Eilers and Peeters (1988) model fitted to the quasi-continuous light curve, using MS Solver. The resulting light levels ($87 - 1400 \mu\text{mol quanta m}^{-2} \text{s}^{-1}$; shown above) were used for all light curves tested in this study, both sequential (SSLC and RLC) and of the SPLC type.

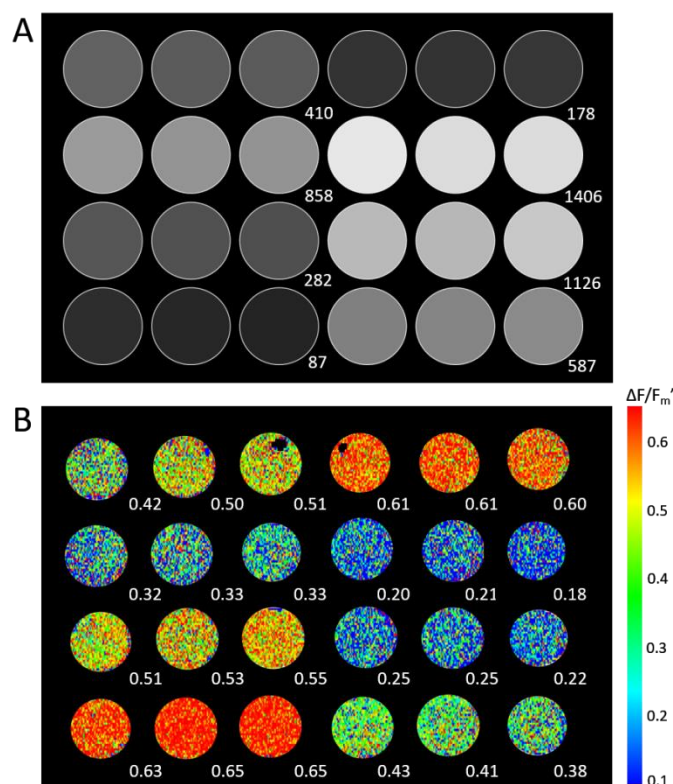


Figure 1. Illustration of the measurement of single-pulse light-response curves (SPLC) of chlorophyll fluorescence on MPB samples. A. Light mask comprising eight areas of actinic light (AAL), and three replicates for each light level ('3 × 8' light mask), designed to fit a well plate containing 24 replicated MPB samples. Numbers indicate the irradiance levels ($\mu\text{mol quanta m}^{-2} \text{s}^{-1}$) applied in each group of three AALs. B. Effective quantum yield of PSII, $\Delta F/F_m'$ (false color scale), as measured for each AAL by applying a single saturating pulse after exposure to the actinic light mask for 120. Numbers indicate the average $\Delta F/F_m'$ values determined for each sample, used for calculating the $rETR$ values plotted in Fig. 2.

Exposure time for reaching steady state

In order to determine the minimum duration of light exposure, necessary to reach a physiological steady state in light curve parameters, sediment samples were treated with the diatom motility inhibitor Latrunculin A (Lat A) to prevent the confounding effects of light-induced vertical migration on the fluorescence response to light. The solution of Lat A (10 μM) was prepared according to Cartaxana and Serôdio (2008). The reaching of a physiological steady state was determined by measuring one SPLC (using the 3 × 8 light mask) at different times (10, 30, 60, 90, 120, 150 and 180 s) following the start of exposure to the actinic light mask. Samples were previously dark acclimated for 2 min. Light curve parameters were estimated for each measuring occasion and their evolution during light exposure was used to determine, for each parameter, the earliest moment that yielded values not statistically different from steady state. Steady-state values were defined as the average value of the measurements that, after a certain time of light exposure, showed no

significant differences from each other. The experiment was also run with samples not treated with Lat A (control), to evaluate the effects of vertical migration.

Light-induced vertical migration

In order to assess the extent of light-induced vertical migration occurring during the period of light exposure required to reach a physiological steady state (determined in the previous experiment), the change in microalgal surface biomass during light exposure was monitored using reflectance-based, physiological-independent biomass index NDVI. Samples were acclimated to darkness and exposed to different light levels as described for the previous experiment. NDVI was measured at 10, 30, 60, 90 and 120 s after the start of light exposure.

Dependence on initial light conditions

To compare the different protocols regarding the influence of initial conditions on the light-response curves, light curves generated using the SPLC method and the conventional sequential protocols used to generate SSLCs or RLCs, were compared on samples acclimated to two contrasting ambient light intensities. Replicated samples were exposed to 50 (low light, LL) and 1000 (high light, HL) $\mu\text{mol quanta m}^{-2} \text{s}^{-1}$ for 15 minutes, in order to induce different photoacclimation states at the start of the measuring of the light-response curves. SPLCs were measured at 10, 30 and 60 s of light mask exposure while sequential RLCs and SSLCs were generated by applying 30 s and 60 s light steps, respectively.

Statistical analysis

Measurements under different treatments were compared by applying Student's *t*-test or one-way ANOVA. Assumptions of normality and homoscedasticity were verified prior to analysis using the Shapiro–Wilk test and Levene's test, respectively. In case of violation of assumptions, data were log transformed. Measurements made on the same samples at different occasions were compared by using repeated measurements ANOVA. When the sphericity assumption was not verified, the Greenhouse & Geiser correction was applied. All statistical analyses were carried out using Statistica 10 (StatSoft Inc., Tulsa, OK, USA).

Assessment

Light curve design: determination of actinic light levels

The light-response curves based on eight light levels and three replicates (using the 3 × 8 light mask; Fig. 1) were very similar to the quasi-continuous response curves obtained by measuring 24 *rETR* values for evenly distributed *E* values. The two curves were virtually identical for irradiances up to ca. 1000 $\mu\text{mol quanta m}^{-2} \text{s}^{-1}$ (Fig. 2). Above this light level, the curves started to diverge, with the quasi-continuous curve showing a tendency for a decrease under the highest irradiances. However, no statistical differences were found between the light curve parameters of the two light response curves, either regarding the light-limited or light-saturated regions of the curve (repeated measurements ANOVA, $F_{1,3} = 2.246$, $P = 0.231$ and $F_{1,3} = 0.028$, $P = 0.877$ for α and $rETR_m$, respectively).

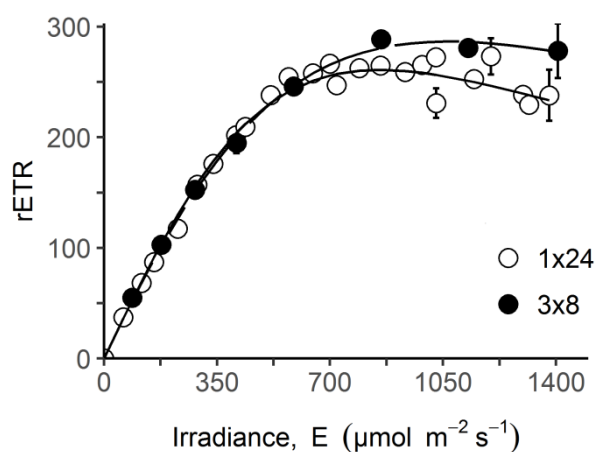


Figure 2. Single-pulse light-response curves of *rETR* as measured on microphytobenthos samples after 120 s of actinic light mask exposure. Comparison of typical quasi-continuous light curve (generated by a light mask with 24 different light levels) and one light curve based on eight light levels (generated by using a 3 × 8 light mask). Lines represent the fit of the Eilers and Peeters (1988) model (Eq. 4). Vertical bars: one standard error.

Exposure time for reaching steady state

Following an initial period of light induction during which light curve parameters varied markedly, a gradual stabilization lead to a steady state which was maintained during the rest of the experiment. During light exposure, the parameter α decreased from 0.77 $\mu\text{mol quanta}^{-1} \text{m}^2 \text{s}$ (10 s of light exposure) until it became not significantly different from the steady-state value (0.62 $\mu\text{mol quanta}^{-1} \text{m}^2 \text{s}$), 120 s upon the start of light exposure (repeated measurements ANOVA, Tukey HSD, MSE = 0.001, P = 0.015) (Fig. 3A).

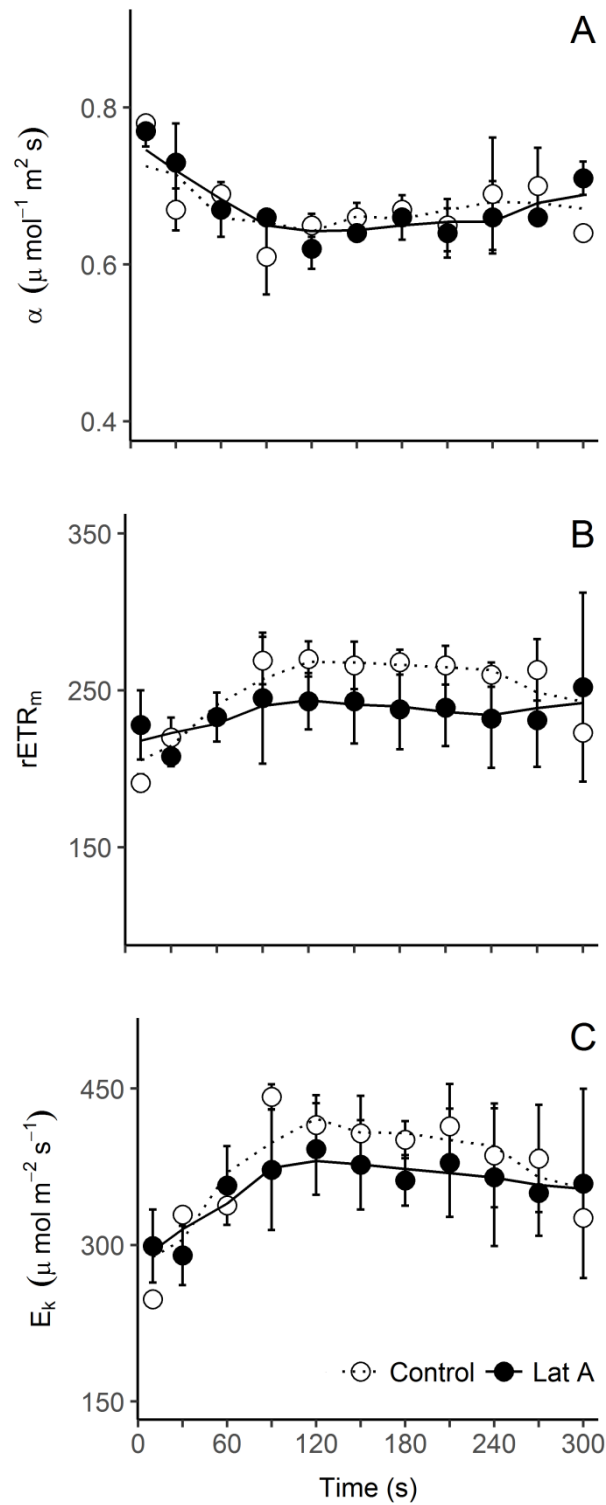


Figure 3. Variation over time of $rETR$ light curve parameters α , $rETR_m$ and E_k upon exposure to actinic light of microphytobenthos samples treated with diatom motility inhibitor Lat A as compared to untreated (control) samples. Lines represent a 3-point moving average of each parameter.

Steady-state values were defined as the average value of the measurements after 120 s (α) or 90 s (ETR_m and E_k) of light exposure. The parameters $rETR_m$ and E_k showed an initial decrease from starting value of 228 and 299 $\mu\text{mol quanta m}^{-2} \text{s}^{-1}$, respectively, rapidly followed by a more gradual increase until reaching steady-state values of 245 to 372 $\mu\text{mol quanta m}^{-2} \text{s}^{-1}$, respectively. Regarding $rETR_m$ (Fig. 3B), no significant changes were detected over the whole period of the experiment (repeated measurements ANOVA, Tukey HSD, MSE = 402.950, $P > 0.697$). Parameter E_k reached values not significantly different from the steady state after 90 s of light exposure (repeated measurements ANOVA, Tukey HSD, MSE = 712.93, $P = 0.012$; Fig. 3C). Variations over time of all light curve parameters were more pronounced in the non-immobilized samples, confirming the importance of vertical migration as a confounding factor for the characterization of the sample photophysiology using fluorescence light-response curves.

Light-induced vertical migration

The migratory response to light exposure was found to be very fast, starting virtually immediately after light exposure (Fig. 4). Even an exposure period as short as 60 s induced a significant decrease in surface biomass (t -test, $t = -2.98$, $df = 14$, $P < 0.01$), for irradiances as low as 87 $\mu\text{mol quanta m}^{-2} \text{s}^{-1}$ (Fig. 4). The change in surface biomass increased with the light level and the time of exposure. However, the changes induced by the tested light intensities and exposure periods were relatively small, with the maximum decrease, observed for the extreme conditions of 1400 $\mu\text{mol quanta m}^{-2} \text{s}^{-1}$ during 120 s, reaching only 22%.

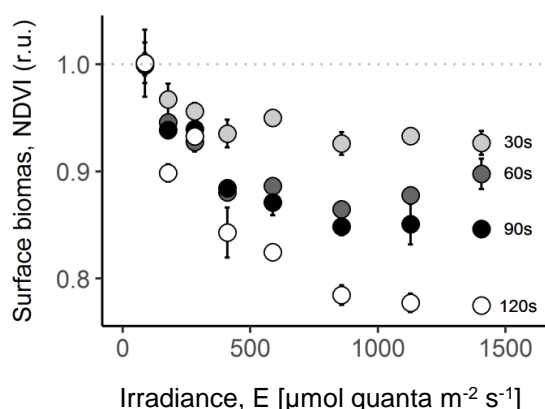


Figure 4. Short-term light-induced changes in microalgal surface biomass under different irradiance levels, as measured by the microalgal biomass reflectance index NDVI (Eq. 3).

Dependence on initial light conditions

Figure 5 summarizes the results of the comparison of the different experimental protocols regarding the effects of initial photoacclimation state on the light curve parameters. Sequential RLCs based on 30 s light steps were strongly affected by the light conditions applied to the samples prior to the start the curve.

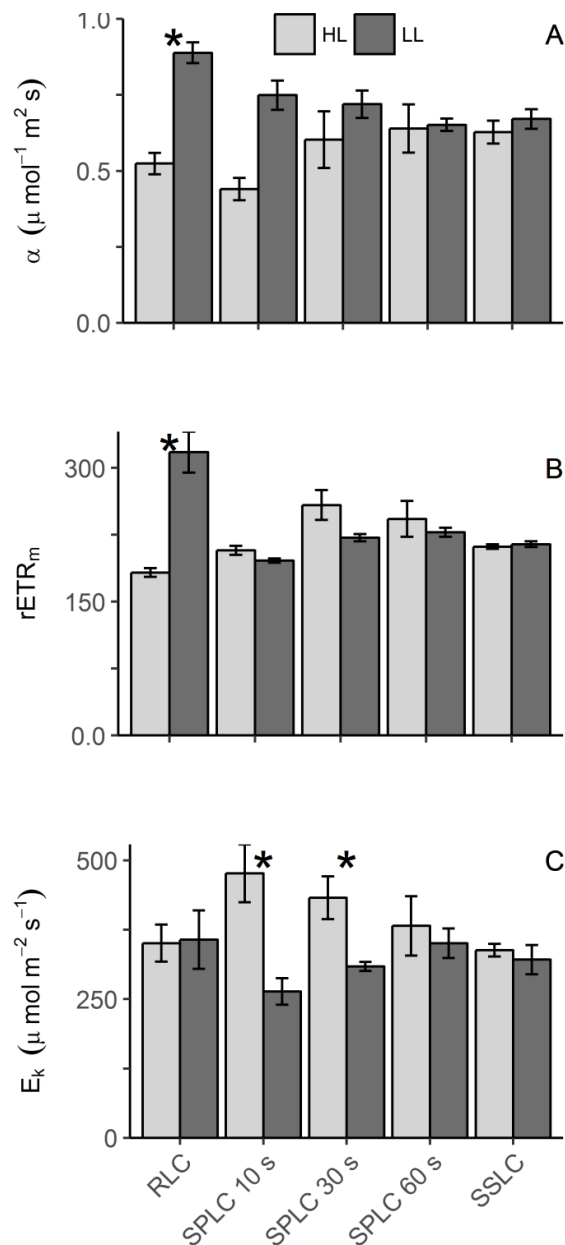


Figure 5. Effects of initial light conditions (LL and HL: 50 and 1000 $\mu\text{mol quanta m}^{-2}\text{s}^{-1}$, respectively) on the parameters of $rETR$ light-response curves α , $rETR_m$ and E_k as measured using different experimental protocols: RLC (10 s light step), SSLC (60 s light step) and SPLC generated after 10, 30 and 60 s of light mask exposure. Mean values of three independent measurements. Vertical bars: one standard error.

Both parameters α and $rETR_m$ were significantly different between samples acclimated to LL and to HL conditions (t -test; α : $t = 9.116$, $df = 4$, $P < 0.001$, $rETR_m$: $t = 3.330$, $df = 4$, $P = 0.029$), reaching significantly higher values for LL-acclimated samples (Fig. 5A,B). Because both α and $rETR_m$ decreased with initial light conditions, E_k did not show significant differences between LL- and HL-acclimated samples (t -test; $t = 0.122$, $df = 4$, $P = 0.909$; Fig. 5C). In contrast, SSLCs were not affected by initial light conditions, as neither of the light parameters varied significantly between LL- and HL-acclimated samples (t -test; α : $t = 1.072$, $df = 4$, $P = 0.344$; $rETR_m$: $t = 0.389$, $df = 4$, $P = 0.717$; E_k : $t = 0.722$, $df = 4$, $P = 0.510$; Fig. 5B). Regarding SPLCs, the results varied with the duration of the light exposure period. For 10 s of light mask exposure, significant differences were found regarding α and E_k (t -test; $t = 6.284$, $df = 4$, $P = 0.003$ and $t = -4.451$, $df = 4$, $P = 0.010$, respectively) but not for $rETR_m$ (t -test; $t = -1.184$, $df = 4$, $P = 0.302$). After 30 s of exposure, both α and $rETR_m$ did not significantly differ between LL- and HL-acclimated samples (t -test; $t = 1.377$, $df = 4$, $P = 0.240$ and $t = 1.234$, $df = 4$, $P = 0.245$, respectively), and only for E_k significant difference were found (t -test, $t = 3.840$, $df = 4$, $P = 0.018$). For a light exposure period of 60 s, the light curves showed no detectable dependency of the initial photoacclimation state, as no significant differences were found for any of the parameters (t -test; $t < 0.638$, $df = 4$, $P > 0.600$ in all cases).

Discussion

A protocol to generate light-response curves that successfully characterize the inherent physiological light response of MPB samples must rely on the tradeoff between the ability to describe the steady-state light response and minimize the main sources of error, identified as the effects on light curve parameters of vertical migration and of initial light acclimation conditions. The results of this study indicate that the non-sequential SPLC protocol represents an advantageous alternative over the conventionally used protocols, based on the sequential exposure of the same sample to various actinic light levels (SSLC and RLC). In essence, the method effectively allows to overcome the main shortcoming of sequential protocols: (i) it provides a close approximation to steady-state light curve parameters in a comparatively short period, which (ii) minimizes the effects of light-induced vertical migration during curve generation, and (iii) eliminates the dependency of short-term photoacclimation prevailing at the start of the measurements.

Approaching steady state while minimizing vertical migration

The evaluation of the SPLC protocol in terms of providing a better tradeoff between estimating steady-state light curve parameters and avoiding the effects of vertical migration was based on the comparison of the kinetics of light curve induction and of downward migration during light activation. The results showed that vertical migration can be induced in timescales shorter than the time required to reach a full steady state in light curve parameters (60 s and 90 s, respectively). This is in agreement with the results of Laviale et al. (2016), who showed for similar samples, that downward vertical migration of benthic diatoms is activated rapidly upon exposure to intensities higher than $250 \mu\text{mol quanta m}^{-2} \text{s}^{-1}$. The results of the present study further confirm that sequential SSLC and even RLC protocols are surely too long to avoid migratory responses capable of causing substantial changes in microalgal biomass and species composition in photic zone of the sediment. In practical terms, this overlapping between the periods required for reaching a full physiological steady state and the induction of vertical migration calls for a compromise between the two processes. In this context, the SPLC protocol appears as particularly advantageous as it is not based on sequential light exposure, that results in the application a long (and often increasing) light stimulus causing cumulative migratory effects. In fact, the presented results showed that an exposure of 60 s represents a satisfactory compromise between approaching the steady state and, while not avoiding completely the occurrence of vertical migration, minimize its effects on the estimation of light curve parameters. Considering the results depicted in Fig. 3, an exposure period of 60 s would underestimate the steady-state light curve parameters by only 6.2% and 6.7% (α ; control and Lat A-treated samples, respectively) and 13.7% and 4.7% (ETR_m ; control and Lat A-treated samples, respectively). To be noted that these results were obtained by exposing the samples to actinic light (various levels of the light mask) after a period of dark acclimation. It may thus be expected that a period shorter than 60 s could be sufficient to reach a steady state if the samples were already light activated. Interestingly, an earlier study on light response curves of microphytobenthos biofilms of different origin concluded that a similar light exposure period (50 s) was required to reach a steady state (Herlory et al. 2007).

Independency of initial conditions

While the SPLC method was shown to effectively allow estimating steady-state light curve parameters with minimum interference from vertical migration, the question remained of how the new method deals with the effects of short-term photoacclimation to the light

conditions prior to the start of the curve. This is of importance if the method is to be applicable on samples exposed to variable light conditions, and their photophysiological state is to be assessed independently of the ambient light conditions. The comparison of the SPLC approach with commonly used protocols for sequential LC (RLCs of 10-30 s and SSLCs of 60 s light steps) confirmed that it is largely independent from initial light conditions. Because SSLC protocols are based on light steps long enough to allow the dissipation of initial short-term photoacclimation state, they allow reaching steady state conditions, and to reveal the inherent photoresponse of the samples (Perkins et al. 2006; Herlory et al. 2007; Cruz and Serôdio 2008; Ihnken et al. 2010; Lefebvre et al. 2011). However, even a relatively short light step of 60 s corresponds to a total period of several minutes of light exposure during the curve construction (8 min if a total 8 light steps), which is expected to cause very large migratory effects.

On the other hand, RLCs were confirmed to be largely dependent on initial light conditions. Due to the short light steps, the short-term photoacclimation established prior to the start of the measurements is not attenuated and prevails during the generation of the curve. The influence of initial light conditions is expected to be especially evident during the first steps of the light curve, affecting more the parameter α than $rETR_m$ (Serôdio et al. 2006b). RLCs may appear preferable because of their expected smaller dependency on vertical migration, but the results of this study indicate that migratory effects may still occur in a significant way. This is because a light step of 30 s corresponds to a total exposure to light of 4 min (if 8 light steps) during the generation of the curve, a period of time expected to result in a substantial migratory response (Laviale et al. 2016).

It is important to note that the conditions tested in these experiments were conservative. The effects of initial light conditions on RLC parameters would likely be much larger if a light step shorter than 30 s had been used. In fact, most studies on benthic microalgae were based on RLCs use protocols use light steps of just 10 s (e.g., McMinn et al. 2005; Serôdio et al. 2005; 2008; Yun et al. 2010; Lefebvre et al. 2011; Du et al. 2012). Also, the differences between RLCs and SSLCs would likely be larger if the later had been carried out applying light steps longer than 60 s, as it is the case of works targeting SSLCs using 2 (Barranguet and Kromkamp 2000) or 3 min (Underwood et al. 2005).

Additional advantages

Besides being a better approach for describing the steady-state photoresponse of MPB samples than the SSLC and RLC protocols, the SPLC method offers some additional advantages. First, in contrast with the often used sequential SSLC and RLC protocols, SPLCs yield truly independent measurements, because each fluorescence measurement originates from a single sample, exposed to only one light level. This has the immediate value of eliminating cumulative light effects, either on sample physiology or species composition in the photic zone. In this regard, SPLCs share the advantages of previously used non-sequential approaches (e.g. Perkins et al. 2006; Lavaud et al. 2007). A second important advantage regards the short time required to complete a light curve. Besides the obvious value of reducing the time required for completing light curves, the method allows to minimize the intrusiveness of the measurements, reducing the effects of light curve generation on the physiology and migratory state of the samples. In turn, this permits to obtain a better time resolution of the measurements, which is especially important in the context of fast changing environmental conditions, sample composition or physiological state, which is characteristic of the intertidal environment and of MPB samples. For example, it makes it easier to study various biofilm samples during the same low tide periods and further allows increasing the level of replication, reducing the error and improving the ability to detect effects.

Another type of benefit of the SPLC approach concerns the flexibility offered in terms of 'light curve design', that is, the possibility of easily and freely adjusting the range and distribution of irradiance levels used for the construction of the light curves. This permits to optimize the description of the light response by adjusting the number and distribution of light levels as a function of the expected change in $rETR$ (or other fluorescence response), e.g., by concentrating data collection in the ranges of irradiances for which $rETR$ is expected to vary more steeply. In this context, the use of an automatic, synoptic light measurement system as the one developed for this study is highly advantageous. The potential of this approach was exemplified in the experiment of Figure 2, in which case the various E levels were determined based on the linear distance between $rETR$ values along the expected light curve. A further use of this approach could be to allocate more measurements in the high end of the light range, to compensate for the increased error in measuring $rETR$ (larger error for measuring smaller values $\Delta F/F_m'$, aggravated by multiplying by larger E values).

Comments and recommendations

This study was centered on the optimization of the measurement of light-response curves of *rETR*. Nevertheless, the method here described can be readily used for the generation of light curves of other fluorescence indices, as the index NPQ (Serôdio et al. 2013). Light-response curves of NPQ are informative on processes associated to photoprotection and photoinhibition, and are often used complementarily to *rETR* vs *E* curves in the characterization of the photophysiology of the photosynthetic organisms (Serôdio and Lavaud 2011). While in principle experiments like those here presented could be carried out for optimizing NPQ vs *E* curves, it must be noted that the measurement of NPQ in MPB samples dominated by motile microalgae is problematic, because this index is strongly affected by vertical migration. The calculation of the NPQ index depends on the absolute values of F_m and F_m' , measured at different points in time, which are directly affected by the rapid changes in microalgal surface biomass occurring during the generation of the curve (Cartaxana and Serôdio 2008).

The method here presented can also be extended to integrate the collection of physiological-independent data on microalgal surface biomass, by measurements of spectral reflectance images (Laviale et al. 2016). Measurements of reflectance-based NDVI index can be carried out in combination with light-response curves of fluorescence, allowing to obtain an integrated response to light of the biofilm, both in terms of photophysiology and migratory behavior.

The results presented in this study were based on homogenized sediment samples, to make it easier to compare the new method with the conventional sequential protocols. However, although this procedure may reduce the variability between replicated samples and favor the application of the method, it is not a requirement of the SPLC approach. SPLCs can be generated using a set of undisturbed (not homogenized) replicated sediment samples, in order to preserve the natural vertical structure and the natural microspatial patchiness of the biofilms. Alternatively, the light mask can be projected directly on a single continuous sediment surface without the need to disrupt the natural biofilm, as has been shown for plant leaves (Serôdio et al. 2013). The only restriction in the later approach is that the AALs have to be sufficiently separated from each other to avoid significant light spillover between adjacent ones.

This work resulted in the recommendation of experimental settings (light levels, time of exposure) that optimize the generation of *rETR* vs *E* curves. However, these settings were determined for the MPB biofilms tested in this study alone and may not be the best for

other samples, as the optimum settings vary with biofilm characteristics such as its inherent light curve parameters and migratory ability. For example, biofilms dominated by mostly non-migratory epipsamic species may allow for longer exposure periods, yielding light curves that better describe the physiological steady state. The procedures here described can nevertheless be followed for optimizing the method to be applied to different types of biofilms.

Acknowledgements

This work was supported by the FCT – Fundação para a Ciência e a Tecnologia, through grant SFRH/BD/86788/2012 (S. Frankenbach) and project MigROS (PTDC/MAR/112473/2009). The authors thank Ivo Mateus and Miguel Rocha for technical assistance on the multi-actinic setup, Gregor Christa for help with R programming and William Schmidt for assistance in field work. We thank three anonymous reviewers for critical comments on the manuscript.

References

- Barranguet, C., and J. Kromkamp. 2000. Estimating primary production rates from photosynthetic electron transport in estuarine microphytobenthos. *Mar. Ecol. Prog. Ser.* 204: 39–52.
- Cartaxana, P., and J. Serôdio. 2008. Inhibiting diatom motility: a new tool for the study of the photophysiology of intertidal microphytobenthic biofilms. *Limnol. Oceanogr. Methods* 6: 466–476.
- Chevalier, E. M., F. Gévaert, and A. Créach. 2010. In situ photosynthetic activity and xanthophylls cycle development of undisturbed microphytobenthos in an intertidal mudflat. *J. Exp. Mar. Bio. Ecol.* 385: 44–49.
- Cohn, S. A., D. Halpin, N. Hawley, A. Ismail, Z. Kaplan, T. Kordes, J. Kuhn, W. Macke, K. Marhaver, B. Ness, S. Olszewski, A. Pike, E. Rice, J. Sbarboro, A. Wolske, and Y. Zapata. 2015. Comparative analysis of light-stimulated motility responses in three diatom species. *Diatom Res.* 30: 213–225.
- Cruz, S., and J. Serôdio. 2008. Relationship of rapid light curves of variable fluorescence to photoacclimation and non-photochemical quenching in a benthic diatom. *Aquat. Bot.* 88: 256–264.
- Du, G. Y., W. T. Li, H. Li, and I. K. Chung. 2012. Migratory responses of benthic diatoms to light and temperature monitored by chlorophyll fluorescence. *J. Plant Biol.* 55: 159–164.
- Eilers, P. H. C., and J. C. H. Peeters. 1988. A model for the relationship between light intensity and the rate of photosynthesis in phytoplankton. *Ecol. Modell.* 42: 199–215.
- Ezequiel, J., M. Laviale, S. Frankenbach, P. Cartaxana, and J. Serôdio. 2015. Photoacclimation state determines the photobehaviour of motile microalgae: The case of a benthic diatom. *J. Exp. Mar. Bio. Ecol.* 468: 11–20.
- Forster, R. M., and J. C. Kromkamp. 2004. Modelling the effects of chlorophyll fluorescence from subsurface layers on photosynthetic efficiency measurements in microphytobenthic algae. *Mar. Ecol. Prog. Ser.* 284: 9–22.
- Frankenbach, S., C. Pais, M. Martinez, M. Laviale, J. Ezequiel, and J. Serôdio. 2014. Evidence for gravitactic behaviour in benthic diatoms. *Eur. J. Phycol.* 49: 429–435.
- Henley, W. J. 1993. Measurement and interpretation of photosynthetic light-response curves in algae in the context of photoinhibition and diel changes. *J. Phycol.* 29: 729–739.

- Herlory, O., P. Richard, and G. F. Blanchard. 2007. Methodology of light response curves: application of chlorophyll fluorescence to microphytobenthic biofilms. *Mar. Biol.* 153: 91–101.
- Ihnken, S., A. Eggert, and J. Beardall. 2010. Exposure times in rapid light curves affect photosynthetic parameters in algae. *Aquat. Bot.* 93: 185–194.
- Jesus, B., C. R. Mendes, V. Brotas, and D. M. Paterson. 2006a. Effect of sediment type on microphytobenthos vertical distribution: modelling the productive biomass and improving ground truth measurements. *J. Exp. Mar. Bio. Ecol.* 332: 60–74.
- Jesus, B., R. G. Perkins, M. Consalvey, V. Brotas, and D. M. Paterson. 2006b. Effects of vertical migrations by benthic microalgae on fluorescence measurements of photophysiology. *Mar. Ecol. Prog. Ser.* 315: 55–66.
- Jones, C. T., S. E. Craig, A. B. Barnett, H. L. Macintyre, and J. J. Cullen. 2014. Curvature in models of the photosynthesis-irradiance response. *J. Phycol.* 50: 341–355.
- Kelly, J. A., C. Honeywill, and D. M. Paterson. 2001. Microscale analysis of chlorophyll-a in cohesive, intertidal sediments: the implications of microphytobenthos distribution. *J. Mar. Biol. Assoc. United Kingdom* 81: 151–162.
- Kromkamp, J., C. Barranguet, and J. Peene. 1998. Determination of microphytobenthos PSII quantum yield efficiency and photosynthetic activity by means of variable chlorophyll fluorescence. *Mar. Ecol. Prog. Ser.* 162: 45–55.
- Lavaud, J., R. F. Strzepek, and P. G. Kroth. 2007. Photoprotection capacity differs among diatoms: Possible consequences on the spatial distribution of diatoms related to fluctuations in the underwater light climate. *Limnol. Oceanogr.* 52: 1188–1194.
- Laviale, M., Frankenbach, S., Serôdio, J., (2016). The importance of being fast: comparative kinetics of vertical migration and non-photochemical quenching of benthic diatoms under light stress. *Mar. Biol.* 163, 1–12.
- Lavaud, J. 2015. Response of intertidal benthic microalgal biofilms to a coupled light-temperature stress: evidence for latitudinal adaptation along the Atlantic coast of Southern Europe. *Environ. Microbiol.* 17: 3662–3677.
- Lefebvre, S., J.-L. Mouget, and J. Lavaud. 2011. Duration of rapid light curves for determining the photosynthetic activity of microphytobenthos biofilm in situ. *Aquat. Bot.* 95: 1–8.
- MacIntyre, H. L., T. M. Kana, T. Anning, and R. J. Geider. 2002. Photoacclimation of photosynthesis irradiance response curves and photosynthetic pigments in microalgae and cyanobacteria. *J. Phycol.* 38: 17–38.

- Mclachlan, D. H., C. Brownlee, A. R. Taylor, R. J. Geider, and G. J. C. Underwood. 2009. Light-induced motile responses of the estuarine benthic diatoms *Navicula perminuta* and *Cylindrotheca closterium* (Bacillariophyceae). *J. Phycol.* 45: 592–599.
- McMinn, A., S. Sellah, W. a. W. A. Llah, M. Mohammad, F. M. S. Merican, W. M. W. Omar, F. Samad, W. Cheah, I. Idris, Y. K. Sim, W. S. Wong, S. H. Tan, and Z. Yasin. 2005. Quantum yield of the marine benthic microflora of near-shore coastal Penang, Malaysia. *Mar. Freshw. Res.* 56: 1047–1053.
- Morris, E. P., R. M. Forster, J. C. Kromkamp, and J. Peene. 2008. Coupling between Photosystem II electron transport and carbon fixation in microphytobenthos. *Aquat. Microb. Ecol.* 50: 301–311.
- Mouget, J., R. Perkins, M. Consalvey, and S. Lefebvre. 2008. Migration or photoacclimation to prevent high irradiance and UV-B damage in marine microphytobenthic communities. *Aquat. Microb. Ecol.* 52: 223–232.
- Nitschke, U., S. Connan, and D. B. Stengel. 2012. Chlorophyll a fluorescence responses of temperate Phaeophyceae under submersion and emersion regimes: a comparison of rapid and steady-state light curves. *Photosynth. Res.* 114: 29–42.
- Perkins, R. G., J. C. Kromkamp, and R. P. Reid. 2007. Importance of light and oxygen for photochemical reactivation in photosynthetic stromatolite communities after natural sand burial. *Mar. Ecol. Prog. Ser.* 349: 23–32.
- Perkins, R. G., J. C. Kromkamp, J. Serôdio, J. Lavaud, B. Jesus, J. L. Mouget, S. Lefebvre, and R. M. Forster. 2010. Chlorophyll a Fluorescence in Aquatic Sciences: Methods and Applications, D.J. Suggett, O. Prášil, and M.A. Borowitzka [eds.]. Springer Netherlands.
- Perkins, R. G., J. L. Mouget, S. Lefebvre, and J. Lavaud. 2006. Light response curve methodology and possible implications in the application of chlorophyll fluorescence to benthic diatoms. *Mar. Biol.* 149: 703–712.
- Perkins, R. G., G. J. C. Underwood, V. Brotas, G. C. Snow, B. Jesus, and L. Ribeiro. 2001. Responses of microphytobenthos to light: primary production and carbohydrate allocation over an emersion period. *Mar. Ecol. Prog. Ser.* 223: 101–112.
- Ralph, P. J., and R. Gademann. 2005. Rapid light curves: a powerful tool to assess photosynthetic activity. *Aquat. Bot.* 82: 222–237.
- Rouse, J., R. Haas, J. Schell, and D. Deering. 1973. Monitoring vegetation systems in the great plains with ERTS, p. 309–317. In *Third Earth Resources Technology Satellite Symposium*, NASA SP-351. NASA.

- Schreiber, U., R. Gademann, P. J. Ralph, and A. W. D. Larkum. 1997. Assessment of photosynthetic performance of *Prochloron* in *Lissoclinum patella* in hospite by chlorophyll fluorescence measurements. 38: 945–951.
- Schreiber, U., U. Schliwa, and W. Bilger. 1986. Continuous recording of photochemical and nonphotochemical chlorophyll fluorescence quenching with a new type of modulation fluorometer. *Photosynth. Res.* 10: 51–62.
- Serôdio, J. 2004. Analysis of variable chlorophyll fluorescence in microphytobenthos assemblages: implications of the use of depth-integrated measurements. *Aquat. Microb. Ecol.* 36: 137–152.
- Serôdio, J., H. Coelho, S. Vieira, and S. Cruz. 2006a. Microphytobenthos vertical migratory photoresponse as characterised by light-response curves of surface biomass. *Estuar. Coast. Shelf Sci.* 68: 547–556.
- Serôdio, J., J. Ezequiel, J. Frommlet, M. Laviale, and J. Lavaud. 2013. A method for the rapid generation of nonsequential light-response curves of chlorophyll fluorescence. *Plant Physiol.* 163: 1089–102.
- Serôdio, J., and J. Lavaud. 2011. A model for describing the light response of the nonphotochemical quenching of chlorophyll fluorescence. *Photosynth. Res.* 108: 61–76.
- Serôdio, J., J. Marques da Silva, and F. Catarino. 2001. Use of in vivo chlorophyll a fluorescence to quantify short-term variations in the productive biomass of intertidal microphytobenthos. *Mar. Ecol. Prog. Ser.* 218: 45–61.
- Serôdio, J., Vieira S., and F. Barroso. 2007. Relationship of variable chlorophyll fluorescence indices to photosynthetic rates in microphytobenthos. *Aquat. Microb. Ecol.* 49: 71–85.
- Serôdio, J., Vieira S., and S. Cruz. 2008. Photosynthetic activity, photoprotection and photoinhibition in intertidal microphytobenthos as studied in situ using variable chlorophyll fluorescence. *Cont. Shelf Res.* 28: 1363–1375.
- Serôdio, J., Vieira, S., Cruz S. and F. Barroso. 2005. Short-term variability in the photosynthetic activity of microphytobenthos as detected by measuring rapid light curves using variable fluorescence. *Mar. Biol.* 146: 903–914.
- Serôdio, J., Vieira, S., Cruz S., and H. Coelho. 2006b. Rapid light-response curves of chlorophyll fluorescence in microalgae: relationship to steady-state light curves and non-photochemical quenching in benthic diatom-dominated assemblages. *Photosynth. Res.* 90: 29–43.

- Ubertini, M., S. Lefebvre, C. Rakotomalala, and F. Orvain. 2015. Impact of sediment grain-size and biofilm age on epipellic microphytobenthos resuspension. *J. Exp. Mar. Bio. Ecol.* 467: 52–64.
- Underwood, G. J. C., R. G. Perkins, M. C. Consalvey, A. R. M. Hanlon, K. Oxborough, N. R. Baker, and D. M. Paterson. 2005. Patterns in microphytobenthic primary productivity: Species-specific variation in migratory rhythms and photosynthetic efficiency in mixed-species biofilms. *Limnol. Oceanogr.* 50: 755–767.
- Waring, J., N. R. Baker, and G. J. C. Underwood. 2007. Responses of estuarine intertidal microphytobenthic algal assemblages to enhanced ultraviolet B radiation. *Glob. Chang. Biol.* 13: 1398–1413.
- White, A. J., and C. Critchley. 1999. Rapid light curves: A new fluorescence method to assess the state of the photosynthetic apparatus. *Photosynth. Res.* 59: 63–72.
- Yun, M. S., S. H. Lee, and I. K. Chung. 2010. Photosynthetic activity of benthic diatoms in response to different temperatures. *J. Appl. Phycol.* 22: 559–562.

Chapter 3

PHOTOINACTIVATION, REPAIR AND THE MOTILITY–PHYSIOLOGY TRADE-OFF IN MICROPHYTOBENTHOS

Published:

Frankenbach S., Schmidt W., Frommlet J.C., Serôdio J. (2018). Photoinactivation, repair and the motility-physiology trade-off in microphytobenthos. *Marine Ecology Progress Series*, 601, 41-57.

DOI: 10.3354/meps12670

Key index words

Microphytobenthos, Diatoms, Photoinactivation, Photoprotection, Repair, Vertical migration, Photoinhibition

Abstract

Microphytobenthos (MPB) inhabiting intertidal flats of estuaries form highly productive diatom-dominated biofilms. The capacity to sustain such high photosynthetic activity under conditions prone to cause photoinhibition is thought to be enabled by efficient photoprotective mechanisms, the main ones being the xanthophyll cycle (XC) and vertical migration (VM). This study compared the photoprotective capacity of two MPB communities inhabiting contrasting sedimentary habitats and relying on distinct light responses: epipelagic communities, colonizing muddy sediments and using motility (VM) to regulate light exposure; and epipsammic communities, inhabiting sandier sediments and relying solely on physiological photoprotection (XC). The efficiency of physiological photoprotection of the two communities was compared regarding Photosystem II (PSII) photoinactivation caused by light stress. Lincomycin was used to distinguish photoinactivation from counteracting repair. Rate constants of PSII photoinactivation (k_{PI}) and repair (k_{REC}) were determined on cell suspensions, based on the light and time dependence of maximum quantum yield of PSII, F_v/F_m , as measured using multi-actinic imaging fluorometry. The results show that motile species, in comparison to epipsammic ones, are inherently more susceptible to photoinactivation (higher k_{PI}), less dependent on the XC for preventing photodamage (smaller increase of k_{PI} induced by nigericin) and more efficient regarding repair capacity (higher k_{REC}). The distinct strategies exhibited by epipelagic and epipsammic communities to cope with light stress support the hypothesized trade-off between photoprotective motility and photophysiology. Motile forms have a diminished physiological capacity for preventing photodamage and compensate using VM and a better repair capacity. Non-motile epipsammic forms rely mostly on physiological mechanisms to optimize photoprotection capacity.

Introduction

Photoprotection against photoinhibition has long been considered crucial for microphytobenthos (MPB) (Admiraal 1984, Kromkamp et al. 1998, Serôdio et al. 2001). These diatom-dominated communities inhabit intertidal and shallow subtidal sedimentary habitats of estuaries and coastal zones, characterized by highly dynamic and extreme abiotic conditions (Serôdio & Catarino 1999, Brotas et al. 2003, Chevalier et al. 2010). These include exposure to fluctuating solar irradiance during prolonged periods (Perkins et al. 2001, Laviale et al. 2015), extreme (high or low) temperature and salinity (Guarini et al. 1997, Serôdio et al. 2008), and nutrient and carbon limitation (Cook & Røy 2006, Vieira et al. 2016). Each of these factors and, more so, their combined effects are prone to cause a decrease in photosynthetic activity due to the photoinactivation of Photosystem II (PSII). Nevertheless, MPB sustain dense biofilms with high photosynthetic activity, and MPB primary productivity is ranked among the highest in marine and estuarine ecosystems, matching or exceeding that of phytoplankton (Underwood & Kromkamp 1999).

The high productivity of MPB under extreme conditions has been thought to be enabled by particularly effective photoprotective mechanisms, allowing them to safely optimize the balance between light exposure and dissipation of excess absorbed light energy (Serôdio et al. 2012). In this context, the motility of benthic diatoms has long been considered to have an important photoprotective value. According to the 'behavioral photoprotection' hypothesis, the ability to vertically migrate within the photic zone of the sediment, covering a large range of light conditions in a short time, could enable motile diatoms to regulate light exposure and optimize photosynthesis while avoiding photodamaging irradiances (Admiraal 1984, Underwood et al. 1999, Consalvey et al. 2004). The photoregulatory nature of vertical migration is supported by increasing experimental evidence: (1) diatom motility is regulated by light intensity (Cohn et al. 2004, 2015, Serôdio et al. 2006, McLachlan et al. 2009); (2) biofilms treated with a motility inhibitor show a marked decrease in photosynthetic activity (Perkins et al. 2010, Serôdio et al. 2012); (3) high light-induced negative phototaxis is associated with susceptibility to photodamage (Ezequiel et al. 2015); and (4) light-induced migration is fast, occurring on time scales comparable to the activation of physiological photoprotection mechanisms (Laviale et al. 2016, Frankenbach & Serôdio 2017, Blommaert et al. 2018).

Motility-based photoprotection could operate complementarily to the physiological processes common to other photoautotrophs, the most important of which is considered to be the thermal dissipation of excessive light energy through the xanthophyll cycle (XC). In

diatoms, the XC relies on the enzyme-mediated, reversible conversion of the PSII antenna pigment diadinoxanthin (DDx) into the energy-dissipation form diatoxanthin (DTx), which depends on the presence of a transthylakoidal proton gradient and on specific LHCx proteins (Blommaert et al. 2017, Lepetit et al. 2017). Compared to higher plants (Ruban et al. 2004), the XC of diatoms was found to operate in a particularly efficient way, especially in coastal and estuarine species (Lavaud 2007). The XC-related de-excitation of the antennae is often quantified by measuring the non-photochemical quenching (NPQ) of chlorophyll fluorescence (Müller et al. 2001, Ruban 2016). Because NPQ comprises several mechanisms of regulated energy dissipation in the PSII antenna, this fluorescence index has been widely used as a measure of photoprotective capacity of MPB (Jesus et al. 2006, Lavaud et al. 2007, Juneau et al. 2015).

A corollary of the ‘behavioral photoprotection’ hypothesis is the existence of a trade-off between motility-based and physiological photoprotective mechanisms: having the possibility to adjust light exposure behaviorally, motile species would rely less on physiological photoprotective processes, thus showing a decreased inherent photoprotective capacity (Serôdio et al. 2001, Barnett et al. 2015, Laviale et al. 2016). The replacement of the physiological photoprotection (at least partially) by motility is supported by the recent finding that high light-induced vertical migration is fast enough to allow the systematic avoidance of exposure to high light (Laviale et al. 2016, Frankenbach & Serôdio 2017), thus avoiding the development of a large physiological photoprotective capacity (Lavaud et al. 2007, Serôdio & Lavaud 2011, Barnett et al. 2015, Blommaert et al. 2018).

The relative importance of behavioral and physiological protection in MPB has been debated extensively in recent years (Serôdio et al. 2001, Van Leeuwe et al. 2008, Mouget et al. 2008, Pniewski et al. 2015, Barnett et al. 2015, Blommaert et al. 2017). This question has been often addressed by comparing 2 types of benthic diatom assemblages, taxonomically closely related and occurring virtually sympatrically (e.g. same tidal flat of the same estuary), but differing markedly regarding motility: the epipelon (EPL), formed by raphid motile species, dominant in fine sediments; and the epipsammon (EPM), composed predominantly of non-motile growth forms, common in coarser sediments, where they live in close association with sediment particles (Jesus et al. 2009, Cartaxana et al. 2011, Barnett et al. 2015, Juneau et al. 2015). The evidence gathered from the comparative study of EPL and EPM species appears to confirm the motility–physiology trade-off hypothesis, in the sense that motile forms tend to show a lower capacity for physiological photoprotection, either by having smaller cellular pools of energy-dissipating pigment DTx (Van Leeuwe et al. 2008, Jesus et al. 2009, Cartaxana et al. 2011, Pniewski et al. 2015) or

by attaining lower maximum NPQ levels than their non-motile equivalents (Barnett et al. 2015, Blommaert et al. 2017, 2018, Pniewski et al. 2017).

The study of the photoprotective role of vertical migration and NPQ, and the trade-off between motility and physiological processes, has been based almost exclusively on the assessment of 'photoinhibition', defined in terms of net photoinactivation, that is, the decrease in photosynthetic activity resulting from the balance between PSII photoinactivation and photorepair, without distinguishing their counteracting effects (e.g. Serôdio et al. 2012, Laviale et al. 2015). However, the evaluation of the actual photoprotective capacity provided by a certain process (e.g. vertical migration) is better attained by quantifying its effect in terms of the induced decrease of the susceptibility to photodamage (Serôdio et al. 2017). This in turn requires the separate quantification of the operation of PSII photoinactivation and repair processes, which can be adequately achieved by measuring the rate constants of inactivation and repair (k_{PI} and k_{REC} , respectively) and their responses to irradiance level (k_{PI} and k_{REC} versus E curves) (Murata et al. 2012, Campbell & Tyystjärvi 2012, Miyata et al. 2012).

This study addresses the comparative study of the inherent physiological photoprotection capacity of EPL and EPM diatom communities, directly testing the motility–physiology trade-off hypothesis based on actual PSII photoinactivation. The rate constant of photoinactivation, k_{PI} , and its variation with irradiance level, were used as a measure of the efficiency of photoprotection processes, testing the hypothesis that EPL species (when not using vertical migration) show a lower physiological photoprotection capacity, being more susceptible to photoinactivation (higher k_{PI}) than their EPM counterparts (lower k_{PI}). The study further intended to (1) test if the hypothesized lower inherent photoprotective capacity of motile species is compensated by a higher capacity for repair, (2) evaluate the effective photoprotective impact of XC-associated NPQ, and (3) characterize the relationship between NPQ and k_{PI} , evaluating the value of the NPQ index as a measure of photoprotection capacity.

Photoinactivation and repair processes were quantified in combination with the assessment of photoacclimation state and potential physiological photoprotection capacity, as conventionally measured by NPQ, taking advantage of a recently developed experimental approach allowing the high-throughput and integrated characterization of light responses and kinetics of photosynthetic samples (multi-actinic imaging fluorometry; Serôdio et al. 2017). The method is based on the combined use of imaging chlorophyll fluorometry and the simultaneous exposure of replicated samples to multiple actinic light levels and periods of exposure, allowing the rapid measurement of the induction and

relaxation kinetics and of the light response of relative PSII electron transport rate ($rETR$; characterizing photoacclimation state) and NPQ (related to processes mediating photoprotection), and of the rate constants k_{PI} and k_{REC} .

Materials and methods

Sampling and sample preparation

Sediment samples were collected on two intertidal flats of the Ria de Aveiro, a mesotidal estuary located off the west coast of Portugal. The sampling sites were selected for their different distinctive characteristics regarding sediment granulometry and diatom species composition. Site Vista Alegre (40° 37' 12" N, 08° 44' 54" W) is composed of fine muddy sediments (97% particles < 63 μm) and is expected to be dominated by EPL species, and will therefore be referred to as VA-EPL. Site Gafanha da Encarnação (40° 35' 18" N, 08° 41' 06" W) is composed of sandy mud (45.3% particles between 63 and 125 μm and 42.7% particles < 63 μm) and is expected to be dominated by EPM species, and will therefore be referred to as GE-EPM. The tidal height of the two sampling sites is similar (ca. 2.3 m relative to hydrographic zero), with a mean duration of low tide (i.e. sediment exposure) of ca. 8 h 30 min (Serôdio et al. 2007). Sampling was carried out during August 2016, on three consecutive days for each site, when low tide took place during the middle of the day. The top 1 cm layer of the sediment was collected using a spatula and then transported to the laboratory, where it was sieved (1 mm mesh) and thoroughly mixed. The sediment was transferred into plastic trays to form a layer of 3–4 cm thick slurry and was maintained overnight immersed in natural seawater collected at the sampling site. The following day, before the start of the low-tide period, the overlying water was carefully removed, and cells were collected using the 'lens tissue' technique (Eaton & Moss 1966). Two layers of lens tissue (Lens cleaning tissue 105, Whatman) were placed on the surface of the sediment exposed to low white light (halogen lamps, 50 $\mu\text{mol quanta m}^{-2} \text{s}^{-1}$) to induce upward migration of motile cells. After ca. 2 h, the upper piece of lens tissue was removed and microalgae were resuspended in filtered natural seawater, producing the cell suspensions used in the experiments.

Photoacclimation state and photoprotection capacity

The photoacclimation state and the potential photoprotection capacity of the samples was characterized by measuring light-response curves and induction kinetics of relative electron transport rate of PSII ($rETR$) and NPQ, respectively (see Notation). $rETR$ was determined by measuring chlorophyll fluorescence parameters F_s and F_m' on samples exposed to irradiance level E (Genty et al. 1989):

$$rETR = E \frac{F_m' - F_s}{F_m'} \quad (1)$$

Because F_m' values measured under low light in MPB samples may be higher than the F_m value measured after dark-adaptation, NPQ was calculated using the adapted NPQ index, based on the relative difference between the maximum fluorescence level measured during the construction of the light- response or induction curves, $F_{m'm}$, and the level measured upon exposure to light, F_m' (Serôdio et al. 2008):

$$NPQ = \frac{F_{m'm} - F_m'}{F_m'} \quad (2)$$

The light-response curves of $rETR$ and NPQ were described by fitting the models of Eilers & Peeters (1988) and Serôdio & Lavaud (2011), respectively. $rETR$ versus E curves were described by model parameters α (the initial slope of the curve), $rETR_m$ (maximum $rETR$) and E_k (the light-saturation parameter). NPQ versus E curves were described by model parameters NPQ_m (maximum NPQ), E_{50} (E corresponding to 50% of NPQ_m) and n (sigmoidicity parameter). Models were fitted and model parameters were estimated by iteratively minimizing a least-squares function, forward differencing, and the default quasi-Newton search method, using a procedure written in MS Visual Basic and based on MS Excel Solver.

Photoinactivation and repair

The rate constants of PSII photoinactivation and repair, k_{PI} and k_{REC} , were measured in the dark following exposure to actinic light. Rates were calculated under the assumptions that (1) the pool of functional PSII can be estimated by the maximum PSII quantum yield, calculated as $F_v/F_m = (F_m - F_0)/F_m$, (2) PSII photoinactivation and repair occur concurrently and can be described as two opposite first-order reactions, and (3) at the beginning of light

exposure all PSII photosystems are functional (Kok 1956, Ni et al. 2017). In this case, the variation of net photoinactivation over time of exposure can be described by:

$$A(E, T) = \frac{k_{REC}(E) + k_{PI}(E) e^{-(k_{PI}(E) + k_{REC}(E))T}}{k_{PI}(E) + k_{REC}(E)} \quad (3)$$

where A is the fraction of functional PSII, measured by the ratio of the $F_v/F_m(E, T)$ values measured after exposure to actinic light level E during a period T , and the initial, pre-stress F_v/F_m values (Campbell & Tyystjärvi 2012). $F_v/F_m(E, T)$ values were measured after 15 min of recovery in darkness. This time period has been used for MPB samples before, as it allows for the relaxation of the XC-associated NPQ (qE), while preventing the build-up of significant sustained NPQ during prolonged darkness (Serôdio et al. 2012). The rate constants k_{PI} and k_{REC} were quantified for each E level as described by Campbell & Tyystjärvi (2012). k_{PI} was measured on samples treated with lincomycin (2 mM; lincomycin hydrochloride, Alfa Aesar; added in the dark 30 min before the start of the experiment), an inhibitor of the de novo synthesis of chloroplast-encoded proteins such as D1, by fitting the simplified form of Eq. (3) (setting $k_{REC} = 0$) to the time series of $A(E, T)$:

$$A(E, T) = e^{-k_{PI}(E)T} \quad (4)$$

k_{REC} was estimated by fitting Eq. (3) to the time series of A values measured in untreated samples and using the corresponding $k_{PI}(E)$ estimates.

The relative quantum yield of photoinactivation, ϕ_{PI} , was determined from the slope of linear regression equation of k_{PI} against irradiance level E (Hakala et al. 2005):

$$\phi_{PI} = \frac{k_{PI}(E)}{E} \quad (5)$$

Because ϕ_{PI} measures directly the susceptibility to inactivation per incident photon, by integrating the effects of all protective mechanisms in operation, it is used in this study as an indicator of the global effectiveness of photoprotection.

In order to evaluate the contribution of XC-related NPQ, rate constants k_{PI} and k_{REC} (and their response to light: ϕ_{PI} and k_{REC} versus E curve) were also measured in samples treated with nigericin (2.67 μ M; nigericin sodium salt, Sigma-Aldrich), an uncoupler that relaxes the transthylakoidal ΔpH by antiporting H^+ and K^+ , thus preventing the induction of the XC and related NPQ (Antal et al. 2011). On lincomycin-treated samples, pH was adjusted to 7.9 ± 0.1 , using 1 M NaOH. Sodium bicarbonate ($NaHCO_3$, 4 mM, Sigma-Aldrich) was added to all samples before each experiment.

Multi-actinic imaging of chlorophyll fluorescence

All described fluorescence parameters and indices used to characterize the photoacclimation state, photoprotection capacity, photoinactivation and repair were measured in a single experiment, by applying the multi-actinic imaging fluorometry protocol described by Serôdio et al. (2017). This approach is based on the combined use of a digital light projector, as source of actinic light, and an imaging chlorophyll fluorescence system, allowing for the simultaneous measurement of the response of a large number of samples subjected to different combinations of light intensity (E) and exposure duration (T). Actinic light was provided by an LCD digital projector (EB-X14; Seiko Epson), comprising one mercury arc lamp providing a maximum light output of 3000 lm. A 'light mask' consisting of a set of 64 circular, spatially separated areas of actinic light (AAL), arranged in an 8 × 8 matrix, was projected on a custom-made 3D-printed 64-well plate containing the samples (Serôdio et al. 2017), so that each AAL covered the whole surface of each sample. The light masks were designed in Microsoft PowerPoint, using a code written in Microsoft Visual Basic defining the number, position, size, shape, light intensity and spectrum (R:G:B ratios) of each individual AAL (Serôdio et al. 2013). The light spectrum was kept constant across light intensities by adjusting the RGB code for each intensity (Frankenbach & Serôdio 2017). Incident PAR irradiance was measured using a calibrated flat PAR sensor (mini quantum sensor LS-C and ULM-500 unit; Heinz Walz) at a distance from the light source that corresponded to the sample surface (bottom of the wells). The imaging fluorometer was a FluorCAM 800MF (Photon System Instruments, PSI), comprising a computer-operated control unit (SN- FC800-082, PSI) and a CCD camera (CCD381, PSI) with an f1.2 (2.8–6 mm) objective (Eneo). Four 13 × 13 cm LED panels emitting red light (emission peak at 621 nm, 40 nm bandwidth) provided modulated measuring light ($< 0.1 \mu\text{mol quanta m}^{-2} \text{s}^{-1}$) and saturating pulses ($> 7000 \mu\text{mol quanta m}^{-2} \text{s}^{-1}$, 0.8 s).

The experiments consisted of 3 phases. An initial period of 30 min of dark acclimation allowed cells to settle in the 64-well plates (working sample volume of 200 μL), after which reference values of F_v/F_m were measured. This was followed by an induction phase of exposure to actinic light, during which light- response curves and induction kinetics were measured by applying saturating pulses every 3.75 min; the samples were arranged in a square 8 × 8 matrix, in which each row corresponded to one of 8 actinic light levels (37, 135, 231, 352, 506, 692, 873 and 1120 $\mu\text{mol quanta m}^{-2} \text{s}^{-1}$), and each column corresponded to one of 8 light exposure periods (T ; 3.75 to 30 min). During the final recovery phase, samples were returned simultaneously to darkness and F_v/F_m was measured after

15 min to allow relaxation of XC- related NPQ. Because each experiment yielded only one estimate of k_{PI} and k_{REC} per E level, experiments were run three times on independent samples collected in each sampling date.

Image analysis and determination of fluorescence parameters

Images (512×512 pixels, 695–780 nm spectral range) of chlorophyll fluorescence parameters F_o , F_m (measured during dark-acclimation) or F_s and F_m' (measured during induction), were captured and processed using the FluorCam7 software (Photon Systems Instruments). For each measurement, 64 'areas of interest' (AOI) were designed as slightly smaller than the corresponding AAL, to avoid misinterpretation due to border effects, having on average 186 pixels (5.8 mm diameter). The fluorescence parameters were measured by averaging all pixel values in each AOI, and by averaging the fluorescence intensity during the 2 s immediately before the saturating pulse (F_o , F_s) and during 0.8 s (F_m , F_m') exposure to the saturating pulse. Fluorescence images were captured at regular time intervals using an AutoHotKey script (www.autohotkey.com), written to automatically run the FluorCam7 protocol used for applying saturating pulses.

Chlorophyll a concentration

Chlorophyll *a* concentration of the suspensions was determined according to Lorenzen (1967). A 2 mL volume of the cell suspension was centrifuged and suspended in cold 90% acetone. Extraction was carried out overnight at 4°C. Samples were centrifuged ($10000 \times g$, 15 min), and the absorbance of the supernatant was measured spectrophotometrically (Spectronic Genesys 6 UV/VIS, Thermo Scientific) at 664 and 750 nm before and after addition of 10% HCl.

Taxonomic composition

Sub-samples of the cell suspensions were fixed in 1% v/v in Lugol's solution (5% Iodine, AppliChem) and viewed under a bright-field microscope for determination of the relative abundance of major taxonomic groups (diatoms, euglenophytes and cyanobacteria). Diatom identification was performed on sub-samples oxidized using concentrated nitric acid (1/4 v/v) and potassium permanganate. Permanent microscopy slides of the frustules were mounted using a high refractive index medium (Naphrax; Northern Biological Supplies). Composition of samples was determined by counting a

minimum of 300 cells or valves on three replicated sub-samples, using a counting chamber (Neubauer-improved, Marienfeld). Diatom identification was based on Round et al. (1990), Ribeiro (2010), and Coste & Rosebery (2011).

Statistical analyses

Measurements under different treatments or times were compared by applying Student's t-test or one-way ANOVA. Assumptions of normality and homoscedasticity were verified prior to analysis using the Shapiro-Wilk test and Levene's test, respectively. In case of violation of assumptions, data were log transformed. Regression equations (slope and intercept) were compared by applying analysis of covariance (ANCOVA). All statistical analyses were carried out using Statistica 10 (StatSoft).

Results

Sample taxonomic composition and chlorophyll content

The biofilms collected at the muddy site (VA-EPL) almost exclusively comprised diatoms (relative abundance 99.5%), being dominated by EPL forms of the genera *Stauroneis* (31%), *Navicula* (24%) and *Craticula* (23%), followed by the less abundant genera *Gyrosigma* (5.7%), *Nitzschia* (3.6%), *Amphora* (2.2%), *Paralibellus* (1.1%), *Achnanthes* (0.8%), *Gomphora* (0.6%), *Suriella* (0.4%) and *Diploneis* (0.2%). The biofilms of the sandy mud site (GE-EPM) had a lower relative abundance of diatoms (82% of total cell counts), and a higher occurrence of euglenophytes (13%) and cyanobacteria (0.2%). The diatom community was more diverse and dominated by EPM species of the genera *Navicula* (30%), *Amphora* (18%), *Achnanthes* (17%) and *Paralibellus* (14%), followed by *Gomphonema* (6.2%) and *Nitzschia* (5.8%). Least abundant were *Pinnularia* (1.2%), *Suriella* (1.1%), *Stauroneis* (1.0%), *Gomphocymbella* (0.9%), *Planothidium* (0.8%), *Cymbella* (0.7%), *Cylindrotheca* (0.5%), *Cocconeis* (0.3%), *Fallacia* (0.1%), *Plagiotropis* (0.1%) and *Ophera* (0.1%). The chlorophyll *a* content of VA-EPL and GE-EPM suspensions used in the experiments averaged 8.4 ± 0.5 and $2.2 \pm 0.6 \mu\text{g mL}^{-1}$, respectively.

Photoacclimation state and photoprotection capacity

The cell suspensions collected from the two habitats responded differently to increasing light intensity (Fig. 1). The samples from VA-EPL, dominated by EPL diatoms, showed a marked decrease in F_m' with increasing irradiance, down to less than 50% of the F_m' value for the maximum applied irradiance ($E = 1120 \mu\text{mol quanta m}^{-2} \text{s}^{-1}$) (Fig. 1A). For some samples, an increase of F_m' under low light ($E < 210 \mu\text{mol quanta m}^{-2} \text{s}^{-1}$) was noticeable, reaching values above F_m , denoting the dissipation of NPQ formed in the dark (data not shown). In contrast, F_s increased slightly under intermediate irradiances, reaching maximum values for $E = 327 \mu\text{mol quanta m}^{-2} \text{s}^{-1}$, then decreasing to a minor extent (ca. 15%) under higher light levels, an indication of little limitation of photochemistry under high irradiance (Fig. 1A). Both F_m' and F_s remained relatively stable over time after 5–15 min of light exposure.

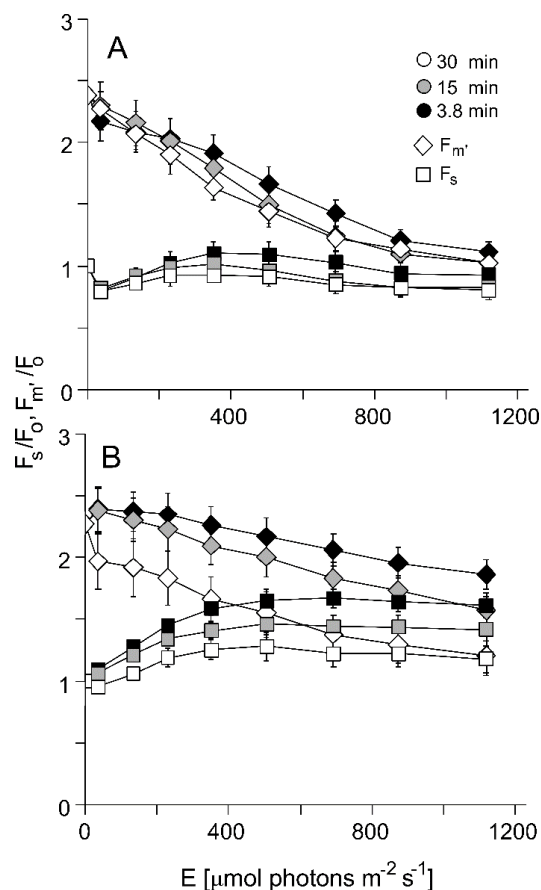


Figure 1. Variation over time of light-response curves of fluorescence parameters F_s and F_m' (normalized to F_0) for samples collected at VA-EPL (A) and GE-EPM (B) sampling sites. Light curves measured at 3.75, 15 and 30 min after the start of light exposure. Data points are mean values of 9 replicated measurements. Error bars represent ± 1 standard error.

In contrast with the VA-EPL samples, the suspensions from the sandy mud site (GE-EPM) showed a smaller decrease of F_m' with increasing irradiance (only ca. 20%; Fig. 1B) during the first periods of light exposure, an indication of a more limited capacity for NPQ induction. Additionally, the light response of F_m' changed markedly over time, with F_m' values continuously decreasing after 7.5 min of light exposure (Fig. 1B). F_m' always decreased monotonically with E and there were no observations of $F_m' > F_m$, reflecting the absence of dark-induced NPQ. Also, in contrast with VA-EPL, F_s increased markedly and continuously with irradiance, reaching values up to 160% of F_o for $E = 506 \mu\text{mol quanta m}^{-2} \text{s}^{-1}$, after which point it remained relatively stable. The large increase of F_s with irradiance was gradually attenuated over time (from 167% of F_o at 3.75 min to only 115% of F_o after 26.25 min of light exposure; Fig. 1B), denoting a limited sink capacity for electrons under high light.

The samples from VA-EPL and GE-EPM also differed substantially regarding the light-response curves of $rETR$ and NPQ (Fig. 2). In the case of VA-EPL, $rETR$ versus E curves were characterized by higher $rETR_m$ values and by not showing saturation under the range of applied irradiances, resulting in relatively high values of α and $rETR_m$ at steady-state and consequently high values of the photoacclimation parameter E_k ($E_k = 416 \mu\text{mol quanta m}^{-2} \text{s}^{-1}$) (Fig. 2A). In contrast, light-response curves of $rETR$ of GE-EPM samples showed a clear saturation, resulting in lower values of light curve parameters ($E_k = 283 \mu\text{mol quanta m}^{-2} \text{s}^{-1}$) (Fig. 2B). In both cases, the $rETR$ versus E curves did not change significantly during the exposure period and a steady state was reached within 30 min, although for the VA-EPL samples the $rETR$ values varied more pronouncedly during the first 15 min of exposure (Fig. 2).

Concerning NPQ, VA-EPL and GE-EPM samples differed regarding the maximum values reached and the variation of the NPQ light response over time. For VA-EPL suspensions, NPQ increased with irradiance almost linearly, not reaching saturation under the applied irradiance levels (Fig. 3A). However, the NPQ light-response curves did not change substantially after 15 min of light exposure (Fig. 3C), suggesting that NPQ induction was fast and reached a steady state during the first minutes of light exposure. At steady-state, NPQ values measured under the highest E level reached around 1.2 while NPQ_m and E_{50} reached 2.7 and $1210 \mu\text{mol quanta m}^{-2} \text{s}^{-1}$, respectively. In contrast, GE-EPM samples reached lower maximum NPQ values (NPQ for the highest $E < 0.6$), although they continued to increase steadily during the whole period of light exposure, not showing signs of saturation.

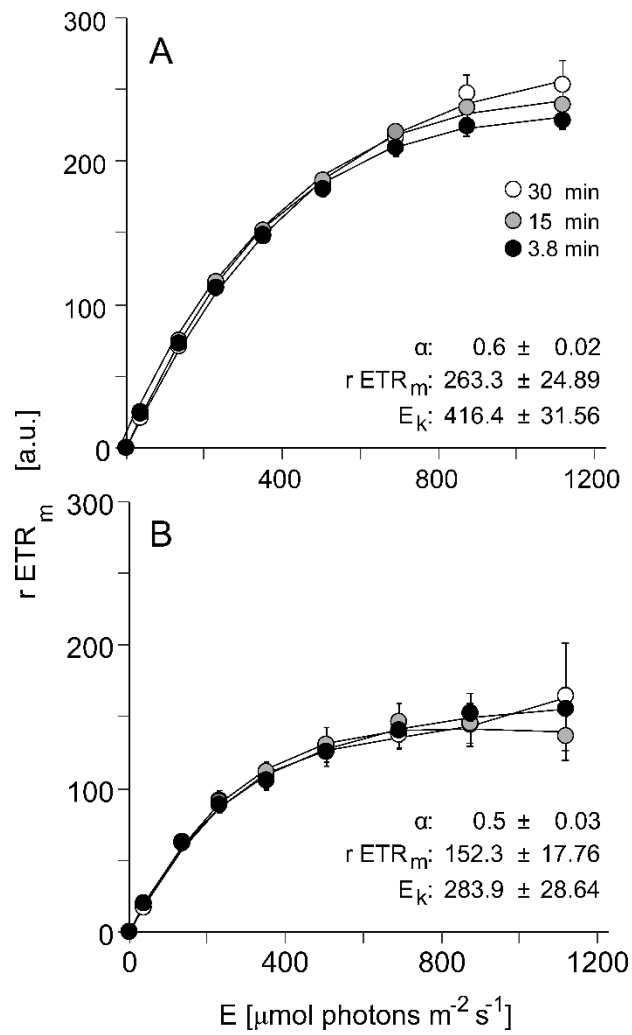


Figure 2. Variation over time of light-response curves of relative electron transport rate at PSII (*rETR*) for samples collected at VA-EPL (A) and GE-EPM (B) sampling sites. Light curves measured at 3.75, 15 and 30 min after the start of light exposure. Data points are mean values of 9 independent measurements. Error bars represent ± 1 standard error. Lines represent the model of Eilers & Peeters (1988) fitted to mean values at each time. Model parameters (α , $rETR_m$ and E_k) at the end of light exposure (30 min).

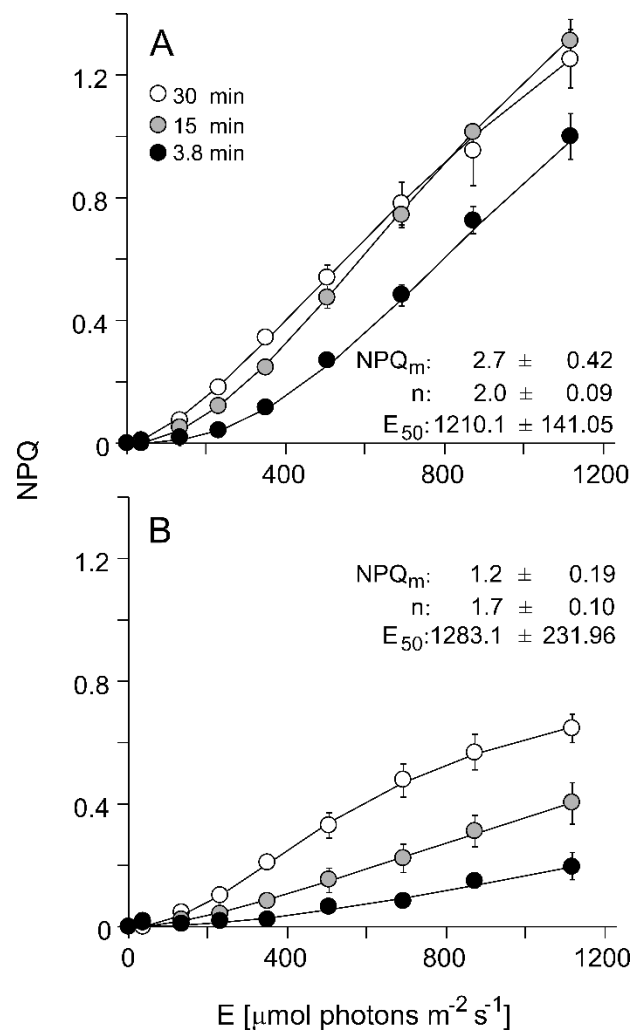


Figure 3. Variation over time of light-response curves of non-photochemical quenching (NPQ) for samples collected at VA-EPL (A) and GE-EPM (B) sampling sites. Light curves measured at 3.75, 15 and 30 min after the start of light exposure. Data points are mean values of 9 independent measurements. Error bars represent ± 1 standard error. Lines represent the model of Serôdio & Lavaud (2011) fitted to mean values at each time. Model parameters (NPQ_m , n and E_{50}) at the end of light exposure (30 min).

Photoinactivation and repair

Fig. 4 illustrates the results obtained when measuring rate constants of photoinactivation and repair for a range of irradiance levels. These results refer to a single set of experiments carried out in a single day for each sampling site but are representative of all results. A striking feature of these results is that, in the case of VA-EPL samples exposed to low and intermediate light levels, A values did not decrease over time as expected but showed a transient increase to values above 1 during the first 10–20 min. Such an increase in F_v/F_m is compatible with the dissipation of NPQ formed in the dark prior to light exposure, and made it impractical to fit Eq. (3) and estimate k_{REC} for most of the light

levels applied ($E < 704 \mu\text{mol quanta m}^{-2} \text{s}^{-1}$). In GE-EPM samples, A did not increase over time as for VA-EPL, but remained relatively constant for the lower light levels. As a result, Eq. (3) could only be fitted, and k_{REC} estimated, for $E > 349 \mu\text{mol quanta m}^{-2} \text{s}^{-1}$ (Fig. 4B). Under high light levels, A reached lower values for the VA-EPL samples (0.75–0.8, for $E = 1120 \mu\text{mol quanta m}^{-2} \text{s}^{-1}$) than for the GE-EPM samples (> 0.9 for the same E), indicating a larger, slowly reversible component of NPQ.

On samples treated with lincomycin (L and L+N), A followed a well-defined negative exponential decay over time for most light levels, the rate of decay increasing with applied irradiance (Fig. 4, L, L+N). The same light- and time-response pattern was observed for VA-EPL and GE-EPM samples, although the rates of decrease were, for comparable E levels, noticeably lower for GE-EPM. In the case of GE-EPM samples, the fit of Eq. (4) resulted in the estimation of $k_{PI} = 0$ for several of the lowest light levels ($E < 349 \mu\text{mol quanta m}^{-2} \text{s}^{-1}$) (Fig. 4B, L). Higher k_{PI} values were measured for VA-EPL samples, reaching up to $3.01 \pm 0.15 \times 10^{-4} \text{s}^{-1}$, while for GE-EPM, maximum values reached only $1.10 \pm 0.18 \times 10^{-4} \text{s}^{-1}$ (average of all measurements). For both types of samples, the addition of nigericin caused an increase of the rate of decay of F_v/F_m . For VA-EPL samples, the addition of nigericin resulted in the complete elimination of the transient increase of A , possibly associated with the NPQ formed in the dark that was observed in the controls and in lincomycin-treated samples (Fig. 4A, L+N).

The availability of k_{PI} estimates for a wide range of irradiances allowed us to quantitatively describe its light response and to estimate the relative quantum yield of photoinactivation, ϕ_{PI} . k_{PI} was found to increase linearly with E for both sampling sites and applied inhibitors (lincomycin and lincomycin + nigericin), as highly significant linear regressions were found in all cases ($p < 0.05$) (Fig. 5). In the case of VA-EPL samples treated with lincomycin, the absence of k_{PI} values for low light levels resulted in a positive x-intercept (y-intercept significantly different from zero; t-test, $t = -4.30$, $df = 6$, $p = 0.007$; Fig. 5). The slopes of the k_{PI} versus E linear regressions for lincomycin-treated samples, direct estimates of ϕ_{PI} , were significantly higher for VA-EPL than for GE-EPM ($\phi_{PI} = 3.25 \times 10^{-7}$ and $1.27 \times 10^{-7} \text{m}^2 \mu\text{mol quanta}^{-1}$ for VA-EPL and GE-EPM, respectively; ANCOVA, $F_{1,8} = 110.3$, $p < 0.001$). The addition of nigericin caused an increase of ϕ_{PI} in both types of samples, but had a smaller effect in samples from VA-EPL than in those from GE-EPM (16.2% and 47.1%, respectively; Fig. 5). This increase was significant at the 5% significance level for both types of samples (ANCOVA, $F_{1,11} = 8.5$, $p = 0.014$ and $F_{1,6} = 8.4$, $p = 0.027$ for VA-EPL and GE-EPM, respectively).

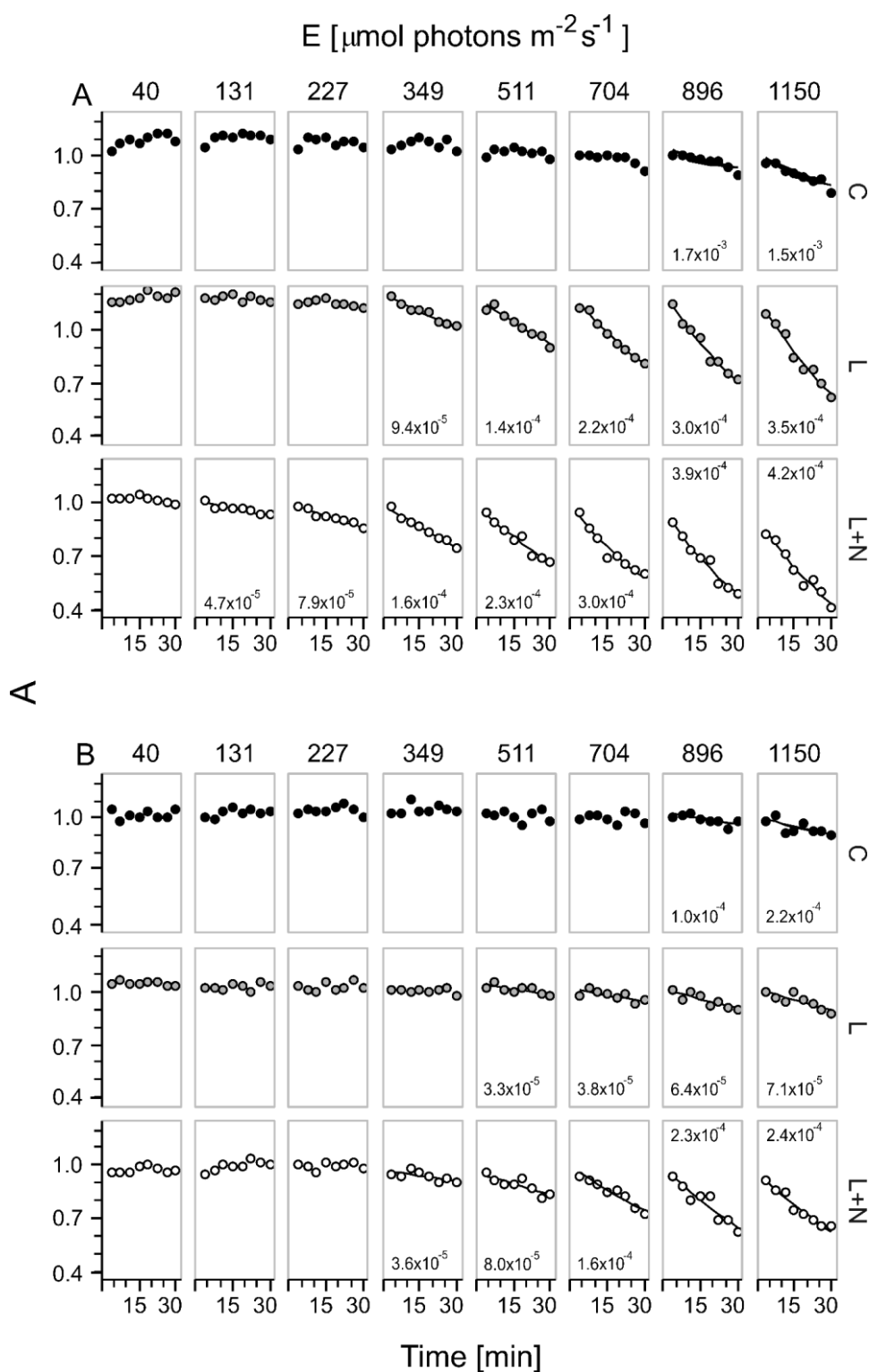


Figure 4. Example of the variation with time of exposure of the fraction of functional PSII (A) under different irradiance levels (numbers at the top), for controls (C), samples treated with lincomycin (L) and samples treated with lincomycin and nigericin (L+N). Results for samples collected at VA-EPL (A) and GE-EPM (B) (8 And 10 August 2016, respectively). Lines represent fitted models (Eqs. 3 and 4 for controls and lincomycin-treated samples, respectively) and numbers are the estimated rate constants (k_{REC} and k_{PI} for controls and lincomycin-treated samples, respectively).

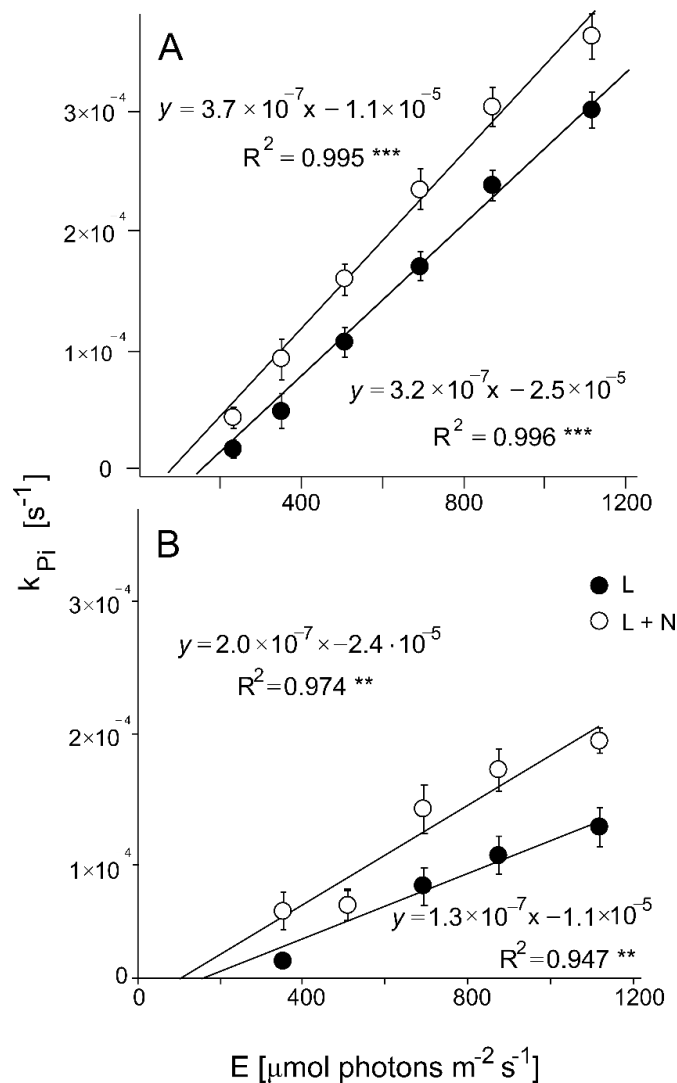


Figure 5. Variation of the rate constants of photoinactivation (k_{Pi}) with irradiance (E), as measured on samples treated with lincomycin (L) and with lincomycin and nigericin (L+N), for samples collected at VA-EPL (A) and GE-EPM (B). Lines represent linear regression equations fitted to k_{Pi} values. Data points are mean values of 9 replicated measurements. Error bars represent ± 1 standard error.

The relative importance of photoinactivation and repair processes can be assessed by comparing the rate constants and k_{Pi} and k_{REC} . However, due to the lack of k_{REC} measurements for most of the E levels, the two rate constants were compared based on the values measured under the highest irradiance level alone ($E = 1120 \mu\text{mol quanta } m^{-2} s^{-1}$) (Fig. 6). Repair rates were significantly higher for VA-EPL than for GE-EPM (17.1 and $2.4 \times 10^{-4} s^{-1}$, respectively; t-test, $t = 5.36$, $df = 14$, $p < 0.001$). More importantly, repair rates were considerably higher for VA-EPL than for GE-EPM when compared to the

corresponding k_{PI} measurements, with the ratio k_{REC}/k_{PI} reaching 5.0 for VA-EPL but only 1.9 for GE-EPM samples.

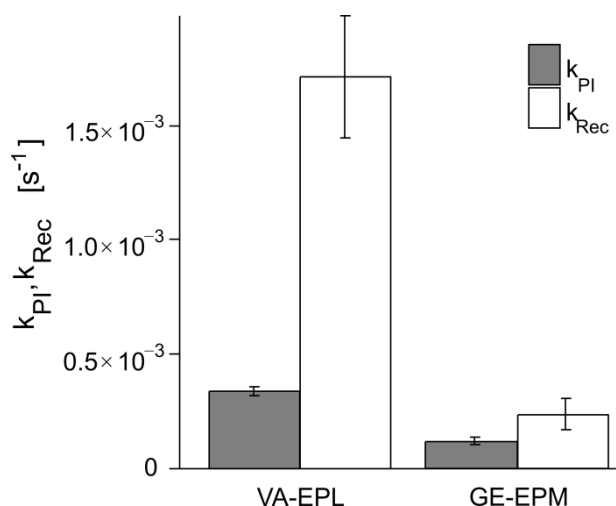


Figure 6. Rate constants of photoinactivation (k_{PI}) and repair (k_{REC}) measured for the highest irradiance applied at each experiment ($1120 \mu\text{mol quanta m}^{-2} \text{s}^{-1}$), for samples collected at VA-EPL and GE-EPM. Data points are mean values of 9 replicated measurements. Error bars represent ± 1 standard error.

Discussion

Light response and induction kinetics of *rETR* and NPQ

The study of the motility–physiology trade-off hypothesis has been mostly based on the comparison of photophysiological properties related to photoprotection capacity of EPL and EPM species or communities. The observation of higher NPQ values (from light-response curves or light stress-recovery kinetics), larger XC pigment pools and depoxidation ratios in natural EPM assemblages (Van Leeuwe et al. 2008, Jesus et al. 2009, Pniewski et al. 2015), and non-motile species (Barnett et al. 2015, Juneau et al. 2015, Blommaert et al. 2017, 2018) has been interpreted as denoting a higher physiological photoprotective capacity to compensate for the lack of motility.

In what regards NPQ, the results of the present study seem to contradict this pattern. The EPL-dominated suspensions (VA-EPL) attained higher NPQ levels and greater rates of formation upon light exposure than the EPM-dominated suspensions (GE-EPM), which can be seen as an indication of a lower capacity of the non-motile cells to withstand the exposure to excess light. However, this apparent contradiction with the motility–physiology

trade-off can be explained by the relatively small light doses applied in this study (maximum irradiance and exposure times lower than in most other studies), which may have prevented the observation of the full development of NPQ and limit the comparison between the EPL- and EPM-dominated samples. In fact, the results suggest that longer exposures could allow a different overall conclusion because, while for the VA-EPL samples NPQ remained constant at all light levels after the quick initial induction, the NPQ of GE-EPM samples continued to increase during the entire period of light exposure, making it likely that higher NPQ levels would be reached if longer incubations were applied.

Another explanation for the observed results is the possibility of latitudinal adaptation, as most of the cited studies were carried out at higher latitudes than the present study, and NPQ has been shown to be higher for MPB communities from higher latitudes (Laviale et al. 2015). However, the results of Jesus et al. (2009), showing higher XC pigment pool for EPM communities at lower latitudes, and of Pniewski et al. (2017, 2018), showing lower NPQ values for EPL communities at higher latitudes, do not support this hypothesis.

It must be mentioned that higher NPQ levels for EPL communities in comparison with EPM ones have also been reported by Pniewski et al. (2017, 2018). However, these studies compared MPB communities from rather distant and different habitats, factors that may have contributed to the observed differences.

These results are nevertheless ecophysiologicaly significant, informing on how the two types of communities deal with high light. EPL species seem capable of a fast activation of NPQ, presumably through the operation of the XC, but a limit in NPQ development, as its maximum is reached within only a few minutes. Thus, while the measured NPQ levels may be higher than for EPM samples (for the applied exposure times), EPL assemblages may in fact have a more limited protection capacity (Fig. 6). Motile cells might use NPQ to quickly respond to fast increases in irradiance, relying on vertical migration to adjust light exposure once the NPQ capacity is reached. In contrast, EPM species do not rely as much on a fast NPQ induction but are capable of maintaining a sustained increase of NPQ levels during long exposure periods. The continued increase of NPQ is consistent with the *de novo* synthesis of XC pigments, and in fact EPM species have also been shown to have a higher capacity for *de novo* synthesis than EPL species (Blommaert et al. 2017, 2018). This strategy is compatible with the idea that EPM cells, being limited in their capacity to regulate light exposure through vertical migration, rely on an enhanced photoprotective physiological processes to minimize the cumulative damaging effects of prolonged exposure to excess light.

EPL and EPM assemblages also differed regarding the light response and induction kinetics of $rETR$. The light-response curves measured in VA-EPL and GE-EPM suspensions were typical of samples photoacclimated to high and low light, respectively, with the former attaining higher α and $rETR_m$, and resulting higher values of the photoacclimation parameter E_k . The high- and low-light photoacclimation responses were also noticeable when analyzing the light response of the fluorescence parameters F_s and F_m' , which indicated that VA-EPL samples were not as photochemically limited and had a larger electron sink capacity under high irradiances than the EPM equivalents. These results may seem unexpected considering the sedimentary light environment of the two sites and the motility of respective dominant species (Serôdio et al. 2007): the higher light attenuation and the steeper light gradients of the muddy site VA-EPL could be expected to favor low-light-acclimated cells, especially if they are able to move away from high light; in contrast, the deeper penetration of light in the GE-EPM sediment and consequent exposure of cells with limited motility to higher light levels would favor the acclimation to high light. Nonetheless, high- and low-light acclimation of EPL and EPM natural assemblages or species, respectively, have been consistently reported (Cartaxana et al. 2011, Barnett et al. 2015, Juneau et al. 2015, Pniewski et al. 2017, 2018)

We hypothesize that the high-light acclimation pattern of EPL species results from the use of motility to search for relatively high light levels within the steep vertical light gradient of muddy sediments. While avoiding accumulation at the surface under very high light levels, a negative phototactic response demonstrated experimentally (Cohn et al. 2004, 2015, Serôdio et al. 2006, Du et al. 2012, Laviale et al. 2016), motile cells could accumulate at sub-surficial layers, being exposed to relatively high light levels, maximizing the use of available light and optimizing photosynthetic carbon fixation and growth. Acclimation to high light allows higher light-saturated photosynthetic rates, supporting higher growth rates, and improves dissipating excitation pressure within PSII through photochemistry, being of clear photoprotective value (Niyogi 1999, Ralph et al. 1999, Gévaert et al. 2003). It also permits the generation of ATP, which is of importance to support the energy-expensive removal of D1 from photoinactivated PSII and subsequent PSII repair (Allakhverdiev et al. 2005, Campbell et al. 2013), found to be particularly efficient in EPL-dominated samples (see below).

The clear differences between the two types of samples were observed despite the well-known selectivity of the 'lens tissue' sampling method for motile cells (Yang et al. 2010). The main potential consequence of this bias is the underrepresentation of non-motile EPM

species in the GE-EPM samples, which could have led to an underestimation of the real differences between the two types of communities.

Susceptibility to photoinactivation

The observed difference between the rate constants of photoinactivation, and their light response, of VA-EPL and GE-EPM samples indicates that epipellic and epipsammic assemblages differ significantly regarding their susceptibility to photoinactivation. Epipellic-dominated samples showed, for comparable irradiances, consistently higher values of k_{PI} , supporting that motile species are inherently (i.e. when impeded from migrating, as in a suspension) more susceptible to photoinactivation than non-motile ones. The linearity between k_{PI} and E , indicative of a reciprocity between the damaging effects of light intensity and time of exposure (Tyystjärvi & Aro 1996, Kou et al. 2012), allows using the slope of the regression of k_{PI} on E , ϕ_{PI} , as a measurement the actual susceptibility to inactivation per incident photon. ϕ_{PI} depends only on the applied light dose, and can thus be used to directly compare results of experiments based on different experimental conditions (light intensity and exposure duration).

The finding of higher values of ϕ_{PI} for epipellic cells than for epipsammic ones supports the postulated existence of a trade-off between photoprotective motility and photophysiology. In comparison to nonmotile species, motile forms appear as having a diminished physiological capacity for minimizing photodamage, which under natural conditions (in the sedimentary microenvironment) could be compensated by migrating vertically across the photic zone of the sediment. Epipsammic species, on the other hand, not being able to behaviorally regulate light exposure and absorption, use physiological mechanisms providing an enhanced global photoprotection capacity.

The ϕ_{PI} values measured in the present study are within the range of published values for natural diatom assemblages, which vary from $1.1 \times 10^{-7} \mu\text{mol quanta}^{-1} \text{m}^2$ for epipellic MPB (Cartaxana et al. 2013) to $3.8 \times 10^{-7} \mu\text{mol quanta}^{-1} \text{m}^2$ for sea ice diatom-dominated samples (Petrou et al. 2010). The former value is the only measurement available for benthic diatoms, and was estimated from the published value of the relative decrease in D1 protein content following light exposure, assuming a negative exponential decay with light dose. The fact that this value is lower than what was observed in the present study for epipellic samples, in spite of the fact that a larger light dose was applied ($1500 \mu\text{mol quanta}^{-1} \text{m}^2$, 60 min), may be explained by the larger error expected from a single endpoint, or by the fact that the published estimate was based on D1 protein content, known to be less

sensitive than fluorescence-based indicators, and that do not always correlate directly with F_v/F_m (Zsiros et al. 2006).

Photoprotective role of NPQ

The addition of nigericin caused an increase in ϕ_{PI} in both VA-EPL and GE-EPM samples. Nigericin is an uncoupler of thylakoid membranes that dissipates the transthylakoidal ΔpH and has long been used for assessing the role of photoprotective NPQ in plants (Park et al. 1996, Ware et al. 2015) and algae (Doerge et al. 2000, Christa et al. 2017), including diatoms (Ting & Owens 1993, Grouneva et al. 2008). An increase in overall PSII photoinactivation (as measured by ϕ_{PI}) resulting from the addition of nigericin is thus indicative of the operation of ΔpH related photoprotective components of NPQ (energy-dependent quenching, qE ; Müller et al. 2001, Ruban 2016) likely including the XC. The comparison of the extent of increase in ϕ_{PI} in EPL and EPM assemblages can therefore be used as a measure of the relative protective importance of NPQ/XC in the two sample types.

The significant nigericin-induced increase in ϕ_{PI} that was observed for both VA-EPL and GE-EPM is an indication of an important photoprotective role of qE and the XC in both types of communities. However, the larger increase in ϕ_{PI} found for GE-EPM samples supports the idea that the XC displays a more important role in the EPM- than in the EPL-dominated assemblages. This result further supports the motility–physiology trade-off hypothesis. Non-motile species, incapable of using vertical migration to regulate light exposure, appear to rely more on efficient inherent physiological photoprotection. In contrast, the smaller increase in PSII photoinactivation in nigericin-inhibited VA-EPL samples shows that the importance of physiological mechanisms is smaller for motile species, which likely rely more on light-induced motility to photoprotect against excess light.

Interestingly, nigericin had the effect of eliminating the transient increase in F_v/F_m observed in VA-EPL samples (Fig. 4A), resulting in x-intercepts closer to zero (Fig. 5A). This result suggests that sustained NPQ formed in the dark may be related to the establishment and maintenance of a transthylakoidal ΔpH , as proposed for planktonic diatoms (Jakob et al. 2001, Dijkman & Kroon 2002, Bailleul et al. 2015). Because the sustained NPQ may also be caused by the permanence, of DTx molecules in the dark, regardless of the presence of a transthylakoidal ΔpH (Lavaud & Lepetit 2013, Giovagnetti & Ruban 2017), the observed effect of nigericin might be due to changes in the activities of XC enzymes DT epoxidase and DD de-epoxidase.

The photoprotective role of motility and XC, and their relative importance, has been addressed in multiple studies. However, none has related the motility or the XC to the effective reduction in PSII photodamage, by distinguishing PSII photoinactivation from repair. An exception is the study by Cartaxana et al. (2013) that, by applying lincomycin and an inhibitor of the DDX-DTx cycle (dithiothreitol; Olaizola et al. 1994) on epipelagic diatoms exposed to a single combination of light intensity and exposure duration, observed a large decrease (ca. -80%) in D1 protein content, supporting a major role of the XC in preventing PSII photodamage. The results of the present study, based on the more robust indicator ϕ_{PI} , pointed to a much lesser importance of physiological processes (ϕ_{PI} increased by 16 and 47% in EPL and EPM samples, respectively). The discrepancy between these results may be due to the different processes targeted by dithiothreitol and nigericin, but also to differences in photoacclimation state, associated with different growth conditions or differences in community composition, highlighting the need for further investigation of the variability of the responses to high light in natural MPB communities.

Photoinactivation versus repair

One advantage of the multi-actinic imaging protocol used in the present study is the possibility to measure paired light responses of rate constants k_{PI} and k_{REC} . However, specific aspects of the response of MPB samples under study limited the measurement of k_{REC} only for the highest applied irradiances. The absence of a clear decrease of F_v/F_m values for a large range of the lowest irradiances made it impossible to fit Eqs. (3) & (4) and to estimate k_{PI} and k_{REC} . The reasons for this differed between EPL and EPM samples. For VA-EPL samples (both untreated and treated with lincomycin), F_v/F_m increased transiently under the lower irradiances, a feature attributable to the build-up of sustained NPQ prior to light exposure. In the case of GE-EPM samples, a light-induced decrease in F_v/F_m of untreated samples was undetectable in most cases, which can be interpreted as resulting from an efficient coping with light under moderate conditions.

Nevertheless, the results regarding k_{PI} and k_{REC} for high light levels allowed for comparison of the relative importance of photoinactivation and repair processes, and point to different strategies of how EPL and EPM species respond to light stress. For both types of assemblages, the capacity of repair exceeds the suffered photodamage, even for the highest irradiance level tested. Yet, EPL forms appear to have the capacity for higher repair rates than EPM forms, the difference being especially relevant when considered in relation to the corresponding photoinactivation rates. EPL diatoms seem to rely more on repair than

on preventing photoinactivation. They are inherently more susceptible to photodamage (higher ϕ_{PI}), but this weaker photoprotective capacity is compensated for by a greater capacity for repair, a strategy also observed in dinoflagellates (Jeans et al. 2013) and coccolithophorids (Ragni et al. 2008). This may explain why, despite showing higher rates of PSII photoinactivation, VA-EPL samples cope better with high light, showing higher light-saturated photosynthetic activity ($rETR_m$). Light-response strategies based on the development of efficient repair mechanisms tend to be favored by acclimation to high light (Ragni et al. 2008, Jeans et al. 2013). Repair capacity is known to increase with growth irradiance by improving the capacity to increase the rate of D1 protein synthesis (Tyystjärvi 2013). PSII repair is a costly process, and efficient use of high light levels, provided by high light acclimation, allows the generation of the necessary ATP and reductant power. Motile diatoms can make use of their motility to exploit the steep sedimentary light gradient and use the high light levels available near the surface in order to generate ATP and support the expensive D1 protein repair.

On the contrary, EPM forms seem to favor the reduction of photoinactivation, based on efficient physiological photoprotection, and thus avoiding the need to develop and support costly repair mechanisms. The inability to move within the photic zone of the sediment and to select a particular light environment leads EPM-dominated samples to appear, comparatively, as low-light acclimated. The evaluation of the balance between susceptibility to photoinactivation versus repair capacity should also consider that diatoms, especially species with a limited capacity for photoprotective energy dissipation, seem to maintain a reservoir of inactive PSII as a means of favoring repair by providing additional substrate for PSII repair (Lavaud et al. 2016).

These results highlight the importance of measuring rate constants of photoinactivation and repair, and their light response, on MPB. It allows for the proper evaluation of the relative importance of the two processes in determining the level net photoinactivation of these communities across the range of ecologically relevant levels of light intensity, which is of interest to characterize their tolerance limits for light stress. The integrated study of photoprotection, photoinactivation and repair is also of interest in the context of the increasing experimental evidence indicating that the light stress acts predominantly by inhibiting repair and not by promoting inactivation (Nishiyama et al. 2006). This shift in paradigm has led to a growing interest in the study of photorepair, now seen as a key determinant of the effective capacity of phototrophs to cope with light stress (Murata et al. 2012).

Photoprotective capacity: NPQ versus ϕ_{PI}

NPQ has been widely used as a measure of photoprotection capacity against photodamage in plants (e.g. Ruban et al. 2004) and algae (e.g. Gévaert et al. 2003, Barnett et al. 2015). In the case of MPB, NPQ (or the associated XC activity) has also been commonly used to ascertain the capacity for photoprotection. It has been used to compare the photoprotection capacity of EPL and EPM communities (XC pigment pools; Van Leeuwe et al. 2008, Cartaxana et al. 2011) or species (NPQ light response and induction/relaxation kinetics; Barnett et al. 2015, Blommaert et al. 2017) or to compare the fast induction of physiological (NPQ induction) and behavioral (negative phototaxis) photoprotection (Laviale et al. 2016). An important result of the present study was the finding that NPQ is not related to the capacity to prevent photodamage. In fact, the susceptibility to PSII photoinactivation, as measured by ϕ_{PI} , varied markedly between EPL and EPM samples, but not as expected from the observed NPQ levels: VA-EPL samples reached higher NPQ levels, but were also the ones that suffered more photodamage; in contrast, GE- EPM samples were more resistant to PSII photoinactivation while reaching lower NPQ values. This contradiction between NPQ levels and actual photoinactivation suggests that NPQ may not be an accurate predictor of actual capacity to prevent photodamage, as it may not account for all photoprotective mechanisms at play, and its action may be complemented by other important protective processes, such as the PSII cyclic electron transfer (Lavaud 2007, Goss & Lepetit 2015), or by enhanced antioxidant activity (Nishiyama et al. 2006). Previous studies comparing NPQ with PSII photoinactivation have also concluded that NPQ offers a relatively low photoprotection, as little as 25% (e.g. Tyystjärvi 2013).

These results call for the use of ϕ_{PI} (or k_{PI} for high light levels) instead of NPQ as a more suitable indicator of photoprotective capacity. Furthermore, particularly in the case of MPB biofilms, the measurement and use of NPQ has long been recognized as problematic, due to the sustained quenching in the dark of F_m values lower than F_m' , and the confounding effects of light-induced vertical migration and light attenuation, and depth-integration of sub-surface fluorescence emission (Forster & Kromkamp 2004, Serôdio 2004, Morelle et al. 2018). In contrast, ϕ_{PI} quantifies the total photodamage actually occurring without the confounding effects of NPQ and repair, integrating the effects of all protective mechanisms in operation, and therefore appears to be a better predictor of the global effectiveness of photoprotection. Measuring ϕ_{PI} , however, is considerably more difficult than measuring NPQ. Hopefully, the further development of experimental approaches such as the one used in the present study may overcome the current experimental limitations.

Acknowledgements

This work was supported by the Fundação para a Ciência e a Tecnologia (FCT), through doctoral scholarship SFRH/BD/86788/2012 (S.F.), Post-Doctoral fellowship SFRH/BPD/111685/2015 (J.C.F.) and CESAM grant UID/AMB/500017/2013 (W.S.). For the financial support, thanks are due to CESAM (UID/AMB/50017 – POCI-01-0145-FEDER-007638), FCT/MCTES through national funds (PID- DAC), and the co-funding by the FEDER, within the PT2020 Partnership Agreement and Compete 2020. The authors thank Gregor Christa for help with R programming, Sandra Craveiro, Carmen Elias and Ana Luís for help with the taxonomical identification, and Dr. Douglas A. Campbell for fruitful discussions on data interpretation. We thank anonymous reviewers for critical comments on the manuscript.

References

- Admiraal W (1984) The ecology of estuarine sediment- inhabiting diatoms. *Prog Phycol Res* 3:269–322
- Allakhverdiev SI, Nishiyama Y, Takahashi S, Miyairi S, Suzuki I, Murata N (2005) Systematic analysis of the relation of electron transport and ATP synthesis to the photodamage and repair of Photosystem II in *Synechocystis*. *Plant Physiol* 137:263–273
- Antal TK, Osipov V, Matorin DN, Rubin AB (2011) Membrane potential is involved in regulation of photosynthetic reactions in the marine diatom *Thalassiosira weissflogii*. *J Photochem Photobiol B* 102:169–173
- Bailleul B, Berne N, Murik O, Petroustos D and others (2015) Energetic coupling between plastids and mitochondria drives CO₂ assimilation in diatoms. *Nature* 524:366–369
- Barnett A, Méléder V, Blommaert L, Lepetit B and others (2015) Growth form defines physiological photoprotective capacity in intertidal benthic diatoms. *ISME J* 9: 32–45
- Blommaert L, Huysman MJJ, Vyverman W, Lavaud J, Sabbe K (2017) Contrasting NPQ dynamics and xanthophyll cycling in a motile and a non-motile intertidal benthic diatom. *Limnol Oceanogr* 62:1466–1479
- Blommaert L, Lavaud J, Vyverman W, Sabbe K (2018) Behavioural versus physiological photoprotection in epipelagic and epipsammic benthic diatoms. *Eur J Phycol* 53: 146–155
- Brotas V, Risgaard-Petersen L, Serôdio J, Ottossen L, Dalsgaard T, Ribeiro L (2003) In situ measurements of photosynthetic activity and respiration of intertidal benthic microalgal communities undergoing vertical migration. *Ophelia* 57:13–26
- Campbell DA, Tyystjärvi E (2012) Parameterization of photosystem II photoinactivation and repair. *Biochim Biophys Acta* 1817:258–265
- Campbell DA, Hossain Z, Cockshutt AM, Zhaxybayeva O, Wu H, Li G (2013) Photosystem II protein clearance and FtsH function in the diatom *Thalassiosira pseudonana*. *Photosynth Res* 115:43–54
- Cartaxana P, Ruivo M, Hubas C, Davidson I, Serôdio J, Jesus B (2011) Physiological versus behavioral photoprotection in intertidal epipelagic and epipsammic benthic diatom communities. *J Exp Mar Biol Ecol* 405:120–127
- Cartaxana P, Domingues N, Cruz S, Jesus B, Laviale M, Serôdio J, Marques Da Silva J (2013) Photoinhibition in benthic diatom assemblages under light stress. *Aquat Microb Ecol* 70:87–92

- Chevalier EM, Gévaert F, Créach A (2010) In situ photosynthetic activity and xanthophylls cycle development of undisturbed microphytobenthos in an intertidal mudflat. *J Exp Mar Biol Ecol* 385:44–49
- Christa G, Cruz S, Jahns P, de Vries J and others (2017) Photoprotection in a monophyletic branch of chlorophyte algae is independent of energy-dependent quenching (q_E). *New Phytol* 214:1132–1144
- Cohn SA, Bahena M, Davis JT, Ragland RL, Rauschenberg CD, Smith BJ (2004) Characterisation of the diatom photophobic response to high irradiance. *Diatom Res* 19: 167–179
- Cohn SA, Halpin D, Hawley N, Ismail A and others (2015) Comparative analysis of light-stimulated motility responses in three diatom species. *Diatom Res* 30:213–225
- Consalvey M, Paterson DM, Underwood GJC (2004) The ups and downs of life in a benthic biofilm: Migration of benthic diatoms. *Diatom Res* 19:181–202
- Cook PLM, Røy H (2006) Advective relief of CO₂ limitation in microphytobenthos in highly productive sandy sediments. *Limnol Oceanogr* 51:1594–1601
- Coste M, Rosebery J (2011) Guide iconographique pour la mise en oeuvre de l'Indice Biologique Diatomée 2007. Action 14: Développement et optimisation des méthodes de bioindication pour les cours d'eau. Cestas Gazinet, Cemagref groupement de Bordeaux, Bordeaux
- Dijkman NA, Kroon BMA (2002) Indications for chlororespiration in relation to light regime in the marine diatom *Thalassiosira weissflogii*. *J Photochem Photobiol B* 66: 179–187
- Doege M, Ohmann E, Tschiersch H (2000) Chlorophyll fluorescence quenching in the alga *Euglena gracilis*. *Photosynth Res* 63:159–170
- Du GY, Li WT, Li H, Chung IK (2012) Migratory responses of benthic diatoms to light and temperature monitored by chlorophyll fluorescence. *J Plant Biol* 55:159–164
- Eaton JW, Moss B (1966) The estimation of numbers and pigment content in epipelagic algal populations. *Limnol Oceanogr* 11:584–595
- Eilers PHC, Peeters JCH (1988) A model for the relationship between light intensity and the rate of photosynthesis in phytoplankton. *Ecol Modell* 42:199–215
- Ezequiel J, Laviale M, Frankenbach S, Cartaxana P, Serôdio J (2015) Photoacclimation state determines the photobehaviour of motile microalgae: the case of a benthic diatom. *J Exp Mar Biol Ecol* 468:11–20

- Forster RM, Kromkamp JC (2004) Modelling the effects of chlorophyll fluorescence from subsurface layers on photosynthetic efficiency measurements in microphytobenthic algae. *Mar Ecol Prog Ser* 284:9–22
- Frankenbach S, Serôdio J (2017) One pulse, one light curve: fast characterization of the light response of microphytobenthos biofilms using chlorophyll fluorescence. *Limnol Oceanogr Methods* 15:554–566
- Genty B, Briantais JMM, Baker NR (1989) The relationship between the quantum yield of photosynthetic electron transport and quenching of chlorophyll fluorescence. *Biochim Biophys Acta* 990:87–92
- Gévaert F, Créach A, Davoult D, Migné A and others (2003) *Laminaria saccharina* photosynthesis measured in situ: photoinhibition and xanthophyll cycle during a tidal cycle. *Mar Ecol Prog Ser* 247:43–50
- Giovagnetti V, Ruban A V. (2017) Detachment of the fucoxanthin chlorophyll a/c binding protein (FCP) antenna is not involved in the acclimative regulation of photoprotection in the pennate diatom *Phaeodactylum tricornutum*. *Biochim Biophys Acta Bioenerg* 1858:218–230
- Goss R, Lepetit B (2015) Biodiversity of NPQ. *J Plant Physiol* 172:13–32
- Grouneva I, Jakob T, Wilhelm C, Goss R (2008) A new multicomponent NPQ mechanism in the diatom *Cyclotella meneghiniana*. *Plant Cell Physiol* 49:1217–1225
- Guarini JM, Blanchard GF, Gros P, Harrison SJ (1997) Modelling the mud surface temperature on intertidal flats to investigate the spatio-temporal dynamics of the benthic microalgal photosynthetic capacity. *Mar Ecol Prog Ser* 153:25–36
- Hakala M, Tuominen I, Keränen M, Tyystjärvi T, Tyystjärvi E (2005) Evidence for the role of the oxygen-evolving manganese complex in photoinhibition of Photosystem II. *Biochim Biophys Acta* 1706:68–80
- Jakob T, Goss R, Wilhelm C (2001) Unusual pH-dependence of diadinoxanthin de-epoxidase activation causes chlororespiratory induced accumulation of diatoxanthin in the diatom *Phaeodactylum tricornutum*. *J Plant Physiol* 158: 383–390
- Jeans J, Campbell DA, Hoogenboom MO (2013) Increased reliance upon photosystem II repair following acclimation to high-light by coral-dinoflagellate symbioses. *Photosynth Res* 118:219–229
- Jesus B, Perkins RG, Consalvey M, Brotas V, Paterson DM (2006) Effects of vertical migrations by benthic microalgae on fluorescence measurements of photophysiology. *Mar Ecol Prog Ser* 315:55–66

- Jesus B, Brotas V, Ribeiro L, Mendes CR, Cartaxana P, Paterson DM (2009) Adaptations of microphytobenthos assemblages to sediment type and tidal position. *Cont Shelf Res* 29:1624–1634
- Juneau P, Barnett A, Méléder V, Dupuy C, Lavaud J (2015) Combined effect of high light and high salinity on the regulation of photosynthesis in three diatom species belonging to the main growth forms of intertidal flat inhabiting microphytobenthos. *J Exp Mar Biol Ecol* 463: 95–104
- Kok B (1956) On the inhibition of photosynthesis by intense light. *Biochim Biophys Acta* 21:234–244
- Kou J, Oguchi R, Fan DY, Chow WS (2012) The time course of photoinactivation of photosystem II in leaves revisited. *Photosynth Res* 113:157–164
- Kromkamp J, Barranguet C, Peene J (1998) Determination of microphytobenthos PSII quantum yield efficiency and photosynthetic activity by means of variable chlorophyll fluorescence. *Mar Ecol Prog Ser* 162:45–55
- Lavaud J (2007) Fast regulation of photosynthesis in diatoms: mechanisms, evolution and ecophysiology. *Funct Plant Sci Biotechnol* 1:267–287
- Lavaud J, Lepetit B (2013) An explanation for the inter-species variability of the photoprotective non-photochemical chlorophyll fluorescence quenching in diatoms. *Biochim Biophys Acta Bioenerg* 1827:294–302
- Lavaud J, Strzepek RF, Kroth PG (2007) Photoprotection capacity differs among diatoms: Possible consequences on the spatial distribution of diatoms related to fluctuations in the underwater light climate. *Limnol Oceanogr* 52:1188–1194
- Lavaud J, Six C, Campbell DA (2016) Photosystem II repair in marine diatoms with contrasting photophysiology. *Photosynth Res* 127:189–199
- Laviale M, Barnett A, Ezequiel J, Lepetit B and others (2015) Response of intertidal benthic microalgal biofilms to a coupled light-temperature stress: evidence for latitudinal adaptation along the Atlantic coast of Southern Europe. *Environ Microbiol* 17:3662–3677
- Laviale M, Frankenbach S, Serôdio J (2016) The importance of being fast: comparative kinetics of vertical migration and non-photochemical quenching of benthic diatoms under light stress. *Mar Biol* 163:1–12
- Lepetit B, Gélín G, Lepetit M, Sturm S and others (2017) The diatom *Phaeodactylum tricornutum* adjusts nonphotochemical fluorescence quenching capacity in response to dynamic light via fine-tuned Lhcx and xanthophyll cycle pigment synthesis. *New Phytol* 214:205–218

- Lorenzen CJ (1967) Determination of chlorophyll and pheopigments: spectrophotometric equations. *Limnol Oceanogr* 12:343–346
- McLachlan DH, Brownlee C, Taylor AR, Geider RJ, Underwood GJC (2009) Light-induced motile responses of the estuarine benthic diatoms *Navicula perminuta* and *Cylindrotheca closterium* (Bacillariophyceae). *J Phycol* 45:592–599
- Miyata K, Noguchi K, Terashima I (2012) Cost and benefit of the repair of photodamaged photosystem II in spinach leaves: roles of acclimation to growth light. *Photosynth Res* 113:165–180
- Morelle J, Orvain F, Claquin P (2018) A simple, user friendly tool to readjust raw PAM data from field measurements to avoid over- or underestimating of microphytobenthos photosynthetic parameters. *J Exp Mar Biol Ecol* 503: 136–146
- Mouget J, Perkins R, Consalvey M, Lefebvre S (2008) Migration or photoacclimation to prevent high irradiance and UV-B damage in marine microphytobenthic communities. *Aquat Microb Ecol* 52:223–232
- Müller P, Li XP, Niyogi KK (2001) Non-photochemical quenching. A response to excess light energy. *Plant Physiol* 125:1558–1566
- Murata N, Allakhverdiev SI, Nishiyama Y (2012) The mechanism of photoinhibition in vivo: Re-evaluation of the roles of catalase, α -tocopherol, non-photochemical quenching, and electron transport. *Biochim Biophys Acta Bioenerg* 1817:1127–1133
- Ni G, Zimbalatti G, Murphy CD, Barnett AB and others (2017) Arctic *Micromonas* uses protein pools and nonphotochemical quenching to cope with temperature restrictions on Photosystem II protein turnover. *Photosynth Res* 131:203–220
- Nishiyama Y, Allakhverdiev SI, Murata N (2006) A new paradigm for the action of reactive oxygen species in the photoinhibition of photosystem II. *Biochim Biophys Acta Bioenerg* 1757:742–749
- Niyogi KK (1999) Photoprotection revisited: genetic and molecular approaches. *Annu Rev Plant Physiol Plant Mol Biol* 50:333–359
- Olaizola M, Roche J, Kolber Z, Falkowski PG, La Roche J, Kolber Z, Falkowski PG (1994) Non-photochemical fluorescence quenching and the diadinoxanthin cycle in a marine diatom. *Photosynth Res* 41:357–370
- Park YI, Chow WS, Anderson JM, Hurry VM (1996) Differential susceptibility of Photosystem II to light stress in light-acclimated pea leaves depends on the capacity for photochemical and non-radiative dissipation of light. *Plant Sci* 115:137–149

- Perkins RG, Underwood GJC, Brotas V, Snow GC, Jesus B, Ribeiro L (2001) Responses of microphytobenthos to light: primary production and carbohydrate allocation over an emersion period. *Mar Ecol Prog Ser* 223:101–112
- Perkins RG, Lavaud J, Serôdio J, Mouget JL and others (2010) Vertical cell movement is a primary response of intertidal benthic biofilms to increasing light dose. *Mar Ecol Prog Ser* 416:93–103
- Petrou K, Hill R, Brown CM, Campbell DA, Doblin MA, Ralph PJ (2010) Rapid photoprotection in sea-ice diatoms from the East Antarctic pack ice. *Limnol Oceanogr* 55: 1400–1407
- Pniewski FF, Biskup P, Bubak I, Richard P, Latała A, Blanchard G (2015) Photo-regulation in microphytobenthos from intertidal mudflats and non-tidal coastal shallows. *Estuar Coast Shelf Sci* 152:153–161
- Pniewski FF, Richard P, Latała A, Blanchard G (2017) Nonphotochemical quenching in epipsammic and epipelagic microalgal assemblages from two marine ecosystems. *Cont Shelf Res* 136:74–82
- Pniewski FF, Richard P, Latała A, Blanchard G (2018) Long- and short-term photoacclimation in epipsammon from non-tidal coastal shallows compared to epipelon from intertidal mudflat. *J Sea Res* 136:1–9
- Ragni M, Airs RL, Leonardos N, Geider RJ (2008) Photoinhibition of PSII in *Emiliania huxleyi* (Haptophyta) under high light stress: The roles of photoacclimation, photoprotection, and photorepair. *J Phycol* 44:670–683
- Ralph PJ, Gademann R, Larkum AWD, Schreiber U (1999) In situ underwater measurements of photosynthetic activity of coral zooxanthellae and other reef-dwelling dinoflagellate endosymbionts. *Mar Ecol Prog Ser* 180:139–147
- Ribeiro L (2010) Intertidal benthic diatoms of the Tagus estuary: taxonomic composition and spatial-temporal variation. PhD thesis, University of Lisbon
- Round FE, Crawford RM, Mann D (1990) The diatoms — biology & morphology of the genera. Cambridge University Press, Cambridge
- Ruban AV (2016) Nonphotochemical chlorophyll fluorescence quenching: mechanism and effectiveness in protecting plants from photodamage. *Plant Physiol* 170: 1903–1916
- Ruban A, Lavaud J, Rousseau B, Guglielmi G, Horton P, Etienne AL (2004) The super-excess energy dissipation in diatom algae: comparative analysis with higher plants. *Photosynth Res* 82:165–175

- Serôdio J (2004) Analysis of variable chlorophyll fluorescence in microphytobenthos assemblages: implications of the use of depth-integrated measurements. *Aquat Microb Ecol* 36:137–152
- Serôdio J, Catarino F (1999) Fortnightly light and temperature variability in estuarine intertidal sediments and implications for microphytobenthos primary productivity. *Aquat Ecol* 33:235–241
- Serôdio J, Lavaud J (2011) A model for describing the light response of the nonphotochemical quenching of chlorophyll fluorescence. *Photosynth Res* 108:61–76
- Serôdio J, Marques da Silva J, Catarino F (2001) Use of in vivo chlorophyll a fluorescence to quantify short-term variations in the productive biomass of intertidal microphytobenthos. *Mar Ecol Prog Ser* 218:45–61
- Serôdio J, Coelho H, Vieira S, Cruz S (2006) Microphytobenthos vertical migratory photoresponse as characterised by light-response curves of surface biomass. *Estuar Coast Shelf Sci* 68:547–556
- Serôdio J, Vieira S, Barroso F (2007) Relationship of variable chlorophyll fluorescence indices to photosynthetic rates in microphytobenthos. *Aquat Microb Ecol* 49:71–85
- Serôdio J, Vieira S, Cruz S (2008) Photosynthetic activity, photoprotection and photoinhibition in intertidal microphytobenthos as studied in situ using variable chlorophyll fluorescence. *Cont Shelf Res* 28:1363–1375
- Serôdio J, Ezequiel J, Barnett A, Mouget JL, Méléder V, Laviale M, Lavaud J (2012) Efficiency of photoprotection in microphytobenthos: role of vertical migration and the xanthophyll cycle against photoinhibition. *Aquat Microb Ecol* 67:161–175
- Serôdio J, Ezequiel J, Frommlet J, Laviale M, Lavaud J (2013) A Method for the rapid generation of nonsequential light-response curves of chlorophyll fluorescence. *Plant Physiol* 163:1089–1102
- Serôdio J, Schmidt W, Frankenbach S (2017) A chlorophyll fluorescence-based method for the integrated characterization of the photophysiological response to light stress. *J Exp Bot* 68:1123–1135
- Ting CS, Owens TG (1993) Photochemical and nonphotochemical fluorescence quenching processes in the diatom *Phaeodactylum tricornutum*. *Plant Physiol* 101: 1323–1330
- Tyystjärvi E (2013) Photoinhibition of Photosystem II. *Int Rev Cell Mol Biol* 300:243–303
- Tyystjärvi E, Aro EM (1996) The rate constant of photoinhibition, measured in lincomycin-treated leaves, is directly proportional to light intensity. *Proc Natl Acad Sci USA* 93:2213–2218

- Underwood GJC, Kromkamp J (1999) Primary production by phytoplankton and microphytobenthos in estuaries. *Adv Ecol Res* 29:93–153
- Underwood GJC, Nilsson C, Sundback K, Wulff A (1999) Short-term effects of UVB radiation on chlorophyll fluorescence, biomass, pigments, and carbohydrate fractions in a benthic diatom mat. *J Phycol* 35:656–666
- Van Leeuwe MA, Brotas V, Consalvey M, Forster RM and others (2008) Photoacclimation in microphytobenthos and the role of xanthophyll pigments. *Eur J Phycol* 43: 123–132
- Vieira S, Cartaxana P, Máguas C, Marques Da Silva J (2016) Photosynthesis in estuarine intertidal microphytobenthos is limited by inorganic carbon availability. *Photosynth Res* 128:85–92
- Ware MA, Belgio E, Ruban AV (2015) Comparison of the protective effectiveness of NPQ in *Arabidopsis* plants deficient in PsbS protein and zeaxanthin. *J Exp Bot* 66: 1259–1270
- Yang H, Flower RJ, Battarbee RW (2010) An improved coverslip method for investigating epipellic diatoms. *Eur J Phycol* 45:191–199
- Zsiros O, Allakhverdiev SI, Higashi S, Watanabe M, Nishiyama Y, Murata N (2006) Very strong UV-A light temporally separates the photoinhibition of photosystem II into light-induced inactivation and repair. *Biochim Biophys Acta Bioenerg* 1757:123–129

Chapter 4

FUNCTIONAL RESILIENCE OF PSII, VERTICAL DISTRIBUTION AND ECOSYSTEM-LEVEL ESTIMATES OF SUBSURFACE MICROPHYTOBENTHOS IN ESTUARINE TIDAL FLATS

Published:

Frankenbach S., Azevedo A., Reis V., Dias D., Vaz L., Dias J.M., Serôdio J. (2019) Functional resilience of PSII, vertical distribution and ecosystem-level estimates of subsurface microphytobenthos in estuarine tidal flats. *Continental Shelf Research* 182, 46–56

DOI: 10.1016/j.csr.2019.05.018

Keywords

Burial, diatoms, epipellic, epipsammic, microphytobenthos, resilience, subsurface, vertical migration

Abstract

Most studies on sediment-inhabiting microphytobenthos are based on the biomass present on the surface layers of intertidal flats. However, large amounts of microalgal biomass are known to exist below the surface. This study tested the role of subsurface microalgal biomass as a potential source of photosynthetically active cells for the biofilm on the surface. The resilience of buried cells was evaluated by exposing samples from various depths to surface conditions and investigating the recovery of photosynthetic activity. Additionally, vertical migration by subsurface epipellic diatoms was followed at sub-millimeter scales to evaluate its role for transporting cells to the vicinity of the sediment surface. Finally the relative importance of subsurface microalgal biomass was assessed by estimating the proportion of subsurface:surface biomass for different types of sediments from the Ria de Aveiro. Vertical profiles of chlorophyll *a*, 10 cm-deep, were measured on samples from three intertidal sites, representative of the range of sediment characteristics found in this estuary. The ratio of total biomass to surface biomass ('subsurface biomass fraction') based on total biomass (0-10 cm depth interval; $C_{sub,total}$) and on viable biomass (between the surface and the maximum depth with significant photosynthetic recovery; $C_{sub,viable}$). The experiments showed that buried cells were able to recover photosynthetic activity within 1.5 to 3 hours of light exposure, with the rate of recovery being dependent on depth and type of sediment. Furthermore, subsurface vertical migration was found to enable motile cells to reach the surface from layers deeper than 1 mm within a low tide period. Overall, the results showed that surface biomass (0-0.5 cm) only accounted for one fifth to one third of the total biomass present between the surface and 10 cm, and that the amount of subsurface viable biomass reached 2-3 times the biomass present at the surface. Applying the estimates of $C_{sub,total}$ and $C_{sub,viable}$ to the whole intertidal area of the Ria de Aveiro, spatially-weighted averages for subsurface biomass fractions were found to reach 3.8 and 2.1 respectively.

Introduction

Microphytobenthos (MPB) comprises the communities of photoautotrophic eukaryotic algae and cyanobacteria living in intertidal and well-lit subtidal sediments (Underwood and Kromkamp, 1999). Diatoms, a highly diverse group that contributes about 20% to the global primary production and about 40% of the total marine primary productivity (Cahoon, 1999; Field, 1998; Sarthou et al., 2005; Tréguer et al., 2018) usually dominate these communities. Diatoms also serve as basis for many marine food webs (Armbrust, 2009), constitute a key carbon source for heterotrophs (Middelburg et al., 2000), and contribute to sediment stabilization through the production of extracellular polymeric substances (EPS) (Cahoon, 1999). Not surprisingly, MPB has been the object of intense research, mostly centered on the seasonal dynamics of biomass and estimation of annual productivity budgets (Benyoucef et al., 2014; Brito et al., 2009; Du et al., 2010b; Koh et al., 2007; Moerdijk-Poortvliet et al., 2018; Pinckney and Zingmark, 1993; Stanley and Howard, 2013).

Most studies have focused on the microalgal biomass within the photic zone, where light penetrates enough to support photosynthetic activity and primary productivity (Herlory et al., 2004; Kelly et al., 2001; MacIntyre and Cullen, 1995; Serôdio et al., 2001). However, large amounts of microalgal biomass can be found well below the surface of the sediment (Brotas and Serôdio, 1995; De Jonge and Colijn, 1994; Fenchel and Straarup, 1971; Mundree et al., 2003; Steele and Baird, 1968). This is especially significant considering that the photic zone in sediments is very thin. It spans from the surface to a few millimeters in sandy sediments, to only fractions of a millimeter, in muddy sediments (Cartaxana et al., 2011; Herlory et al., 2004; Kelly et al., 2001).

MPB cells are continuously buried below the surface due to bioturbation and resuspension/deposition events caused by waves and currents during high tide (de Jonge and van Beusekom, 1995; Kingston, 1999; Plecha et al., 2014; Ubertini et al., 2015). Conversely, buried cells can return to the surface, being passively transported either during bioturbation and resuspension events, or due to the reworking or removal of upper layers of sediment by grazers like snails or fish (Almeida et al., 1993; Hagerthey et al., 2002), exposing cells in a newly created surface. While these processes occur in all types of sediments, in the case of muddy sediments the resurfacing of cells may be enhanced by vertical cell migration. In contrast with sandy sediments, where the diatom communities are mainly formed by non-motile lifeforms (epipsammic) living attached to the large sediment particles, in muddy sediments the MPB is dominated by raphid pennate diatoms (epipellic),

able to actively move between the fine sediment particles (Admiraal, 1984; Cahoon et al., 1995).

Although most studies have focused on the effect of vertical migration on the biomass present at the surface or in the photic zone (Easley et al., 2005; Round and Palmer, 1966; Serôdio et al., 2001), motile diatoms may undertake vertical migratory movements at sedimentary depths below the illuminated layers (Frankenbach et al., 2014; Pinckney et al., 1994). However, subsurface vertical migration has been poorly studied and its potential importance for reaching newly-created surface layers is unknown.

Subsurface biomass has been hypothesized to represent a source of photosynthetically competent cells capable of 're-inoculating' the depleted surface, and thus allowing the attenuation of in the biomass the photic zone and biofilm productivity (Delgado et al., 1991; Easley et al., 2005). This requires that the buried diatoms survive prolonged periods in continuous darkness, and regain their photosynthetic activity quickly (faster than growth of remaining cells) following exposure to surface conditions. In order to contribute to this process, buried epipelagic species need to retain their capability to migrate vertically to reach the photic zone.

This study tested the importance of subsurface microalgal biomass as a potential source of photosynthetically active cells for surface MPB biofilms. This was pursued by addressing the following objectives in the described ways:

(i) to investigate if buried cells can regain photosynthetic activity in a short time if exposed to surface conditions; to determine until which depth can cells recover their photosynthetic competence. These questions were addressed by following the recovery of photosynthetic activity of subsurface MPB samples, from various depths, following resurfacing and exposure to ambient light.

(ii) in the case of epipelagic MPB communities, to test if vertical migration occurring below the surface are capable of transporting cells to the vicinity of the sediment surface. This was studied by measuring vertical migration at sub-millimeter vertical scales, using a recently-developed method for obtaining thin sediment sections.

(iii) to estimate how much microalgal biomass is present below the surface, relative to surface levels, and to determine if the proportion subsurface:surface biomass varies with sediment type. These questions were addressed by measuring vertical profiles of MPB biomass for various sediment types and quantifying the subsurface MPB biomass, distinguishing 'total' biomass (down to 10 cm deep) and 'viable' (down to the depth determined in (i)).

(iv) to estimate the amount of subsurface MPB biomass present at the ecosystem level. This was estimated considering the proportion of subsurface biomass for different types of sediments and associated MPB communities, and the spatial distribution of sediment types throughout the intertidal areas of one estuarine ecosystem, the Ria de Aveiro (Portugal).

Material and methods

Sampling sites

The Ria de Aveiro is a mesotidal coastal lagoon on the northwest coast of Portugal (40°38'N - 08°45'W) (Tomás et al., 2014). Detailed characterization of physical, geomorphological, and ecological features of the Ria de Aveiro can be found in Bueno-Pardo et al., (2018); Dias et al.,(2003, 1999); Tomás et al., (2014). Sampling was carried out on intertidal sites considered as representative of the overall variability in sediment type. MPB assemblages were collected in two channels of the lagoon: Gafanha da Encarnação (GE; in Canal de Mira, 40°35'18" N, 08°41'06" W), and Vista Alegre (VA; in Canal de Ílhavo, 40°37'12" N, 08°44'54" W). The sampling sites differ in grain size, salinity (Tomás et al., 2014; Vargas et al., 2017), and water retention time (Dias et al., 2003). Sediment granulometry ranged from sand (45.3% particles between 63 µm and 125 µm; 42.7% below 63 µm) at GE, to fine mud (97% of the grains smaller the 63 µm) at VA (percentages of dry weight; Serôdio et al., 2007). The MPB communities of the two sites have distinct taxonomic composition and photophysiological characteristics (Frankenbach et al., 2018; Serôdio et al., 2007). To increase the spatial resolution of the estimation of the subsurface biomass at the ecosystem-level, a third sampling site was added. This site is located in the Canal de Ovar, in front of Torreira (TO; 40°35" N, 8°,42" W)

Recovery of photosynthetic activity

On three consecutive days in July 2016, 12 sediment cores were collected using 2 cm-diameter, 20 cm-long acrylic corers during daytime low tide and taken to the laboratory. There, the cores were sectioned horizontally into 5 mm-thick sections. The sections started at depth 0, 5, 20 and 40 mm (VA) or 0, 20, 45 and 60 mm (GE) below the surface. In the case of GE samples, the depth intervals were adjusted to reach deeper layers because in sandy sediments resuspension and bioturbation are expected to cause sediment mixing down to greater depths. Each section was cut with a separate blade,

forming the base of a circular plastic ring 5-mm thick, avoiding cross contact and transfer of sediments between sections. Three replicated cores for each sampling site were used.

Shortly after sectioning, the undisturbed samples were exposed to constant low white light ($50 \mu\text{mol quanta m}^{-2} \text{s}^{-1}$), provided by a LCD digital projector (EMP-1715; Epson, Suwa, Japan) for six hours, simulating the exposure to surface conditions following resurfacing. This light intensity is high enough to induce photosynthetic activity and promote upward migration of MPB, but low enough to avoid damaging light stress (Serôdio et al. 2006, Laviale et al. 2016). During this period, the photosynthetic activity of the cells in the newly exposed sediment surfaces was monitored by measuring Φ_{PSII} , the effective quantum yield of photosystem II (PSII), every 30 min. At the end of this period, the samples were used to quantify the Chl *a* and water content, as well as for determination of taxonomic composition (see below). Φ_{PSII} was measured using a Pulse Amplitude Modulated (PAM) fluorometer (WATER-EDDF-Universal PAM, Gademann Instruments; (Serôdio, 2004), using a 6 mm-diameter optical fiber to deliver measuring light and saturating pulses (peaking at 450 nm) and to capture the emitted fluorescence. Φ_{PSII} was determined by measuring steady state (F_s) and maximum (F_m') fluorescence levels ($\Phi_{PSII} = (F_m' - F_s)/F_m'$) (Genty et al. 1989). Three independent saturating pulses were applied to each sample by positioning the optical fiber at different non-overlapping areas (1 mm from the surface, 45°). The average Φ_{PSII} for each sample and time point was used in subsequent calculations. The variation of Φ_{PSII} over time during light exposure was described by a rate constant of Φ_{PSII} recovery, k_t (min^{-1}), estimated by fitting the following model:

$$\Phi_{PSII}(t) = \Phi_{PSII}(ss) + [\Phi_{PSII}(t_0) - \Phi_{PSII}(ss)]e^{-k_t t} \quad (1)$$

where $\Phi_{PSII}(t_0)$ and $\Phi_{PSII}(ss)$ are the PSII effective quantum yields at the beginning of the exposure (t_0) and after reaching a steady state.

In order to verify the source of the observed fluorescence signal at each depth, three additional cores were sliced and exposed to comparable light conditions (intensity and duration) using a second LCD digital projector (EB-X14; Seiko, Japan). The cells were harvested at the end of the experiment by carefully scraping off the uppermost surface layer. Samples were then fixed in Lugol's solution (concentrated, 5% Iodine, AppliChem GmbH, Germany) and stored at 4 °C. The abundance of the major photoautotroph taxonomic groups was examined using a Nageotte counting chamber (Marienfeld-Superior, Germany). Observed cells were grouped into three categories; diatoms, cyanobacteria, and

euglenoids. Cells that were not possible to identify were grouped as 'others' to avoid overestimation of abundance for other groups.

Subsurface vertical migration

To test the capacity of cells displaced to layers below the surface to migrate vertically, homogenized slurries were used to simulate a disturbance event such as bioturbation or resuspension/deposition. During low tide, sediment was collected from the top 1 cm using a spatula and deposited in a tray overnight in the laboratory. The following day, at the time coinciding with the beginning of low tide exposure in the field, the samples were thoroughly mixed using a spatula, and the homogenized slurries were poured into 24-wellplates as described in Frankenbach and Serôdio (2017). Immediately after the sample preparation, a first sampling was carried out by collecting surface samples of different thickness (of 0.1, 0.25, 0.5 and 1.0 mm-thick) using the cryo-sampling technique "crème brûlée" (Laviale et al., 2015). This procedure was repeated during the subjective low tide period, once at the time of the low peak tide in the field, and 90 min before and 90 min after that time. The sediment samples were immediately transferred into pre-weighted Eppendorf-caps and shock frozen in liquid N₂, and microalgal biomass was later quantified by measuring Chl *a* content. The changes in biomass at each depth interval allowed to follow the variation of biomass over time and along vertical profiles, with sub-millimeter resolution. Biomass present in each depth interval below the surface (0.1-0.25, 0.25-0.5 and 0.5-1.0 mm) was estimated by subtracting the Chl *a* content of a sample of a certain thickness from the Chl *a* content of the sample of thickness immediately higher. Three replicates were obtained for each time and depth interval. This experiment was carried out exclusively for samples from VA, as the communities from GE are dominated by epipsammic forms, and therefore not expected to show significant motility.

Vertical distribution of subsurface biomass

Vertical profiles of Chl *a* were measured in samples collected from the three sampling sites described above. Sediment cores (36 mm diameter, 20 cm long) were collected during low tide. The cores were sectioned into 5 mm-thick sections in the uppermost 20 mm, and 20 mm-thick from 20 mm down to 100 mm below the surface. Chl *a* depth profiles were quantitatively described by fitting a simple negative exponential model, based on the one proposed by Brotas and Serôdio (1995). The model used in the present study contains a

new parameter, C_d , representing the minimum background level approached by the Chl *a* content as depth increases:

$$C(z) = C_0 e^{-k_c z} + C_d \quad (2)$$

where $C(z)$ and C_0 are the Chl *a* content at any depth z and at the surface ($z = 0$), respectively, and k_c represents the rate constant of Chl *a* decay with depth. When fitting the model, the median depth of each sediment section was used as z . The model was used to calculate, for each type of sediment, the ratio of total biomass (including surface and subsurface) to surface biomass:

$$C_{sub,total} = \frac{\int_0^{z_t} C(z) dz}{\int_0^{z_s} C(z) dz} \quad (3)$$

where z_t is the maximum depth where Chl *a* was found (considered here as 10 cm) and z_s is the depth defining the 'surface' layers (here considered 5 mm). This ratio, the 'subsurface biomass fraction' (C_{sub}) allows to estimate the total, depth-integrated MPB biomass from surface biomass measurements (see below). C_{sub} was also calculated based on the 'viable' biomass, defined as the depth-integrated Chl *a* content present between the surface and the maximum depth at which significant recovery was observed following exposure to surface conditions:

$$C_{sub,viable} = \frac{\int_0^{z_v} C(z) dz}{\int_0^{z_s} C(z) dz} \quad (4)$$

where z_v is the maximum depth where potentially viable cells are present. z_v was determined from the results of the experiments on photosynthetic resilience (see above).

Ecosystem-level subsurface biomass fraction

The fraction of MPB subsurface biomass was estimated for the whole intertidal area of the Ria de Aveiro, considering the relationship between C_{sub} values and sediment type (granulometry) observed for the sampling sites and the distribution of granulometry throughout the intertidal areas of the estuary. Information on the grain size of the sediments of the Ria de Aveiro was obtained from Costa et al. (2018) and Plecha et al. (2014). The available data is the form of a D_{35} matrix, values that correspond to the size of particles where 35% of all particles have a lower diameter than the announced value. For the three sampling sites, the D_{35} values were 2.9×10^{-4} m (VA), 3.3×10^{-4} m (TO) and 6×10^{-5} m

(GE), respectively, meaning that sediments from GE have comparably larger particles (sandy) and VA the finest (muddy). The geographic information system software ArcGIS (ERSI, USA) was used to create a map of the lagoon under different tidal conditions, based on Google Earth's satellite imagery. Multiple images of different tidal cover situations were used to map the intertidal and subtidal areas of the estuary. For each intertidal area polygon constructed, the correspondent C_{sub} values were defined according with D_{35} data matrix. The software calculated the areas automatically, after the correct georeferencing.

Chlorophyll a quantification

The samples used for testing recovery of PSII functionality and vertical migration were extracted in 2 mL cold acetone (90%). For Chl *a* vertical profiles samples, the water content of three replicated cores was determined for each depth on additional replicates and the average value was used to calculate the volume of acetone (100%) to be added to achieve a final concentration of 90%. Chl *a* content is given as weight of Chl *a* per dry weight of sediment. The dry weight was determined by drying the samples at 120 °C for 24 h. In all cases, Chl *a* extraction was made in the dark, 4 °C for 24 h. Chl *a* concentration was calculated according to Lorenzen (1967). Extracts were centrifuged (10 min, 18000 g, 4 °C). The absorbance of the supernatant was measured at 664 and 750 nm before and after acidification (10 μ L, 1 N HCl), using a spectrophotometer (Thermo Spectronic, Rochester, NY, USA).

Statistical analysis

The Φ_{PSII} values measured at different depths and at the surface were compared by applying a two-tailed Student's *t*-test.

Results

Recovery of photosynthetic activity

The exposure of buried cells to surface conditions resulted in significant and relatively fast recovery of Φ_{PSII} in both types of sediments. However, the Φ_{PSII} recovery capacity varied markedly with depth and sediment type. In both types of samples, the initial values of Φ_{PSII} decreased with depth. In VA samples, $\Phi_{PSII}(t_0)$ decreased from 0.68 ± 0.03 at the surface to 0.46 ± 0.06 and 0.38 ± 0.02 at the depths of 2.0 and 4.0 cm, respectively (Fig.1a). During

light exposure, cells present at the surface showed only a slight increase in Φ_{PSII} , which stabilized at around 0.71 ± 0.02 within the first hour. On samples from deeper layers, light exposure caused substantial increases in Φ_{PSII} , up to 64% (4.0 cm deep, after 3 h) (Fig 1a). After 6 h of light exposure, Φ_{PSII} increased by about 0.4% (0.69 ± 0.007 surface), 8% (0.68 ± 0.021 0.5 cm) and 42% (0.65 ± 0.235 ; 2.0 cm), 56% (0.59 ± 0.026 ; 4 cm). For all depths, the steady state values of Φ_{PSII} were significantly lower than the ones at the surface (*t*-test, $P < 0.001$). Plotting the same data as a function of depth highlights how most of the recovery of Φ_{PSII} happened within the first 3 hours (Fig. 1b).

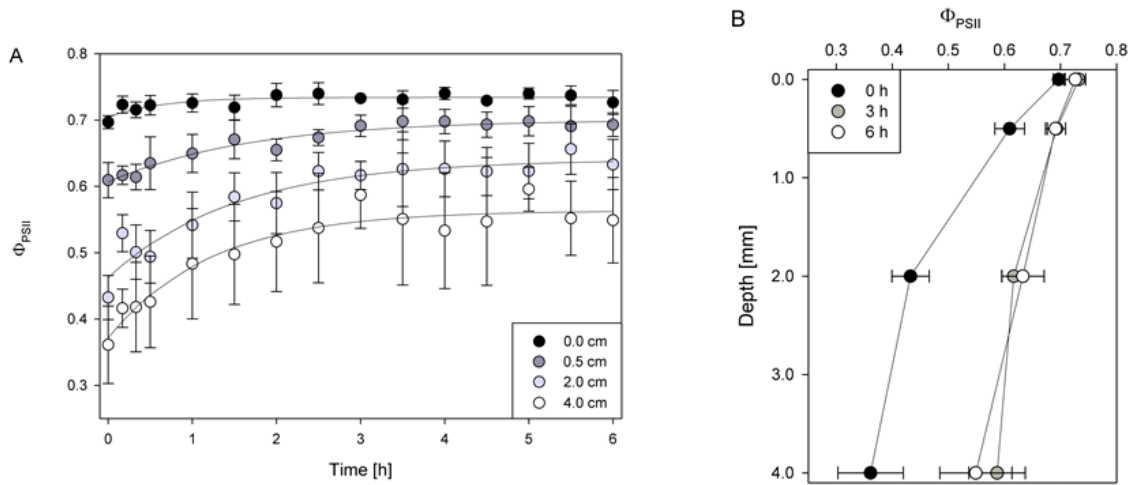


Figure 1. Recovery of PSII effective quantum yield (Φ_{PSII}) of samples collected at VA following exposure to surface conditions, for different depths. (A) Variation of Φ_{PSII} over time for four different depths. Lines represent the fitting of Eq. (1) to data collected for each depth. (B) Φ_{PSII} plotted against depths for three time points. Average of three independent measurements. Error bars indicate one standard error.

In contrast with VA samples, $\Phi_{PSII}(t_0)$ of GE samples was generally lower, although the variation with depth was less pronounced. Furthermore, the recovery of photosynthetic activity was essentially limited to the top 2.0 cm. Starting from values of $\Phi_{PSII} = 0.540 \pm 0.028$, surface samples showed a small increase to 0.620 ± 0.001 , reaching a steady state within the first hour of light exposure. At 2.0 cm, Φ_{PSII} increased 66%, from 0.20 ± 0.05 to 0.43 ± 0.019 in the first 90 min of light exposure, after which no further changes were observed (Fig. 2a). This was comparable to the increase of Φ_{PSII} observed for VA at 4.0 cm after 3 h of light exposure. Samples from deeper layers (4.5 and 6.0 cm) showed only a very small recovery of Φ_{PSII} from about 0.22 ± 0.01 to 0.26 ± 0.02 and 0.22 ± 0.03 to 0.26 ± 0.04 respectively, after 6 h of light exposure. Vertical profiles of Φ_{PSII} highlight how recovery was limited to the top layers, mostly to the layers 2.0 cm deep (Fig. 2b).

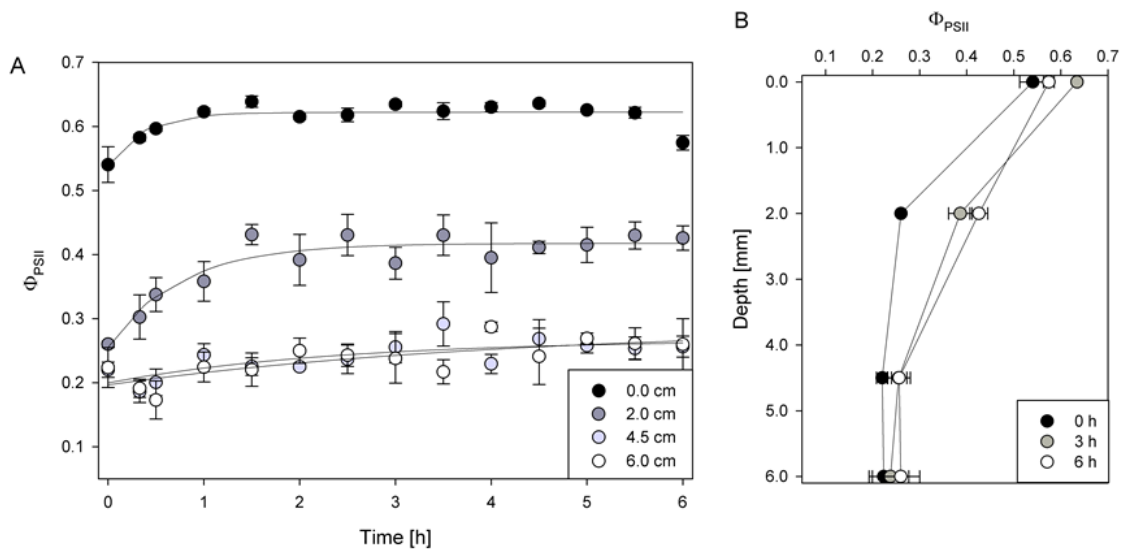


Figure 2. Recovery of PSII effective quantum yield (Φ_{PSII}) of samples collected at GE following exposure to surface conditions, for different depths. (A) Variation of Φ_{PSII} over time for four different depths. Lines represent the fitting of Eq. (1) to data collected for each depth. (B) Φ_{PSII} plotted against depths for three time points. Average of three independent measurements. Error bars indicate one standard error.

The different recovery capacity of VA and GE samples is confirmed by the rate constant of Φ_{PSII} , k_t , and its variation with depth (Fig. 3). While for GE, k_t reaches high values ($> 1.25 \text{ min}^{-1}$ for surface and depth 2.0 cm) and decreases considerably with depth, for VA samples k_t remained below 1.0 min^{-1} , and varied much less with increasing depth.

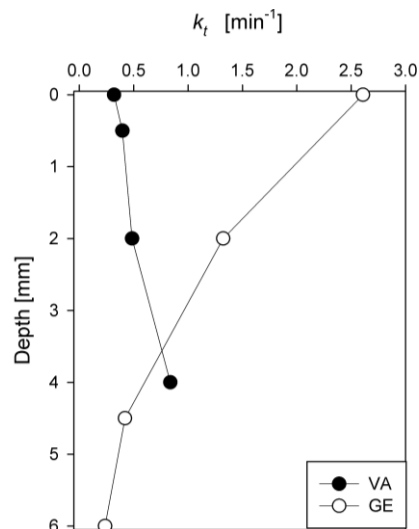


Figure 3. Variation with depth of the rate constant of Φ_{PSII} recovery (k_t) for samples collected at VA and GE.

The relative distribution of the main taxonomic groups with depth is shown in Fig. 4. Both VA and GE samples showed a clear dominance of diatoms at all depths, with the minimum diatom abundance being observed for GE samples at 6.0-6.5 cm with

$72 \pm 4.28\%$. Cyanobacteria were present in almost all samples (the exception GE samples, at 6.0 cm) and euglenoids were observed only in VA samples.

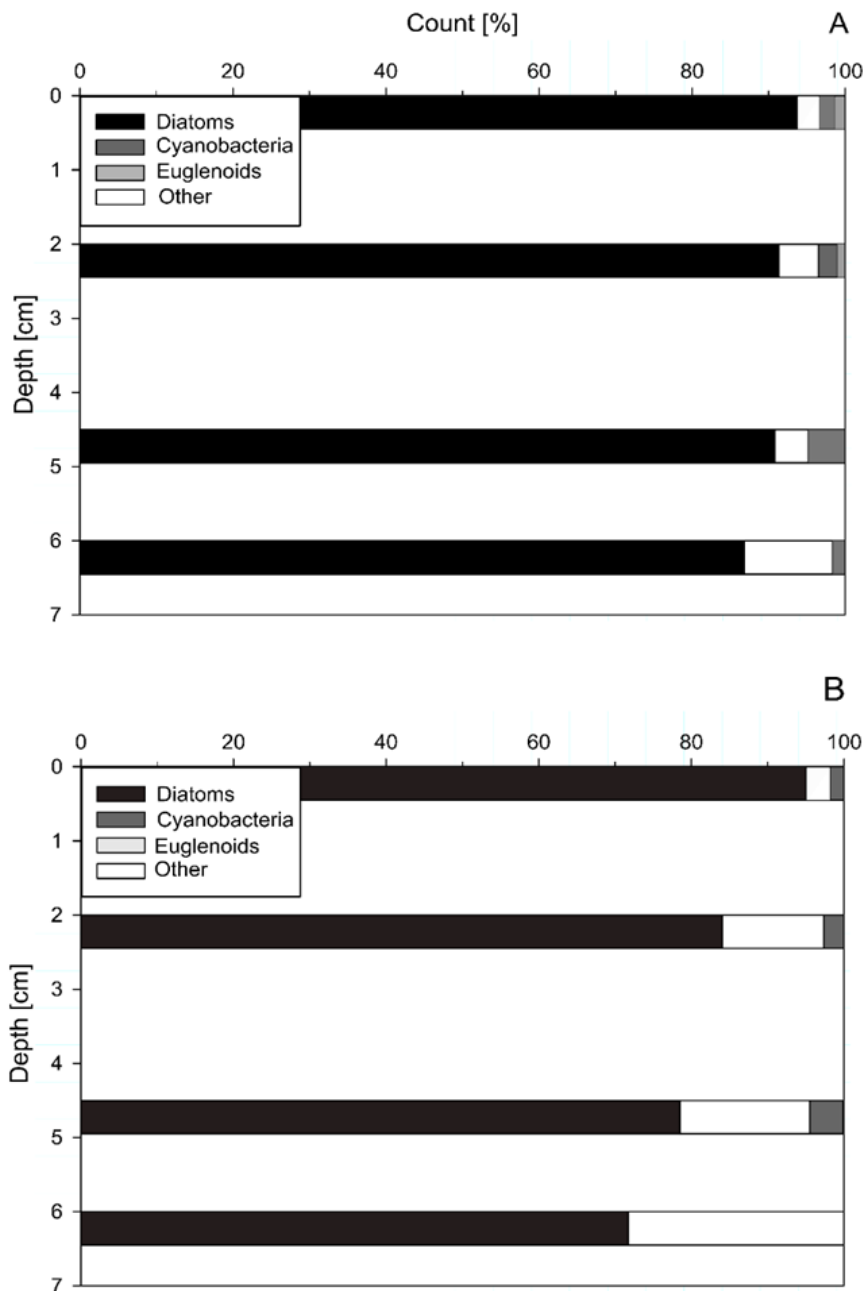


Figure 4. Variation with depth of the relative abundance of three main taxonomical groups (diatoms, cyanobacteria and euglenoids) in sampling sites VA (A) and GE (B). Cells categorized as 'other' were in most cases unidentified.

Subsurface vertical migration

Fig. 5 shows the results of two independent experiments following the variation of sub-millimeter vertical profiles of Chl *a* concentration during a low tide period. In both cases, a clear surface accumulation of microalgal biomass was observed in all sampled depths, but mainly above 0.4 mm. On some occasions, a subsurface maximum was observed, denoting the upward movement of cells toward the surface. Although the experiments started from homogenized slurries, already in the first sampling occasion some cell accumulation towards the surface was observed, indicating that vertical migration towards the surface started immediately after the homogenization of the sediment. Maximum Chl *a* concentrations (308.9 and 275.7 $\mu\text{g mm}^{-3}$) were reached at the time coinciding with the time of low tide in the field, which was 3 h after the start of the experiment. Thereafter, a downward bulk movement appeared to have started, corresponding to the downward migration anticipating the incoming tide in the field. In both experiments, the total Chl *a* in the uppermost 1 mm increased over time, denoting the accumulation of cells originating from deeper layers due to vertical migration occurring below the surface (Fig. 5).

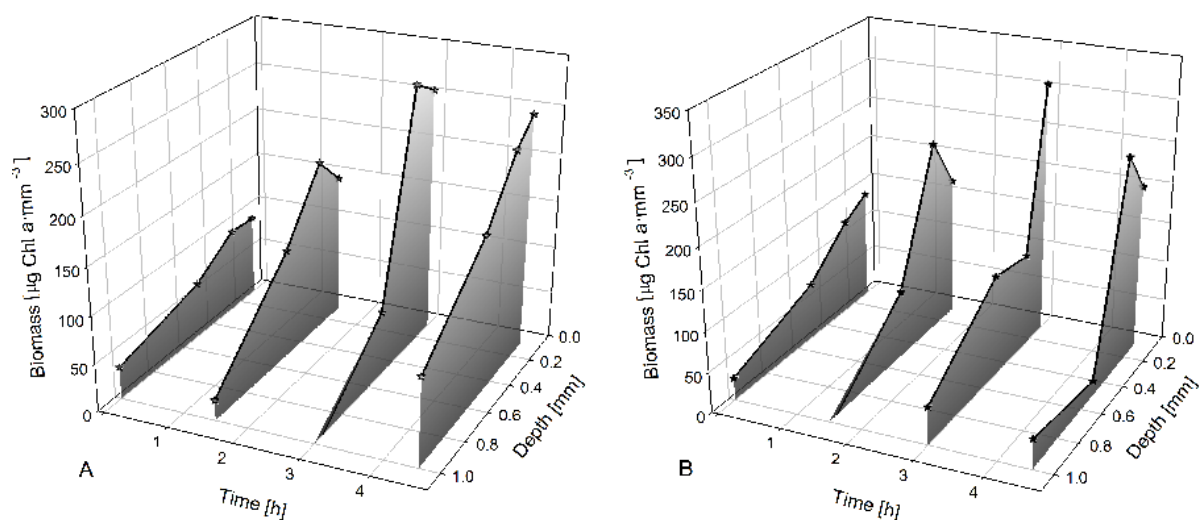


Figure 5. Variation of sub-millimeter scale Chl *a* vertical profiles over the time course of a diurnal low tide exposure. Panels A and B refer to two independent experiments. Average of three independent samples.

The two experiments differed such that in the latter (Fig. 5B), the total Chl *a* reached a maximum and started to decrease before the end of the measuring period, while in the former (Fig. 5A) it continued to increase throughout the whole sampling period (Fig. 6).

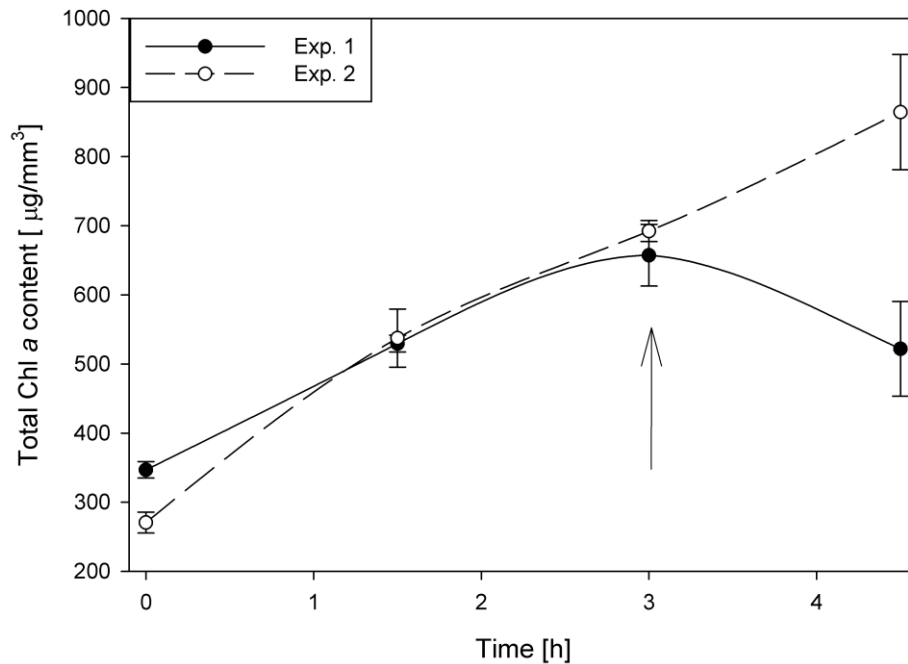


Figure 6. Depth-integrated Chl *a* content over the time course of a diurnal low tide exposure, during two independent experiments (from data shown in Fig. 5). Arrow indicates the low tide peak at the corresponding sampling side.

Vertical distribution of MPB biomass

Sediment cores sampled in VA showed the highest Chl *a* content at the surface, averaging $28.4 \pm 1.93 \mu\text{g Chl } a \text{ g}^{-1}$, which gradually decreased with depth to a minimum of $4.0 \pm 0.96 \mu\text{g Chl } a \text{ g}^{-1}$ at 10 cm (Fig. 7a). The lowest surface Chl *a* content was measured in GE samples, reaching only $5.5 \pm 1.58 \mu\text{g Chl } a \text{ g}^{-1}$, and decreasing to a minimum of $0.90 \pm 0.31 \mu\text{g Chl } a \text{ g}^{-1}$ at the depth of 10 cm (Fig. 7c). Sediment cores sampled in TO showed intermediate values, reaching $15.85 \pm 2.22 \mu\text{g Chl } a \text{ g}^{-1}$ at the surface and minimum values of $4.57 \pm 1.58 \mu\text{g Chl } a \text{ g}^{-1}$ at 10 cm (Fig. 7b). In all cases, the decrease with depth followed a negative exponential-like pattern, which enabled a very good fit of Eq. (2) ($r^2 > 0.96$ in all cases) and estimation of parameters C_0 , k_C , and C_d for each type of sediment (Fig. 7). The values of k_C were similar in VA and GE samples (1.11 and 1.26 cm^{-1} , respectively), despite the large difference in Chl *a* content of the two profiles (Fig. 7). The TO samples showed an intermediate Chl *a* content and a much lower rate of decrease ($k_C = 0.53 \text{ cm}^{-1}$), indicating a more vertically homogeneous profile. In all cases, the profiles tend to a non-null constant Chl *a* content level (C_d).

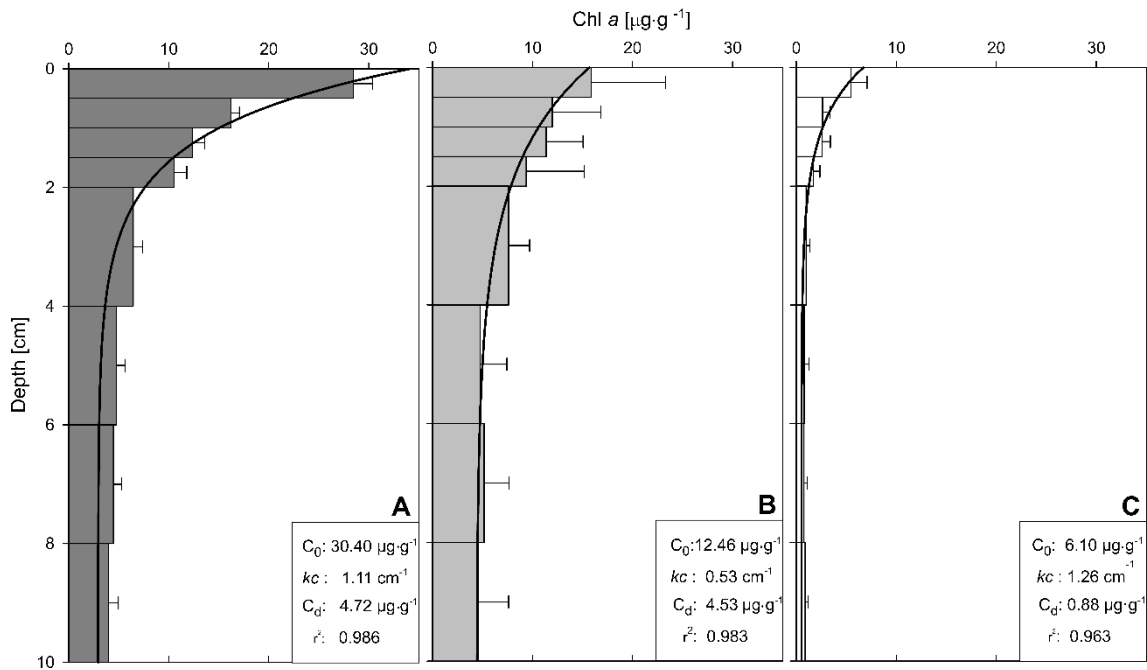


Figure 7. Depth profiles of Chl a content in the three sampling sites VA (A), TO (B) and GE (C). Line represents the fitting of Eq. (2). The estimated values of the parameters of Eq. (2) C_0 , k_C , and C_d are shown. Average Chl a concentration of nine sediment cores. Error bars indicate one standard error.

Using the estimates of the parameters C_0 , k_C , and C_d for each site, the subsurface fraction $C_{sub,total}$ was calculated by applying Eq. (3), resulting in the following values: 4.95 (VA), 5.17 (TO) and 2.96 (GE). These values indicate that the surface MPB biomass (0-5 mm depth range) only accounts for around one fifth to one third of the total MPB biomass present in the sediment (considered down to 10 cm). The subsurface fraction for potentially viable biomass was calculated by applying Eq. (4), and, considering the values for z_v of 3.0 cm (VA) and 2.0 cm (TO, GE), resulted in the following values: 3.14 (VA), 2.30 (TO) and 1.92 (GE). These results indicate that the proportion of subsurface MPB biomass capable of regaining photosynthetic activity after surfacing reaches roughly 2-3 times the biomass present in the top 5 mm.

Ecosystem-level subsurface biomass fraction

Making use of the known distribution of sediment granulometry and of the C_{sub} values for the sampled sediments, maps of the spatial distribution of the fraction of total and viable subsurface MPB biomass were produced (Fig. 8). These maps allowed classifying the intertidal areas according to the relative amount of subsurface MPB biomass. By calculating the total area of each type of sediment and corresponding C_{sub} values, spatially-weighted

averages for subsurface biomass fraction for the entire Ria de Aveiro was estimated: 3.78 for $C_{sub,total}$ and 2.14 for $C_{sub,viable}$.

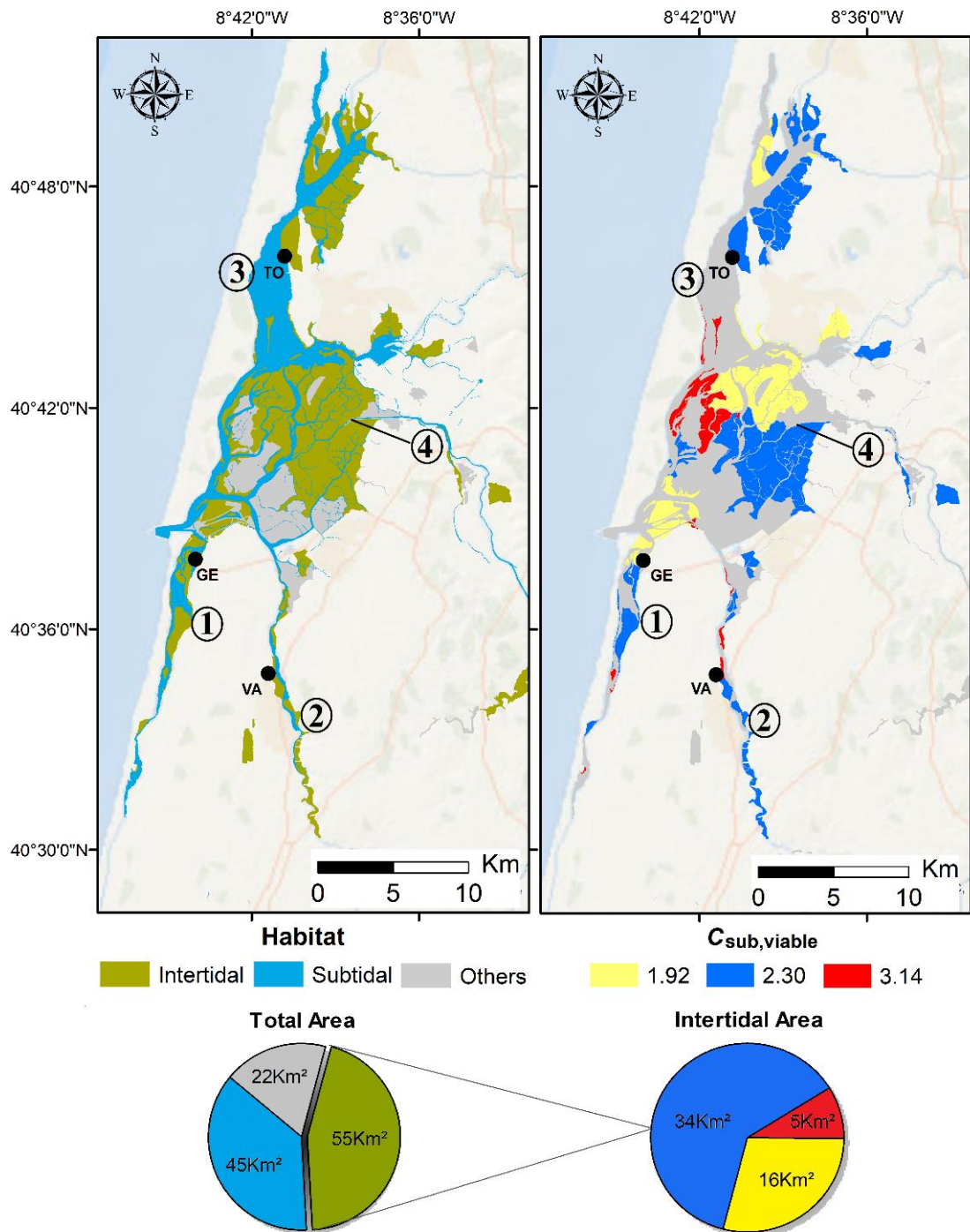


Figure 8. Classification of the intertidal areas Ria de Aveiro regarding the ratios of total biomass and of total viable biomass to surface biomass ($C_{sub,total}$ and $C_{sub,viable}$, respectively). Values of $C_{sub,total}$ and $C_{sub,viable}$ determined for each intertidal habitat were applied to the total intertidal area. Numbers identify the main channels: Mira Channel (1) Ilhavo Channel (2), São Jacinto Channel (3), Espinheiro Channel (4).

Discussion

Photosynthetic resilience

This study showed that buried MPB cells can regain PSII functionality shortly after being exposed to surface conditions, although it varied between the two sediment types. These results expand the findings of Wasmund (1989) on subtidal MPB, which demonstrated that buried microalgae are able to fix CO₂ after exposure to light in one sediment sample. The present study includes, however, photosynthetic recovery kinetics in muddy and sandy sediments inhabiting MPB. Samples from muddy sediments (VA) showed that the capacity to recover was extended to deeper layers than those of the sandy site GE. The capacity to recover was related to the initial physiological status at each depth, as initial Φ_{PSII} levels decreased with depth. Cell viability was seen to decrease with depth in both sampling sites, and cells found in deeper layers can be thought to have spent longer periods away from the surface. The idea that cells from GE spend more time buried may contradict what is expected from the fact that muddy sediments are typically more cohesive than sandier ones. However, its distinct life form (no motile, epipsammic in sandy, vs motile eipipelic forms in dominated in muddy sediments) might be part of the explanation. Furthermore, surface biomass in VA was higher than in GE, thus may have been less prone to resurface buried cells by vertical mixing (Delgado et al., 1991). However, the higher k_C values observed for GE samples, representing a steeper vertical variation in Chl *a*, is indicative of a lower degree of vertical mixing. When exposed to photosynthesis-promoting conditions, buried MPB cells recovered PSII activity in a relatively short period (3 h), but only to a fraction of the Φ_{PSII} values observed at the surface. It may be hypothesized that the recovery of the photosynthetic activity occurs in a two-step process: the described fast induction leading to intermediate, depth-dependent Φ_{PSII} levels, being followed by a longer acclimation process leading to the full recovery of Φ_{PSII} to values comparable to those at the surface.

Viable cells were found at depths considerably larger (cm-scale) than the depth of the photic zone or its vicinity (sub-millimeter scale). Together with the ability to regain PSII functionality within 3h, demonstrates its ecological relevance. This buried fraction of MPB biomass allows to act as a reservoir for replacing cells at the surface which may be suddenly removed by resuspension or grazing. This could attenuate fluctuations in the productive biomass formed by microalgal cells present in the photic zone. This in turn may contribute to increase the resilience of MPB communities in face of external perturbations, and to

reinforce the role of MPB as source of cells for phytoplankton (Barnett et al., 2015; Guarini et al., 2004; Lewis et al., 1999).

This functional resilience requires that benthic diatoms (i) can survive for long periods in darkness and in anoxia and (ii) maintain the capacity to promptly resume photosynthetic activity. There is solid experimental evidence that some diatoms can survive long periods of darkness (Antia and Cheng, 1970; Itakura et al., 1997; Murphy and Cowles, 1997; Peters and Thomas, 1996; Reeves et al., 2011; Smayda and Mitchell-Innes, 1974). Already in the 1970s (Antia and Cheng, 1970) it was found that *Phaeodactylum tricornutum* was able to survive up to six months in the dark, with a few individuals surviving up to 17 months. Subsequent studies have confirmed that planktonic centric diatoms species were also capable of withstanding long dark periods. *Thalassiosira antarctica*, *T. tunida* and *Proboscis inermis* were shown to survive from four to nine months in the dark, maintaining high levels of photosynthesis during the first three months (Peters and Thomas, 1996).

Survival in darkness or while buried is supported by the formation of morphological unchanged resting cells (Jewson et al., 2006; McQuoid and Hobson, 1996), or sporulation (Sugie and Kuma, 2008). The latter was shown by both laboratory (Durbin, 1978; Jochem, 1999; Lewis et al., 1999) and field studies, using diatoms from deep sea (Cahoon et al., 1995; Wasmund, 1989), Antarctic sediments (Wulff, 2008), or the alteration of the gene expression level of the LHCx family as described by Nymark et al., (2013). Diatoms thus have the capacity to live heterotrophically, enabling survival based on organic energy sources (Kamp et al., 2011; Lewin, 1953; McMinn and Martin, 2013; Schaub et al., 2017; Tuchman et al., 2006). Facultative heterotrophy of diatoms is a long-known mechanism enabling survival in the absence of light (Lewin, 1953). Although it seems more common among pennate, benthic forms (Lewin and Hellebust, 1970; Rivkin and Putt, 1987), it was shown to also occur in centric diatoms (Kamp et al., 2013; White, 1974). Peters, (1996) suggested a re-utilization of organics derived from senescent members of the population, which is a plausible scenario in the case of buried MPB populations.

The reactivation of photosynthetic activity of diatoms after prolonged dark periods has also been shown to occur in a variety of conditions and for different species. The pennate species *P. tricornutum* and several other diatom species are able to resume growth in light after 24 to 68 weeks in the dark (Antia and Cheng, 1970), and ice diatoms are able to resume photosynthetic activity after 64 days in darkness (Wulff et al., 2008). The fast recovery of photosynthetic activity seems to be based on the ability of diatoms to maintain a functional photosynthetic apparatus during dark periods (Nymark et al., 2013), supported by a very slow degradation of photosynthetic pigments during long periods of darkness and

anoxia (Jewson et al., 2006; Kamp et al., 2013; Larson and Sundbäck, 2012; Wasmund, 1989).

The significance of buried MPB regaining its photosynthetic activity presented in this study nevertheless is limited in two main ways: first, they do not provide any indication on how long the cells had been buried before being exposed to light and air. This makes it difficult to compare the results with ones performed under controlled laboratory conditions (e.g. known time of darkness), or to relate the rates of vertical decrease of Chl *a* with temporal processes. A second limitation regards the fact that the techniques used cannot determine the fraction of buried cells that remain viable, as chlorophyll fluorescence indices like Φ_{PSII} are largely independent of the absolute number of photosynthetic cells. Therefore, it will only detect signals emitted from functional cells, even if present in small numbers (Franklin et al., 2009).

Subsurface vertical migration

Vertical migration by benthic pennate diatoms in tidal sediments has been extensively studied (Coelho et al., 2011; Consalvey et al., 2004; Easley et al., 2005; Herlory et al., 2004; Janssen et al., 1999; Round, 1979; Underwood et al., 2005). The migratory behavior of pennate diatoms is partially controlled by endogenous rhythms, responsible for triggering movement in the absence of external stimuli (Coelho et al., 2011; Frankenbach et al., 2014). Most studies have been centered on the effects of vertical migration on surface MPB biomass as a main factor controlling the photosynthetic biomass in the photic zone, and thus the instantaneous rates of carbon fixation (Serôdio et al., 2001). In comparison, only a few studies have addressed the occurrence of vertical migration below the photic zone and the changes in mm-scale Chl *a* vertical profiles over time (Du et al., 2010b; Kingston, 1999; Pinckney et al., 1994).

The present work introduced the quantification of Chl *a* profiles with sub-millimeter vertical resolution to monitor fluxes of microalgal biomass between the photic zone and subsurface layers. This technique demonstrated that subsurface vertical migration can contribute to ‘reinoculate’ the photic zone. This is of great importance after a significant disturbance (bioturbation, resuspension/deposition) causing the removal of cells from the surface layers. As an increase over time of depth-integrated biomass in the 0-1.0 mm depth interval was observed (Fig. 5), migration seems to occur at layers deeper than those sampled. Therefore, it is possible that support that cells buried down to several millimeters below the surface may reach the photic zone not only passively, as via

resuspension/deposition, but as well actively, due to vertical migration. Although light incident at the sediment surface may have stimulated the upward migration of diatoms present in the illuminated layers, endogenous behavior likely played a role as well, because cells at depths of 1.0 mm may already be in the dark due to the strong light attenuation in such fine sediments.

Earlier studies have measured vertical speeds of diatom migration between 0.17 and 0.28 $\mu\text{m s}^{-1}$ in natural sediment (Consalvey et al., 2004). Considering that upward migration may start more than four hours before the low tide and light exposure (Coelho et al., 2011; Frankenbach et al., 2014), motile diatoms could cover a vertical distance of about 3.2 mm along one low tide event.

Vertical distribution of subsurface biomass

Significant amounts of microalgal Chl *a* can be found at depths of several centimeters below the sediment surface (De Jonge and Colijn, 1994; Du et al., 2010a; Kingston, 1999; Sun et al., 1991). Most of these works quantified continuous cm-scale vertical profiles of Chl *a* of MPB, from the surface to depths often greater than those tested in the present study (10 cm) (Steele and Baird, 1968). The simple first-order exponential model of Eq. (2) captured the main features of the vertical distribution of Chl *a* in all studied sediments (De Jonge and Colijn, 1994; Delgado et al., 1991; Du et al., 2010b; Sun et al., 1991; Weiqiu et al., 2013). The fitting of the model to experimental data was found to be significantly improved by adding a term for background biomass. This does not exclude however that this basal level (ranging from 0.88 to 4.72 $\mu\text{g Chl } a \text{ g}^{-1}$) may not remain constant with depth and may tend to zero in deeper vertical profiles.

The estimated depth-integrated biomass decreased with increasing grain size (highest in VA and lowest in GE, intermediate values for TO), confirming earlier studies where Chl *a* profiles were compared between muddy and sandy sediments and where MPB biomass was consistently found to be higher in the former than the latter (Brotas and Serodio, 1995; Jack J. Middelburg et al., 2000). The fitting of Eq. (2), and particularly the estimation of the decay rate k_C , allows comparing the various sites regarding the shape of the vertical Chl *a* profile. Based on the estimates of the decay rate k_C and of background biomass, C_d , two different patterns emerged. Despite showing very different absolute values at the surface, samples from VA and GE showed similar vertical decay rates (1.11 and 1.26 cm^{-1} , respectively), while the value estimated for TO was substantially lower ($k_C = 0.52 \text{ cm}^{-1}$). It is evident by comparing the ratio of surface biomass to C_d of VA and TO that sediments

from TO appear to conceal more biomass below the surface. While surface biomass in VA was about twice as high as in TO, C_d values were similar (4.46 to 4.42 $\mu\text{g g}^{-1}$ for VA and TO, respectively). The steepness of Chl *a* gradients is expected to decrease with mixing and increase with Chl *a* degradation (Middelburg et al., 2000; Sun et al., 1991). As such, the steeper profile observed in VA and GE may be due to lower mixing or higher pigment degradation. The observed differences may also be explained by different impacts of resuspension, as previously shown (Middelburg et al., 2000; Sun et al., 1991). Considering the data available for the Ria de Aveiro on sediment granulometry (Plecha et al., 2014), bathymetry (Dias et al., 2003; Vargas et al., 2017), and water velocity (Lopes and Dias, 2015), the results match the prediction that sediments in GE are mixed up more thoroughly than in VA.

Application of Eq. (2) also evaluated the fraction of subsurface Chl *a*, to our knowledge not done in previous studies which characterized cm-scale vertical profiles of Chl *a* in estuarine or marine sediments (Du and Chung, 2009; Weiqiu et al., 2013). The proportion of MPB biomass below the surface layers was found to reach substantial values, as indicated by the large $C_{sub,total}$ values that were estimated, which ranged from close to 3 (GE) to values around 5 (VA and TO). These values may, however, be considered conservative estimates, since they are based on relatively short vertical profiles (0-6 cm deep, when Chl *a* has been reported to be found at deeper layers), and because 'surface' biomass was considered the top 5 mm depth interval, a depth range clearly much larger than the actual photic zone, which even for the sandy site should not exceed 1-2 mm.

Based on the results of this study, the MPB can be categorized into three functional layers, i) a 'canopy', formed by the cells at the uppermost layers, which are photosynthetically active, and therefore actively contributing to primary production, ii) a 'cell reserve', formed by cells capable to quickly replace the ones in the surface layer through vertical migration, within minutes to a few hours, and iii) a large repository of cells serving as a 'backup' but also acting as a carbon sink.

Ecosystem-level subsurface biomass and 'blue carbon' budgets

The proportion of total:subsurface MPB biomass (here quantified as $C_{sub,total}$) may be used to estimate the amount of potentially productive subsurface biomass from available surface values. Traditionally, MPB 'surface' biomass has been measured by sampling the top layers of sediment, in the range 2-10 mm (Du and Chung, 2009; Kelly et al., 2001), when studies target to measure the biomass implicated in primary productivity (Laviale et

al., 2015; MacIntyre and Cullen, 1995; Serôdio et al., 2001; Taylor and Paterson, 1998). More recently, optical methods such as remote sensing, based on reflectance measurements or solar-induced fluorescence became an extensively used method to estimate Chl *a* concentrations and create km-scale maps of MPB biomass and annual rates of primary production (Benyoucef et al., 2014; Bouman et al., 2017; Combe et al., 2005; Daggars et al., 2018; Huete et al., 2015; Kazemipour et al., 2012; Ryu et al., 2014; van der Wal et al., 2010). Thus, 'observable' MPB biomass is limited to the top surficial layers of sediment, missing an important fraction of standing stock of MPB biomass. Upscaling of local estimates of the fraction of Chl *a* present below the surface to the whole intertidal area of the Ria de Aveiro confirmed the relevance of the subsurface MPB biomass at the ecosystem level. In what can be a conservative estimate, the spatially-weighted average of $C_{\text{sub,total}}$ reached 3.78, indicating that more than 3/4 of the MPB biomass in the top 10 cm is sub-superficial. Considering only the potentially resilient biomass, the subsurface fraction is still substantial, with spatially-weighted $C_{\text{sub,viable}}$ reaching a value above 2.

The quantification of MPB subsurface biomass is relevant in the context of the ongoing discussion on the importance of unvegetated estuarine intertidal areas as contributors of ecosystem-level 'blue carbon' budgets (Oakes and Eyre, 2014; Oreska et al., 2018). Although the estimates in the present study were based on Chl *a* and not directly on carbon content, being therefore more closely related to the content in particulate organic carbon, the produced results clearly support the idea that 'naked sediments' colonized by MPB are major contributors to ecosystem-level blue carbon. As more than half of the intertidal area of the Ria de Aveiro are unvegetated sediments, the present results support several recent studies raising awareness for the role of these areas as major sites of blue carbon location (Oakes and Eyre, 2014; Oreska et al., 2018). As recognized by Wolanski et al. (2009), unvegetated estuarine areas have received much less attention than vegetated areas (seagrass beds, saltmarshes, mangroves). However, recent studies using ^{13}C *in situ* labeling experiments showed that most sediment organic carbon is derived by MPB in both vegetated and unvegetated coastal habitats, and therefore contributed to the overall sediment organic contribution (Oakes and Eyre, 2014; Oreska et al., 2018). Furthermore, the findings of this study also show that, not only is there a significant amount of microalgal-associated carbon that is 'captured and hold' (configuring the 'blue carbon' paradigm), but that this biomass stored in the sediments is (at least partially) photosynthetically functional, being readily mobilizable to carry out additional carbon fixation. The results of this study show that the large amounts of MPB biomass in sub-photic layers are likely an important contributor to productive biomass, replenishing surface levels

and attenuating effects of local disturbances, and function not merely as primary producers but also as a major carbon sink.

Acknowledgements

This work was supported by the Fundação para a Ciência e a Tecnologia (FCT), through doctoral fellowship SFRH/BD/86788/2012 to S. Frankenbach and by CESAM (UID/AMB/50017 – POCI-01-0145- FEDER-007638), FCT/MCTES through national funds (PID- DAC), and the co-funding by the FEDER, within the PT2020 Partnership Agreement and Compete 2020. We thank William Schmidt for revising the manuscript, and two anonymous reviewers for their critical comments.

References

- Admiraal, W., 1984. The ecology of estuarine sediment-inhabiting diatoms. *Prog. Phycol. Res.* 3, 269–322.
- Almeida, P.R., Moreira, F., Costa, J.L., Assis, C.A., Costa, M.J., 1993. The feeding strategies of *Liza ramada* (Risso, 1826) in fresh and brackish water in the River Tagus, Portugal. *Journal of Fish Biology. J. Fish Biol.* 42, 95–107.
- Antia, N.J., Cheng, J.Y., 1970. The survival of axenic cultures of marine planktonic algae from prolonged exposure to darkness at 20°C. *Phycologia* 9, 179–183.
- Armbrust, E.V., 2009. The life of diatoms in the world's oceans. *Nature* 459, 185–92.
- Barnett, A., Méléder, V., Blommaert, L., Lepetit, B., Gaudin, P., Vyverman, W., Sabbe, K., Dupuy, C., Lavaud, J., 2015. Growth form defines physiological photoprotective capacity in intertidal benthic diatoms. *ISME J.* 9, 32–45.
- Benyoucef, I., Blandin, E., Lerouxel, A., Jesus, B., Rosa, P., Méléder, V., Launeau, P., Barillé, L., 2014. Microphytobenthos interannual variations in a north-European estuary (Loire estuary, France) detected by visible-infrared multispectral remote sensing. *Estuar. Coast. Shelf Sci.* 136, 43–52.
- Bondoc, K.G. V., Lembke, C., Lang, S.N., Germerodt, S., Schuster, S., Vyverman, W., Pohnert, G., 2018. Decision-making of the benthic diatom *Seminavis robusta* searching for inorganic nutrients and pheromones. *ISME J.*
- Bouman, H.A., Platt, T., Doblin, M., Figueiras, F.G., Gudfinnsson, H.G., Huang, B., Hickman, A., Jackson, T., Lutz, V.A., Rey, F., Pepin, P., Segura, V., Tilstone, G.H., Dongen-Vogels, V. Van, 2017. Photosynthesis-irradiance parameters of phytoplankton: synthesis of a global data set marine. *Earth Syst. Sci. Data Discuss.* 251–266.
- Brito, A., Newton, A., Tett, P., Fernandes, T.F., 2009. Temporal and spatial variability of microphytobenthos in a shallow lagoon: Ria Formosa (Portugal). *Estuar. Coast. Shelf Sci.* 83, 67–76.
- Brotas, V., Serodio, J., 1995. A mathematical model for the vertical distribution of chlorophyll *a* in estuarine intertidal sediments. *Netherlands J. Aquat. Ecol.* 29, 315–321.
- Bueno-Pardo, J., García-Seoane, E., Sousa, A.I., Coelho, J.P., Morgado, M., Frankenbach, S., Ezequiel, J., Vaz, N., Quintino, V., Rodrigues, A.M., Leandro, S., Luis, A., Serôdio, J., Cunha, M.R., Calado, A.J., Lillebø, A., Rebelo, J.E., Queiroga, H., 2018. Trophic web structure and ecosystem attributes of a temperate coastal lagoon (Ria de Aveiro, Portugal). *Ecol. Modell.* 378, 13–25.

- Cahoon, L.B., 1999. The role of benthic microalgae in neritic ecosystems. *Oceanogr. Mar. Biol. an Annu. Rev.* 37, 47–86.
- Cahoon, L.B., Lawst, R.A., Thomas, C.J., 1995. Viable diatoms and chlorophyll a in continental slope sediments off Cape Hatteras, North Carolina. *Deep. Res. II* 41, 767–782.
- Cartaxana, P., Ruivo, M., Hubas, C., Davidson, I., Serôdio, J., Jesus, B.M., 2011. Physiological versus behavioral photoprotection in intertidal epipelagic and epipsammic benthic diatom communities. *J. Exp. Mar. Bio. Ecol.* 405, 120–127.
- Coelho, H., Vieira, S., Serôdio, J., 2011. Endogenous versus environmental control of vertical migration by intertidal benthic microalgae. *Eur. J. Phycol.* 463, 271–281.
- Combe, J.P., Launeau, P., Carrère, V., Despan, D., Méléder, V., Barillé, L., Sotin, C., 2005. Mapping microphytobenthos biomass by non-linear inversion of visible-infrared hyperspectral images. *Remote Sens. Environ.* 98, 371–387.
- Consalvey, M., Paterson, D.M., Underwood, G.J.C., 2004. The ups and downs of life in a benthic biofilm: Migration of benthic diatoms. *Diatom Res.* 19, 181–202.
- Costa, S., Picado, A., Vaz, N., Coelho, C., Portela, L., Dias, J.M., 2018. Climate change effects on suspended sediment dynamics in a coastal lagoon: Ria de Aveiro (Portugal). *J. Coast. Res.* 85, 521–525.
- Daggers, T.D., Kromkamp, J.C., Herman, P.M.J., van der Wal, D., 2018. A model to assess microphytobenthic primary production in tidal systems using satellite remote sensing. *Remote Sens. Environ.* 211, 129–145.
- De Jonge, V.N., Colijn, F., 1994. Dynamics of microphytobenthos biomass in the Ems Estuary. *Mar. Ecol. Prog. Ser.* 104, 185–196.
- De Jonge, V.N., van Beusekom, J.E.E., 1995. Wind- and tide-induced resuspension of sediment and microphytobenthos from tidal flats in the Ems estuary. *Limnol. Oceanogr.* 40, 776–778.
- Delgado, M., de Jonge, V.N., Peletier, H., 1991. Experiments on resuspension of natural microphytobenthos populations. *Mar. Biol.* 108, 321–328.
- Dias, J.M., Lopes, J.F., Dekeyser, I., 2003. A numerical system to study the transport properties in the Ria de Aveiro lagoon. *Ocean Dyn.* 53, 220–231.
- Dias, J.M., Lopes, J.F., Dekeyser, I., 1999. Hydrological characterisation of Ria de Aveiro, Portugal, in early summer. *Oceanol. Acta* 22, 473–485.
- Du, G.Y., Chung, I.K., 2009. Estimating areal production of intertidal microphytobenthos based on spatio-temporal community dynamics and laboratory measurements. *Ocean Sci. J.* 44, 189–197.

- Du, G.Y., Oak, J.-H.H., Li, H., Chung, I.-K.K., 2010a. Effect of light and sediment grain size on the vertical migration of benthic diatoms. *Algae* 25, 133–140.
- Du, G.Y., Son, M., An, S., Chung, I.K., 2010b. Temporal variation in the vertical distribution of microphytobenthos in intertidal flats of the Nakdong River estuary, Korea. *Estuar. Coast. Shelf Sci.* 86, 62–70.
- Durbin, E.G., 1978. Aspects of the biology of resting spores of *Thalassiosira nordenskiöldii* and *Detonula confervacea*. *Mar. Biol.* (1978) 45: 31.
- Easley, J.T., Hymel, S.N., Plante, C.J., 2005. Temporal patterns of benthic microalgal migration on a semi-protected beach. *Estuar. Coast. Shelf Sci.* 64, 486–496.
- Fenchel, T., Straarup, B.J., 1971. Vertical distribution of photosynthetic pigments and the penetration of light in marine sediments. *Oikos*, 22, 172–182.
- Field, C.B., 1998. Primary production of the biosphere: integrating terrestrial and oceanic Components. *Science*. 281, 237–240.
- Frankenbach, S., Pais, C., Martinez, M., Laviale, M., Ezequiel, J., Serôdio, J., 2014. Evidence for gravitactic behaviour in benthic diatoms. *Eur. J. Phycol.* 49, 429–435.
- Frankenbach, S., Serôdio, J., 2017. One pulse, one light curve: Fast characterization of the light response of microphytobenthos biofilms using chlorophyll fluorescence. *Limnol. Oceanogr. Methods* 15, 554–566.
- Franklin, D.J., Choi, C.J., Hughes, C., Malin, G., Berges, J.A., 2009. Effect of dead phytoplankton cells on the apparent efficiency of photosystem II. *Mar. Ecol. Prog. Ser.* 382, 35–40.
- Guarini, J.M., Gros, P., Blanchard, G., Richard, P., Fillon, A., 2004. Benthic contribution to pelagic microalgal communities in two semi-enclosed, European-type littoral ecosystems (Marennes-Oléron Bay and Aiguillon Bay, France). *J. Sea Res.* 52, 241–258.
- Hagerthey, S.E., Defew, E.C., Paterson, D.M., 2002. Ulvae on Intertidal Benthic Diatom Assemblages Under Different Nutrient and Temperature Regimes. *Mar. Ecol. Prog. Ser.* 245, 47–59.
- Herlory, O., Guarini, J.M., Richard, P., Blanchard, G.F., 2004. Microstructure of microphotobenthic biofilm and its spatio temporal dynamics in an intertidal mudflat (Aiguillon Bay, France). *Mar Ecol Prog Ser* 282, 33–44.
- Hopkins, J.T., 1966. The role of water in the behaviour of an estuarine mud-flat diatom. *J. Mar. Biol. Assoc. United Kingdom* 46, 617–626.
- Huete, A., Ponce-campos, G.E., Zhang, Y., Restrepo-Coupe, N., Ma, X., Moran, M.S., 2015. Monitoring Photosynthesis from Space. pp. 3–22.

- Itakura, S., Imai, I., Itoh, K., 1997. "Seed bank" of coastal planktonic diatoms in bottom sediments of Hiroshima Bay, Seto Inland Sea, Japan. *Mar. Biol.* 128, 497–508.
- Janssen, M., Hust, M., Rhiel, E., Krumbein, W.E., 1999. Vertical migration behaviour of diatom assemblages of Wadden Sea sediments (Dangast, Germany): A study using cryo-scanning electron microscopy. *Int. Microbiol.* 2, 103–110.
- Jewson, D.H., Lowry, S.F., Bowen, R., 2006. Co-existence and survival of diatoms on sand grains. *Eur. J. Phycol.* 41, 131–146.
- Jochem, F.J., 1999. Dark survival strategies in marine phytoplankton assessed by cytometric measurement of metabolic activity with fluorescein diacetate. *Mar. Biol.* 135, 721–728.
- Kamp, A., de Beer, D., Nitsch, J.L., Lavik, G., Stief, P., 2011. Diatoms respire nitrate to survive dark and anoxic conditions. *Proc. Natl. Acad. Sci.* 108, 5649–5654.
- Kamp, A., Stief, P., Knappe, J., De Beer, D., 2013. Response of the ubiquitous pelagic diatom *Thalassiosira weissflogii* to darkness and anoxia. *PLoS One* 8, 1–11.
- Kazemipour, F., Launeau, P., Méléder, V., 2012. Microphytobenthos biomass mapping using the optical model of diatom biofilms: Application to hyperspectral images of Bourgneuf Bay. *Remote Sens. Environ.* 127, 1–13.
- Kelly, J.A., Honeywill, C., Paterson, D.M., 2001. Microscale analysis of chlorophyll-a in cohesive, intertidal sediments: the implications of microphytobenthos distribution. *J. Mar. Biol. Assoc. United Kingdom* 81, 151–162.
- Kingston, M.B., 1999. Wave Effects on the Vertical Migration of Two Benthic Microalgae: *Hantzschia virgata* var. *intermedia* and *Euglena proxima*. *Estuaries* 22, 81.
- Koh, C.-H., Khim, J.S., Araki, H., Yamanishi, H., Koga, K., 2007. Within-day and seasonal patterns of microphytobenthos biomass determined by co-measurement of sediment and water column chlorophylls in the intertidal mudflat of Nanaura, Saga, Ariake Sea, Japan. *Estuar. Coast. Shelf Sci.* 72, 42–52.
- Larson, F., Sundbäck, K., 2012. Recovery of microphytobenthos and benthic functions after sediment deposition. *Mar. Ecol. Prog. Ser.* 446, 31–44.
- Laviale, M., Ezequiel, J., Pais, C., Cartaxana, P., Serôdio, J., 2015. The "crème brûlée" sampler: A new high-resolution method for the fast vertical sampling of intertidal fine sediments. *J. Exp. Mar. Bio. Ecol.* 468, 37–44.
- Lewin, J., Hellebust, J.A., 1970. Heterotrophic nutrition of the marine pennate diatom, *Cylindrotheca fusiformis*. *Can. J. Microbiol.* 16, 1123–1129.
- Lewin, J.C., 1953. Heterotrophy in diatoms. *J. Gen. Microbiol.* 9, 305–313.

- Lewis, J., Harris, A.S.D., Jones, K.J., Edmonds, R.L., 1999. Long-term survival of marine planktonic diatoms and dinoflagellates in stored sediment samples. *J. Plankton Res.* 21, 343–354.
- Lopes, C.L., Dias, J.M., 2015. Tidal dynamics in a changing lagoon: Flooding or not flooding the marginal regions. *Estuar. Coast. Shelf Sci.* 167, 14–24.
- Lorenzen, C.J., 1967. Determination of Chlorophyll and Pheo-Pigments: Spectrophotometric Equations. *Limnol. Oceanogr.* 12, 343–346.
- MacIntyre, H.L., Cullen, J.J., 1995. Fine-scale vertical resolution of chlorophyll and photosynthetic parameters in shallow-water benthos. *Mar. Ecol. Prog. Ser.* 122, 227–238.
- McLachlan, D.H., Brownlee, C., Taylor, A.R., Geider, R.J., Underwood, G.J.C., 2009. Light-induced motile responses of the estuarine benthic diatoms *Navicula perminuta* and *Cylindrotheca closterium* (bacillariophyceae). *J. Phycol.* 45, 592–599.
- McMinn, A., Martin, A., 2013. Dark survival in a warming world. *Proc. R. Soc. Biol. Sci.* 280, 20122909.
- McQuoid, M.R., Hobson, L.A., 1996. Diatom resting stages. *J. Phycol.* 32, 889–902.
- Middelburg, J.J., Barranguet, C., Boschker, H.T.S., Herman, P.M.J., Moens, T., Heip, C.H.R., 2000. The fate of intertidal microphytobenthos carbon: An in situ ¹³C-labeling study. *Limnol. Oceanogr.* 45, 1224–1234.
- Moerdijk-Poortvliet, T.C.W., van Breugel, P., Sabbe, K., Beauchard, O., Stal, L.J., Boschker, H.T.S., 2018. Seasonal changes in the biochemical fate of carbon fixed by benthic diatoms in intertidal sediments. *Limnol. Oceanogr.* 63, 550–569.
- Mundree, S., Perissinotto, R., Nozais, C., 2003. Seasonal variations in the vertical distribution of benthic microalgae in the upper sediment of the Mdloti Estuary, South Africa. *Bot. Mar.* 46, 323–331.
- Murphy, A.M., Cowles, T.J., 1997. Effects of darkness on multi-excitation in vivo fluorescence and survival in a marine diatom. *Limnol. Oceanogr.* 42, 1444–1453.
- Nymark, M., Valle, K.C., Hancke, K., Winge, P., Andresen, K., Johnsen, G., Bones, A.M., Brembu, T., 2013. Molecular and photosynthetic responses to prolonged darkness and subsequent acclimation to re-illumination in the diatom *Phaeodactylum tricorutum*. *PLoS One* 8.
- Oakes, J.M., Eyre, B.D., 2014. Transformation and fate of microphytobenthos carbon in subtropical, intertidal sediments: Potential for long-term carbon retention revealed by ¹³C-labeling. *Biogeosciences* 11, 1927–1940.

- Oreska, M.P.J.J., Wilkinson, G.M., McGlathery, K.J., Bost, M., Mckee, B.A., 2018. Non-seagrass carbon contributions to seagrass sediment blue carbon. *Limnol. Oceanogr.* 63, S3–S18.
- Perkins, R.G., Lavaud, J., Serôdio, J., Mouget, J.L., Cartaxana, P., Rosa, P., Barille, L., Brotas, V., Jesus, B.M., 2010. Vertical cell movement is a primary response of intertidal benthic biofilms to increasing light dose. *Mar. Ecol. Prog. Ser.* 416, 93–103.
- Peters, E., 1996. Prolonged darkness and diatom mortality: II. Marine temperate species. *J. Exp. Mar. Bio. Ecol.* 207, 43–58. [https://doi.org/10.1016/S0022-0981\(96\)02520-8](https://doi.org/10.1016/S0022-0981(96)02520-8)
- Peters, E., Thomas, D.N., 1996. Prolonged darkness and diatom mortality I: Marine antarctic species. *J. Exp. Mar. Bio. Ecol.* 207, 25–41.
- Pinckney, J., Piceno, Y., Love, C.R., 1994. Short-term changes in the vertical distribution of benthic microalgal biomass 9, 143–153.
- Pinckney, J.L., Zingmark, R.G., 1993. modeling the annual production of intertidal benthic microalgae in estuarine ecosystems. *J. Phycol.* 29, 396–407.
- Plecha, S., Picado, A., Chambel-Leitão, P., Dias, J.M., Vaz, N., 2014. Study of suspended sediment dynamics in a temperate coastal lagoon: Ria de Aveiro (Portugal). *J. Coast. Res.* 70, 604–609.
- Reeves, S., McMinn, A., Martin, A., 2011. The effect of prolonged darkness on the growth, recovery and survival of Antarctic sea ice diatoms. *Polar Biol.* 34, 1019–1032.
- Rivkin, R.B., Putt, M., 1987. Diel periodicity of photosynthesis in polar phytoplankton: Influence on primary production. *Science.* 238, 1285–1288.
- Round, F.E., 1979. A diatom assemblage living below the surface of intertidal sand flats. *Mar. Biol.* 54, 219–223.
- Round, F.E., Palmer, J.D., 1966. Persistent, vertical-migration rhythms in benthic microflora.: II. Field and laboratory studies on diatoms from the banks of the river avon. *J. Mar. Biol. Assoc. United Kingdom* 46, 191–214.
- Ryu, J.H., Choi, J.K., Lee, Y.K., 2014. Potential of remote sensing in management of tidal flats: A case study of thematic mapping in the Korean tidal flats. *Ocean Coast. Manag.* 102, 458–470.
- Sarthou, G., Timmermans, K.R., Blain, S., Tréguer, P., 2005. Growth physiology and fate of diatoms in the ocean: A review. *J. Sea Res.* 53, 25–42.
- Schaub, I., Wagner, H., Graeve, M., Karsten, U., 2017. Effects of prolonged darkness and temperature on the lipid metabolism in the benthic diatom *Navicula perminuta* from the Arctic Adventfjorden, Svalbard. *Polar Biol.* 40, 1425–1439.

- Serôdio, J., 2004. Analysis of variable chlorophyll fluorescence in microphytobenthos assemblages: Implications of the use of depth-integrated measurements. *Aquat. Microb. Ecol.* 36, 137–152.
- Serôdio, J., Coelho, H., Vieira, S., Cruz, S., 2006. Microphytobenthos vertical migratory photoresponse as characterised by light-response curves of surface biomass. *Estuar. Coast. Shelf Sci.* 68, 547–556.
- Serôdio, J., Da Silva, J.M., Catarino, F., 2001. Use of in vivo chlorophyll a fluorescence to quantify short-term variations in the productive biomass of intertidal microphytobenthos. *Mar. Ecol. Prog. Ser.* 218, 45–61.
- Serôdio, J., Marques da Silva, J., Catarino, F., 1997. Nondestructive tracing of migratory rhythms of intertidal benthic microalgae using in vivo chlorophyll a fluorescence. *J. Phycol.* 33, 542–553.
- Serôdio, J., Silva, R., Ezequiel, J., Calado, R., 2011. Photobiology of the symbiotic acoel flatworm *Symsagittifera roscoffensis*: Algal symbiont photoacclimation and host photobehaviour. *J. Mar. Biol. Assoc. United Kingdom* 91, 163–171.
- Serôdio, J., Vieira, S.S., Barroso, F., 2007. Relationship of variable chlorophyll fluorescence indices to photosynthetic rates in microphytobenthos. *Aquat. Microb. Ecol.* 49, 71–85.
- Smayda, T.J., Mitchell-Innes, B., 1974. Dark survival of autotrophic, planktonic marine diatoms. *Mar. Biol.* 25, 195–202.
- Stanley, R.H.R., Howard, E.M., 2013. Quantifying photosynthetic rates of microphytobenthos using the triple isotope composition of dissolved oxygen. *Limnol. Oceanogr. Methods* 11, 360–373.
- Steele, J.H., Baird, I.E., 1968. Production ecology of a sandy beach. *Limnol. Oceanogr.* 14–25.
- Sugie, K., Kuma, K., 2008. Resting spore formation in the marine diatom *Thalassiosira nordenskiöldii* under iron- and nitrogen-limited conditions. *J. Plankton Res.* 30, 1245–1255.
- Sun, M., Aller, R.C., Lee, C., 1991. Early diagenesis of chlorophyll-a in Long Island Sound sediments: A measure of carbon flux and particle reworking. *J. Mar. Res.* 49, 379–401.
- Taylor, I.S., Paterson, D.M., 1998. Microspatial variation in carbohydrate concentrations with depth in the upper millimetres of intertidal cohesive sediments. *Estuar. Coast. Shelf Sci.* 46, 359–370.

- Tomás, L.M., Rodrigues, M., Fortunato, A.B., Azevedo, A., Leitão, P.C., Oliveira, A., Rocha, A., Lopes, J.F., Dias, J.M., 2014. Salinity modelling accuracy of a coastal lagoon: a comparative river flow analysis of basin model vs. traditional approaches. *J. Coast. Res.* 70, 586–591.
- Tréguer, P., Bowler, C., Moriceau, B., Dutkiewicz, S., Gehlen, M., Aumont, O., Bittner, L., Dugdale, R., Finkel, Z., Iudicone, D., Jahn, O., Guidi, L., Lasbleiz, M., Leblanc, K., Levy, M., Pondaven, P., 2018. Influence of diatom diversity on the ocean biological carbon pump. *Nat. Geosci.* 11, 27–37.
- Tuchman, N.C., Schollett, M.A., Rier, S.T., Geddes, P., 2006. Differential heterotrophic utilization of organic compounds by diatoms and bacteria under light and dark conditions. *Hydrobiologia* 561, 167–177.
- Ubertini, M., Lefebvre, S., Rakotomalala, C., Orvain, F., 2015. Impact of sediment grain-size and biofilm age on epipelagic microphytobenthos resuspension. *J. Exp. Mar. Bio. Ecol.* 467, 52–64.
- Underwood, G.J.C., Kromkamp, J., 1999. Primary production by phytoplankton and microphytobenthos in estuaries. *Adv. Ecol. Res.* 29, 93–153.
- Underwood, G.J.C., Perkins, R.G., Consalvey, M.C., Hanlon, A.R.M., Oxborough, K., Baker, N.R., Paterson, D.M., 2005. Patterns in microphytobenthic primary productivity: Species-specific variation in migratory rhythms and photosynthetic efficiency in mixed-species biofilms. *Limnol. Oceanogr.* 50, 755–767.
- van der Wal, D., Wielemaker-van den Dool, A., Herman, P.M.J., 2010. Spatial synchrony in intertidal benthic algal biomass in temperate coastal and estuarine ecosystems. *Ecosystems* 13, 338–351.
- Vargas, C.I.C., Vaz, N., Dias, J.M., 2017. An evaluation of climate change effects in estuarine salinity patterns: Application to Ria de Aveiro shallow water system. *Estuar. Coast. Shelf Sci.* 189, 33–45.
- Wasmund, N., 1989. Micro-autoradiographic determination of the viability of algae inhabiting deep sediment layers. *Estuar. Coast. Shelf Sci.* 28, 651–656.
- Weiqiu, L., Jielong, Z., Guanghong, T., Hualin, X., Xiaohua, Y., 2013. Temporal and vertical distribution of microphytobenthos biomass in mangrove sediments of Zhujiang (Pearl River) Estuary. *Acta Oceanol. Sin.* 32, 82–88.
- White, W.A., 1974. Uptake of organic compounds by two facultatively heterotrophic marine centric diatoms. *J. Phycol.* 433–438.

- Wolanski, E.; Brinson, M.M.; Cahoon, D.R.; Perillo, G.M.E. (2009). Coastal wetlands: a synthesis, *in*: Perillo, G.M.E. *et al.* (Ed.) *Coastal wetlands: an integrated ecosystem approach*. pp. 1-62
- Wulff, A., Roleda, M.Y., Zacher, K., Wiencke, C., 2008. Exposure to sudden light burst after prolonged darkness—a case study on benthic diatoms in Antarctica. *Diatom res.* 23, 519–532.

Chapter 5

SYNOPTIC SPATIO-TEMPORAL VARIABILITY OF THE PHOTOSYNTHETIC PRODUCTIVITY OF MICROPHYTOBENTHOS AND PHYTOPLANKTON IN A TIDAL ESTUARY

Publication in preparation:

Silja Frankenbach, João Ezequiel, Sandra Plecha, Johannes Gössling, Leandro Vaz, Michael Kühl, João Dias, Nuno Vaz, João Serôdio. Synoptic spatio-temporal variability of the photosynthetic productivity of microphytobenthos and phytoplankton in a tidal estuary To be submitted to *Frontiers in Marine Science*.

Key index words

Chlorophyll *a* fluorescence, estuaries, diatoms, microphytobenthos, photoacclimation, photosynthesis, phytoplankton, productivity, sediment

Abstract

Tidal estuaries and shallow coastal zones are regarded as highly important ecosystems, mostly due to their high primary productivity and associated role as carbon sinks. In these ecosystems, primary productivity is mainly due to the photosynthetic carbon fixation by phytoplankton and microphytobenthos. Most studies have assessed the productivity of the two communities separately, and productivity rates for the same estuary that can be directly comparable are still relatively scarce. The present study aimed to characterize the spatio-temporal variability of primary productivity of phytoplankton and microphytobenthos in a tidal estuarine system, the Ria de Aveiro (Portugal), and to estimate the ecosystem-level budget for photosynthetic carbon fixation. Photosynthetic productivity rates of phytoplankton and intertidal microphytobenthos were determined based on synoptic *in situ* measurements of absolute rates of electron transport rate of photosystem II, using PAM fluorometry. Measurements of chlorophyll fluorescence indices were accompanied by measurements of salinity, temperature, water turbidity, solar irradiance, and planktonic and benthic microalgal biomass. Measurements were carried out hourly, along four spring-neap tidal cycles distributed along one year, on three contrasting sites of the estuary, allowing to cover a wide range of spatial and temporal scales of variability. Both phytoplankton and microphytobenthos were found to vary seasonally and along the spring-neap tidal cycle, regarding biomass, photophysiology and productivity. The most pronounced trends in the spatio-temporal variability of the photophysiology and productivity of two communities included: (i) maximum biomass and productivity were reached later for microphytobenthos (summer-autumn) than for phytoplankton (spring-summer); (ii) absorption cross-section of PSII was generally higher for phytoplankton; (iii) the two groups showed a similar photoacclimation state, but there was a tendency for the microphytobenthos to appear as high light-acclimated when compared to phytoplankton. Biomass-specific productivity was on average much higher for phytoplankton than for microphytobenthos, averaging 68.0 and 19.1 mg C mg Chl $a^{-1} d^{-1}$, respectively. However, because of the larger amounts of photosynthetic biomass contributing to benthic production, the areal, depth-integrated production rates of microphytobenthos were generally higher

than the ones of phytoplankton, averaging 264.5 and 140.0 mg C m⁻² d⁻¹, respectively. On an annual basis, phytoplankton productivity averaged 49.9 g C m⁻² yr⁻¹ while the productivity of microphytobenthos averaged 105.2 g C m⁻² yr⁻¹. When upscaling for the whole estuary, annual primary production rates of the phytoplankton and the microphytobenthos reached 4894.3 and 7534.0 t C yr⁻¹, respectively, representing 60.6% and 39.4% of the combined total of 12428.3 t C yr⁻¹ determined for the Ria de Aveiro.

Introduction

Estuaries and coastal zones support a number of key ecosystem services, while being under direct threat from heavy human use (Barbier et al., 2011). The importance attributed to these areas is largely justified by their high rates of primary productivity, ranking among the highest in both aquatic and terrestrial ecosystems (McLusky and Elliott, 2007). In tidal estuaries and shallow coastal zones, primary productivity is mostly due to the photosynthetic carbon fixation by phytoplankton and microphytobenthos (Underwood and Kromkamp, 1999). Although estuarine primary productivity is often considered to be mainly due to phytoplankton photosynthetic activity, the contribution of microphytobenthos can be significant in tidal systems, having been estimated to represent up to 50% of ecosystem-level carbon fixation (Underwood and Kromkamp, 1999). This is because in tidal systems the productivity of phytoplankton is limited by the high turbidity of the water column, caused by strong tidal currents and resulting sediment resuspension and, on the other hand, because of the large intertidal areas formed during low tide, that harbor dense and highly productive microphytobenthos communities (Van Colen et al., 2014).

The assessment of the primary productivity of estuarine areas is crucial to evaluate their role as carbon sinks, a question particularly relevant in the current context of increasing of atmospheric carbon levels due to anthropogenic action. However, the primary productivity of phytoplankton and microphytobenthos communities have been generally studied separately and only a relatively small number of studies have attempted to provide directly comparable estimates of carbon fixation rates of the two groups in the same estuary (Underwood & Kromkamp, 1999; Tagliarolo and Scharler 2018, Caffrey et al 2014). This is probably due to differences in the methodologies used to quantify photosynthetic activity and carbon fixation in the water column and in the sediment. The difficulties in obtaining comparable estimates for phytoplankton and microphytobenthos have been long recognized (Underwood and Kromkamp, 1999) and are based on the drastic differences in the vertical scale of the photic zone in the water column (meters) and the sediment

(micrometers). This has hampered not only the evaluation of the relative importance of both communities but also the estimation of integrated pelagic-benthic production budgets.

This work aimed to assess the integrated pelagic-benthic productivity in a tidal estuarine system, the Ria de Aveiro (Portugal). Photosynthetic rates were estimated based on measurements of *in vivo* chlorophyll fluorescence indices, combining the functional absorption cross section and the electron transport rate of photosystem II (PSII). This enabled the calculation of absolute rates of electron transport rate, which are closely correlated with rates of photosynthetic carbon fixation (Migné et al., 2007; Kromkamp et al., 1998; Schreiber et al., 2012, Morelle et al. 2018b). Measurements were carried out on phytoplankton and microphytobenthos samples in parallel, on different sites of the estuary, selected to cover a wide range of conditions (canals and tidal flats), including water depth, tidal height and grain size, and covering the main scales of temporal variability in the estuarine environment (hourly, fortnight and seasonal). This approach allowed for the detailed characterization and comparison of the spatio-temporal variability of benthic and pelagic photosynthetic activity, ultimately supporting the estimation of an ecosystem-level budget of photosynthetic carbon fixation for the whole estuary.

Material and Methods

Study area, sampling and sample processing

The study was carried out in the Ria de Aveiro a coastal lagoon located in the northwest coast of Portugal (40°38'N, 08°45'W). Detailed characterization of physical, geomorphological, and ecological features of the Ria de Aveiro can be found elsewhere (Bueno-Pardo et al., 2018; Dias et al., 1999, 2003; Tomás et al., 2014). The Ria de Aveiro comprises into four main channels (S. Jacinto, Mira, Ílhavo and Espinheiro), receiving fresh water from four rivers (Vouga, Antuã, Boco and Fontão). It connects to the Atlantic Ocean by a single artificial inlet, allowing water circulation patterns typical of a tidal estuary (Vaz and Dias, 2008).

Three sampling sites were selected, based on their contrasting characteristics, namely location (channels, distance to the ocean), hydrodynamics, salinity and sediment granulometry (Fig. 1): Gafanha da Encarnação, located in the Mira channel and closest to the mouth of the estuary, characterized by sandy sediments (GE; 40°35'18" N, 08°41'06" W); Vista Alegre, located in the Canal de Ílhavo, characterized by fine muddy sediments (VA; 40°37'12" N, 08°44'54" W); Torreira, in the S. Jacinto channel, characterized by

coarser muddy sand (TO; 40.758403 N, 8.676949 W). The three sampling sites are described in more detail in (Frankenbach et al., 2019). At each sampling site, samples of intertidal sediment and of overlying water were collected to allow measurements on microphytobenthos and phytoplankton, respectively.

Sampling was carried along four spring-neap tidal cycles, distributed over the period between July 2013 and June 2014, to assess seasonal variability (summer: 16-18 and 23-25 July 2013; autumn: 29-31 October and 4-6 November 2013; winter: 12-13 and 18-20 February 2014; spring: 27-29 May and 3-5 June 2014). For each neap or spring tidal period, sampling was carried out on the three sites on consecutive days, one for each site. During each sampling day, samples were collected hourly, from sunrise to sunset, and all measurements were carried out *in situ* (see below) immediately following collection. Sediment samples were collected only during daytime low tide exposure. Water samples were collected from surface water, from the shoreline (GE, TO) or from an overlying bridge (VA) using a bucket and transferred into 1.5 L bottles.

Water samples were used for measurements of chlorophyll *a* fluorescence, carried out immediately after collection (see below). Sediment samples were collected using Plexiglas corers (3.6 cm internal diameter) and used immediately for chlorophyll *a* fluorescence measurement.

Afterwards, cores were subsampled for quantification of chlorophyll *a*, as an indicator of surface biomass (see below) by cryo-sampling using mini contact cores (“*crème brûlée*” technique; (Laviale et al., 2015)). Different sample depths were collected for each sampling site, to match the expected depth of the photic zone on each type of sediment (0.25, 0.5 and 2.0 mm for VA, GE and TO respectively). Sub-samples were flash frozen immediately after collection and kept in liquid nitrogen until further analysis in the laboratory.

Microphytobenthos cell suspensions were collected from the sediment surface using the lens tissue technique, (Eaton and Moss, 1966). Two layers of lens tissue (Lens cleaning tissue 105, Whatman) were placed on the surface of the sediment for one hour and the upper piece was collected and resuspended in tubes with 10 ml of filtered seawater. Chlorophyll *a* fluorescence was measured immediately after preparation of the suspensions (1.25 mL).

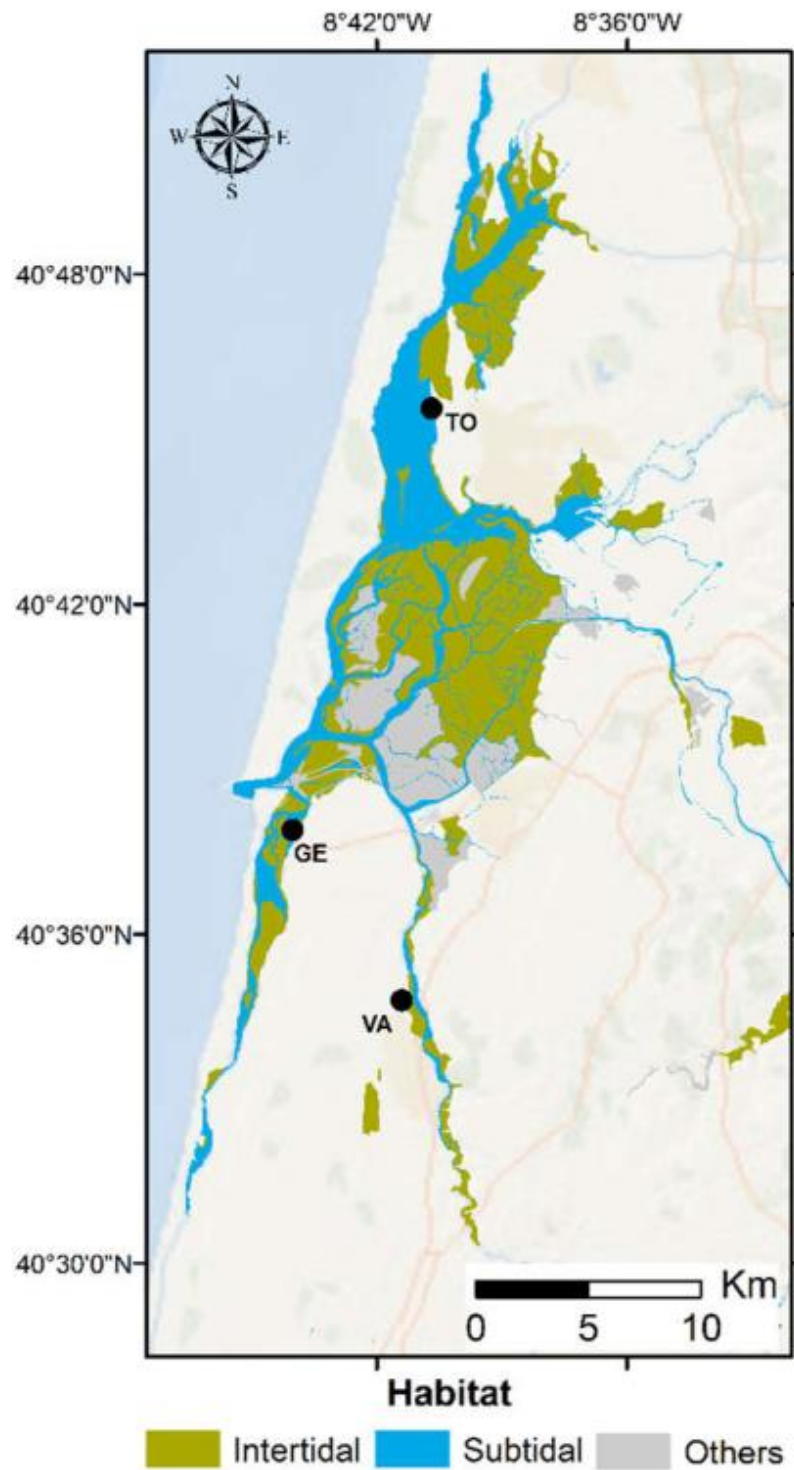


Figure 1. Ria de Aveiro, Portugal. The different habitats are highlighted in green, for intertidal areas, blue for subtidal areas, and grey for other. Sampling sites are marked with a black dot: Vista Alegre (VA), Gafanha da Encarnação (GE), and Torreira (TO).

Physical parameters

Photosynthetic active radiation ($\mu\text{mol quanta m}^{-2} \text{ s}^{-1}$) was measured hourly, at the time of sample collection, using a Quantum Meter with a separate sensor (Model MQ-200, Apogee Instruments, Logan, Utah, USA). Sediment temperature was measured using an infrared thermometer (ScanTemp 410, Tematec GmbH, Hennef, Germany). Water temperature, salinity and turbidity (NTU) were measured using a multi-parameter Sonde YSi 6600 (YSI incorporated, Yellow Springs, Ohio, USA). The sonde measured salinity in a range from 0 to 70 ppt (± 0.1 ppt), temperature from -5 to 50 °C ($\pm 0.15^\circ$) and turbidity from 0 to 1000 NTU (± 0.3 NTU), being suitable to survey water properties in shallow turbid systems like the Ria de Aveiro.

Biomass

Phytoplankton and microphytobenthos biomass were quantified through chlorophyll *a* concentration. Water samples (1 L, one replicate per sampling point) were filtered in cellulose nitrate filters (0.8 μm pore size, 47 mm \varnothing) and immediately frozen at -80°C until pigment extraction. Sediment samples (three replicates per sampling point), collected with mini contact cores, were freeze-dried during 48h, prior to the extraction. Suspensions of benthic cells, collected via the lens tissue technique (three replicates per sampling point), were stored in a -80°C freezer until pigment extraction. Prior to the extraction, cell suspensions were centrifuged, and the supernatant discarded. Chlorophyll *a* content was quantified spectrophotometrically following Lorenzen (1967). In the case of sediments, the adaptations proposed by Plante-Cuny (1974) were used. Pigments from all samples were extracted in centrifuge tubes (15 ml falcons), with 90% aqueous acetone. Samples were homogenized in a vortex, to ensure a good mixing between the sample (filters, sediments or pellets, depending on the sample type) and the extraction solvent. Extraction was done in the dark, at 4 °C, for 24 hours. Samples were centrifuged at (3000 g, 10 min, 4 °C) and the absorbance of the supernatant was read in a spectrophotometer (Thermo Fisher Scientific, Waltham, USA) at 664 and 750 nm, with acetone 90% used as a blank. Acidification was done by adding 12 μl of HCl 1M. Chlorophyll *a* content was calculated following Lorenzen (1967) and expressed per volume as mg m^{-3} (phytoplankton) or per area mg m^{-2} (microphytobenthos).

Chlorophyll *a* fluorescence

Chlorophyll *a* fluorescence was measured using a Multi-Color PAM fluorometer, controlled by the PamWin V3.12w software (Heinz Walz GmbH, Effeltrich, Germany). Blue light (440 nm) was used for the measuring and actinic light, as well as for the saturation pulses. In the MCP-D detector unit, a RG 665 long pass filter (> 650 nm, 3 mm RG665, Schott) was used. Fluorescence of cell suspensions (phytoplankton and microphytobenthos) was measured in a 10 × 10 mm quartz cuvette using the ED-101US/MD optical unit, coupled to a magnetic stirrer (PHYTO-MS Miniature Magnetic Stirrer, Walz). Fluorescence of undisturbed microphytobenthos samples was measured using the MCP-BK Optical Unit for Leaf Measurements (Walz). The fluorometer was zeroed using filtered seawater as a blank (cells suspensions) or by pointing the MCP-BK Optical Unit to empty space (undisturbed microphytobenthos samples). Measurements were carried out by running a user-defined Script-file, comprising the following steps: 30 s darkness, measurement of the absorption cross section of PSII (σ_{II} ; see below), 30 s of darkness, rapid light curves (RLC; see below), 60 s of actinic light (intensity matching the solar irradiance at the moment of sample collection), measurement of the effective quantum yield ($\Delta F/F_m$; see below). During the periods of darkness, far-red illumination (725 nm) was applied, to induce the fully re-oxidation of the PQ-pool. The first measurement of the RLC was taken as a proxy for the maximum quantum yield of PSII, F_v/F_m . Samples were magnetically stirred between measurements. At each measuring occasion, measurements were carried out on three independent replicates.

Absorption cross section of PS II

The absorption cross section of PS II, σ_{II} [nm^2], was measured from the O–I1 rise kinetics, the initial rise of fluorescence yield, corresponding to the kinetics of Quinone (QA)-reduction, in the presence of an oxidized Plastoquinone (PQ)-pool (Schreiber et al., 2012). The O–I1 rise kinetics was measured under strong multi turnover (MT) saturation pulse, (SP) light (440 nm), using the pre-programmed Sigma 1000_MT.FTM fast trigger file. σ_{II} was calculated by running the special fitting routine O-I1 Fit (PamWin V3.12w software, Walz), based on the reversible radical pair model of PS II (Schreiber et al., 2012).

Effective quantum yield and relative electron transport rate of PSII

The effective quantum yield ($\Delta F/F_m'$) and the relative electron transport rate of PSII ($rETR$) were calculated from the fluorescence parameters F_s and F_m' (steady-state and maximum fluorescence of a light adapted sample, respectively) and the incident PAR irradiance E (measured *in situ* or applied as actinic light by the fluorometer), by (Genty et al., 1989):

$$\frac{\Delta F}{F_m'} = \frac{F_m' - F_s}{F_m'} \quad (1)$$

and

$$rETR = E \frac{F_m' - F_s}{F_m'} \quad (2)$$

Light-response curves of $rETR$

Rapid light-response curves (RLCs) were generated by sequentially applying 12 incremental light steps E (between 0 and 2179 $\mu\text{mol quanta m}^{-2} \text{s}^{-1}$), with each light step taking 10 s. At the end of each 10 s light exposure period, a saturating pulse was applied, F_s and F_m' were measured and $rETR$ was calculated. RLCs were characterised by estimating the initial slope (α), maximum $rETR$ ($rETR_m$) and the photoacclimation parameter E_k , by fitting the model of Eilers and Peters (1988).

Absolute ETR and carbon fixation rates

Absolute rates of electron transport of PSII were estimated following the rationale described by (Schreiber et al., 2012), based on the determination of the rate of quantum absorption per PSII (electrons $\text{PSII}^{-1} \text{s}^{-1}$):

$$ETR = \sigma_{II} L E \frac{\Delta F/F_m'}{F_v/F_m'} \quad (3)$$

where L is the Avogadro's constant (0.6022 mol^{-1}). Carbon fixation rates P^B [biomass-specific photosynthetic hourly rates; $\text{mg C mg Chl a}^{-1} \text{ h}^{-1}$] were estimated from (i) hourly rates of O_2 evolution [$\text{mmol O}_2 \text{ mg Chl a}^{-1} \text{ s}^{-1}$], estimated by (Schreiber et al., 2012):

$$rO_2 = \frac{ETR}{PSU \cdot n_e(O_2) \cdot M(\text{Chl})} \quad (4)$$

where PSU is number of chlorophyll *a* molecules per photosynthetic unit, $ne(O_2)$ is the number of electrons required for evolution of 1 molecule of O_2 and $M(Chl)$ is the molar mass of chlorophyll *a* ($893.49 \text{ g mol}^{-1}$); and (ii) from the ratio of oxygen produced to carbon fixed (photosynthetic quotient, PQ; mol C:mol O_2):

$$P^B = \frac{r_{O_2}}{PQ} M(C) 3600 \quad (5)$$

where $M(C)$ is the molar mass of carbon (12.01 g mol^{-1}) and 3600 is the conversion factor for hourly rates. PSU and $ne(O_2)$ were assumed to be equal to 600 Chl PSII⁻¹ and $5 e^- O_2^{-1}$, respectively, based on the experimental data compiled by (Suggett et al., 2010). PQ was assumed to be 1.1 mol C:mol O_2 (Kromkamp et al., 2008). All these parameters were assumed to remain constant across sampling sites and dates of sampling. Daily carbon fixation rates were calculated by summing the hourly rates for each daytime period.

Areal rates of carbon fixation

Areal rates of carbon fixation were estimated by integrating over depth the biomass-specific photosynthetic rates calculated by Eq. (5), using the method described by MacIntyre et al., (1996b). For each depth z below the surface of the water (phytoplankton) or the sediment (microphytobenthos): (i) the downwelling irradiance $E(z)$ was calculated from light the attenuation coefficient k_w or k_s (for the water column or the sediment, respectively; see below) assuming an exponential decrease; (ii) the biomass-specific photosynthetic rate $P^B(z)$ was calculated from the light-response curve (P^B vs E) measured for the corresponding sampling time and site, using $E(z)$ as an input; light-response curves of P^B were calculated by applying Eqs. 3-5 to the rETR vs E curves (RLC). $P^B(z)$ was calculated for depth intervals Δz of 10^{-6} mm (sediment) or 10^{-6} m (water column) and depth-integrated rate P [$\text{mg C m}^{-2} \text{ h}^{-1}$] was calculated summing over all depth intervals and multiplying by the chlorophyll *a* concentration, C [mg Chl a m^{-3}]:

$$P = \sum_z P^B(z) \Delta z C \quad (6)$$

For the microphytobenthos, $P^B(z)$ was calculated based on the light curves measured on cells collected in lens tissues, integrated numerically over depth using the attenuation coefficient measured for each type of sediment. Chlorophyll *a* concentration [mg Chl a m^{-3}] was calculated considering the volume sampled the contact core used for each sampling site. For the phytoplankton, $P^B(z)$ was depth integrated from the surface until the maximum depth of the water column at each sampling moment.

Light attenuation coefficients

Spectral scalar irradiance profiles of PAR (400-700 nm) in sediments from the three sampling sites were measured with a custom-made scalar field radiance probe connected to a spectrophotometer (USB 2000+, Ocean Optics, Duiven, Netherlands), and recorded using the spectral acquisition software Spectra Suite (Ocean Optics). The custom-made sensor consisted of a light diffusing sphere with a diameter of 90 μm was attached to the coated tip of a tapered optical fiber (Rickelt et al., 2016). The sensor was mounted on a motorized micromanipulator and positioned on the sediment surface in a 45° angle to minimize self-shading. To account for the insertion angle, the sensor was moved downwards in 141.4 μm steps to record spectral irradiance profiles in vertical depths of 100 μm increments. Spectral data were normalized to the incident downwelling spectral irradiance, which was recorded on a black non-reflective surface at the same position relative to light source and sediment surface. The light attenuation coefficients (k_s , mm^{-1}) were determined by the slope of the linear decay of the natural logarithm transformed percentage of incident light intensity as a function of depth, down to a maximum depth of 0.8 mm (Kühl, 2005). Measurements were replicated on three different samples per sampling site.

For the water column, the light extinction coefficient, k_w (m^{-1}), was estimated from measurements of turbidity (TURB, NTU), assuming to be proportional to the concentration of cohesive sediments (C_{ss} , mg L^{-1}), using the following relationships (Vaz et al., 2019):

$$C_{ss} = 3.42 \text{ TURB} + 3.0 \quad (7)$$

and

$$k_w = 0.036 C_{ss} + 1.24 \quad (8)$$

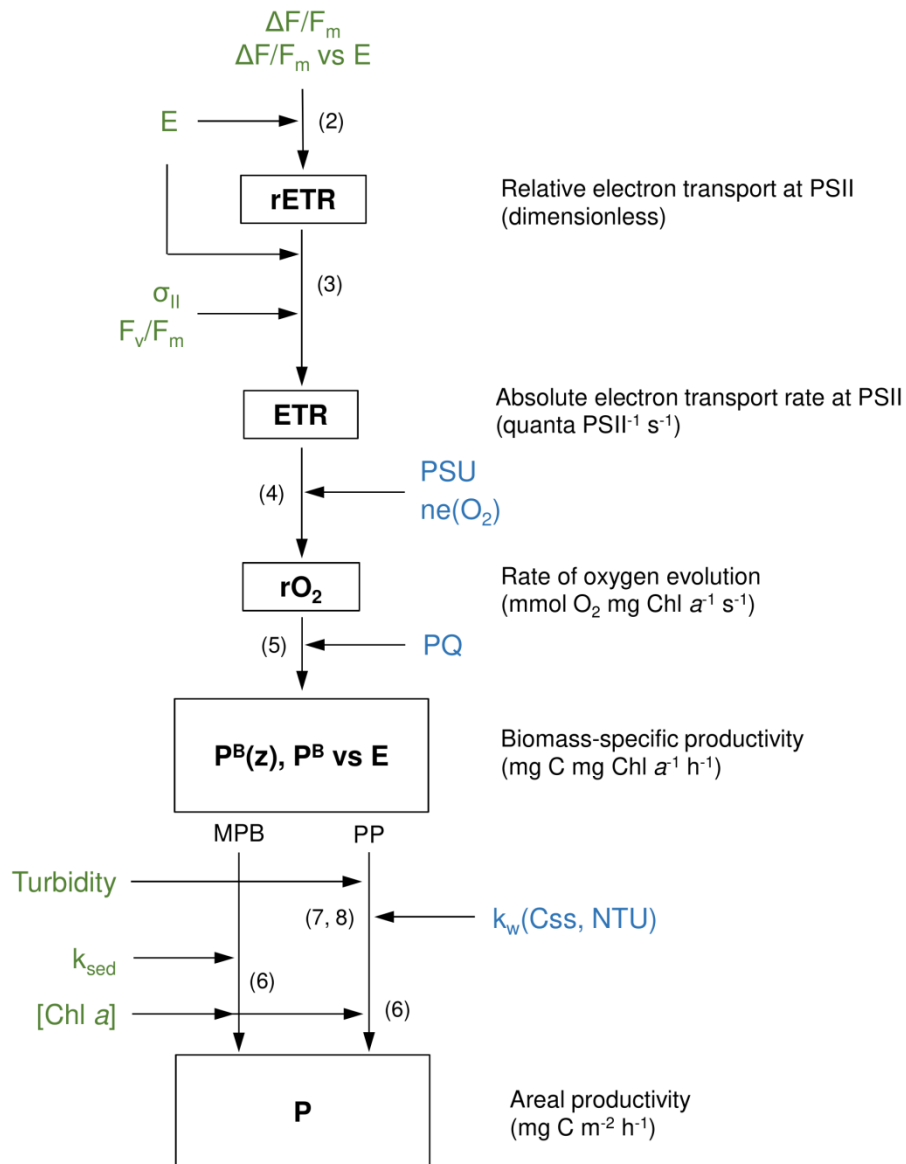


Figure 2. Schematic describing the modelling workflow followed in this study. Biomass-specific productivity rates (P^B , mg C mg Chl a⁻¹ h⁻¹) were calculated from irradiance (E) and fluorescence-based parameters (F_v/F_m , $\Delta F/F_m$, σ_{II}). Productivity per unit area was calculated by depth-integrating P^B using light-response curves of P^B , chlorophyll a content, and light attenuation. Depth-integration was carried out differently for phytoplankton and microphytobenthos, using light attenuation coefficient for the water column (k_w) and the sediment (k_s), respectively. Parameters in green were measured in this study. Parameters in blue were taken from published sources. Numbers represent the equations describing each step.

Estimation of ecosystem-level annual primary productivity

A preliminary estimate of the annual primary productivity of the Ria de Aveiro was calculated by multiplying the daily rates P , measured in each season and tidal cycle (spring vs neap), by the number of days of each season (1/4 of the whole year, 91 days)

corresponding to spring tides or to neap tides (45 days). Daily rates were calculated by adding the hourly rates determined for each day of sampling. Upscale for the entire estuary was done by considering the total area of the estuary (phytoplankton) and the area corresponding to intertidal flats (microphytobenthos). The former was estimated from the mean value between the area covered by water during mean high tide and during mean low tide (89.2 and 64.9 km², respectively; (Lopes et al., 2013). The areas corresponding to each type of sediment type were the ones determined in (Frankenbach et al., 2019): 34, 16 and 5 km² for TO, GE and VA, respectively. The area corresponded to the phytoplankton was estimated to reach 100 km², by adding the subtidal and the total intertidal areas calculated by (Frankenbach et al., 2019). The modelling approach used to estimate the area rates of carbon fixation by phytoplankton and microphytobenthos is summarized in the schematic of Figure 2.

Statistical analysis

Measurements made on different sampling sites and times were compared by applying an ANOVA. Assumptions of normality and homoscedasticity were verified prior to analysis using the Shapiro-Wilk test and Levene's test, respectively. In case of violation of assumptions, data were log transformed. All statistical analyses were carried out using Statistica 10 (StatSoft).

Results

Hourly variability in physical conditions, photophysiology, and biomass-specific productivity

Figs. 3-5 show the typical hourly variability in physical and photophysiological parameters in the three sampling sites during the course of two days, on neap and spring tides, during July 2013. A marked hourly variability in abiotic factors was observed in both the water column and intertidal sediments. In the sampling sites of the Ria de Aveiro, low tide tended to occur at mid-day during spring tides, and early in the morning and in late afternoon during neap tides. This caused a strong fortnight pattern of variability in physical conditions, particularly in the intertidal areas. The solar irradiance received varied between maximum values during spring tides to minimum values during neap tides, when direct exposure to light was restricted to two short periods, during early morning and late afternoon.

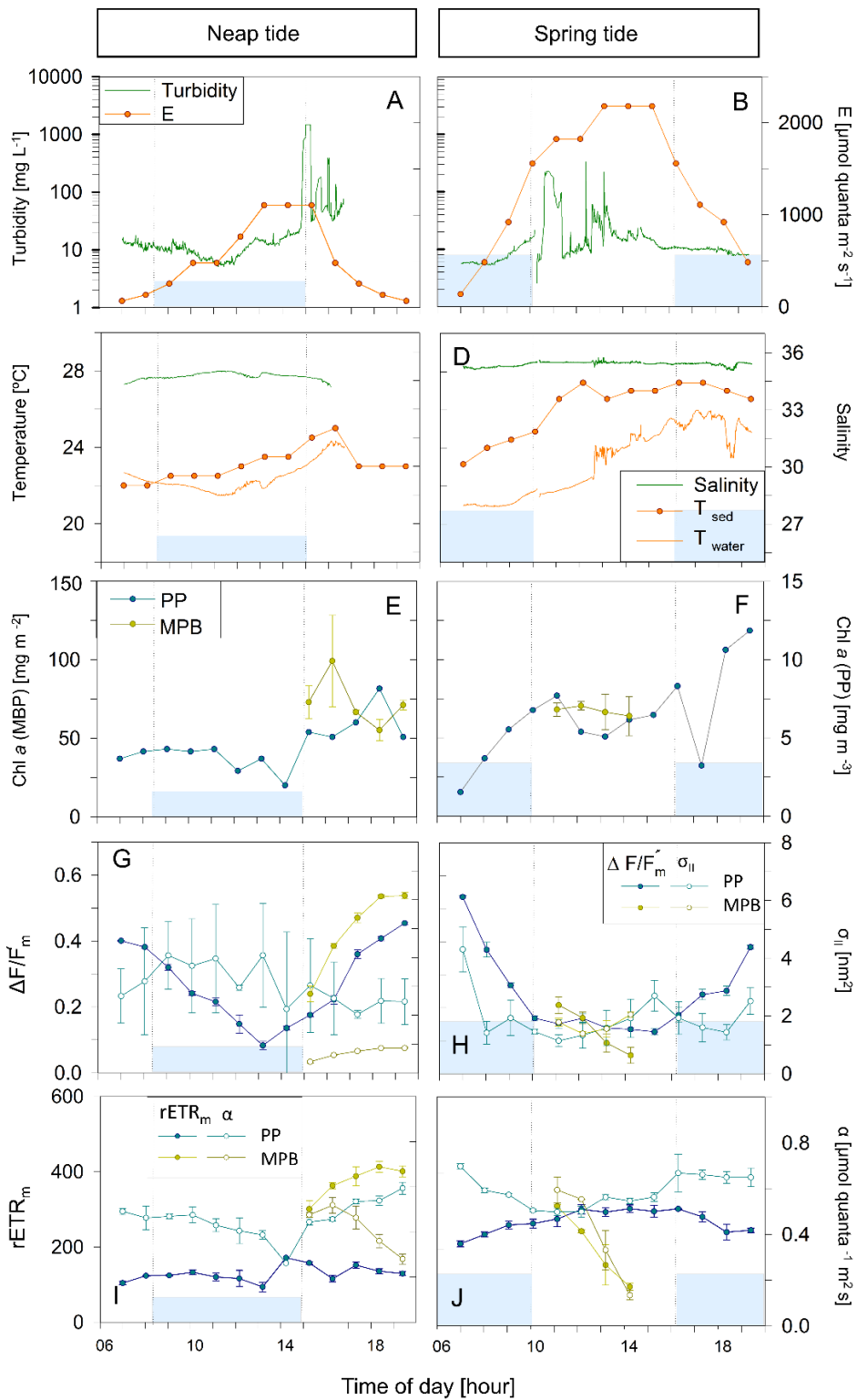


Figure 3. Hourly variation of abiotic (A-D) and photophysiological (E-J) parameters along one day in Torreira (TO) during neap (A, C, E, G, I) and spring tide (B, D, F, H, J) in July 2013. Blue areas represent high tide; vertical bars demonstrate the beginning/end of the high tide. Mean values of three replicates. Error bars represent one standard error.

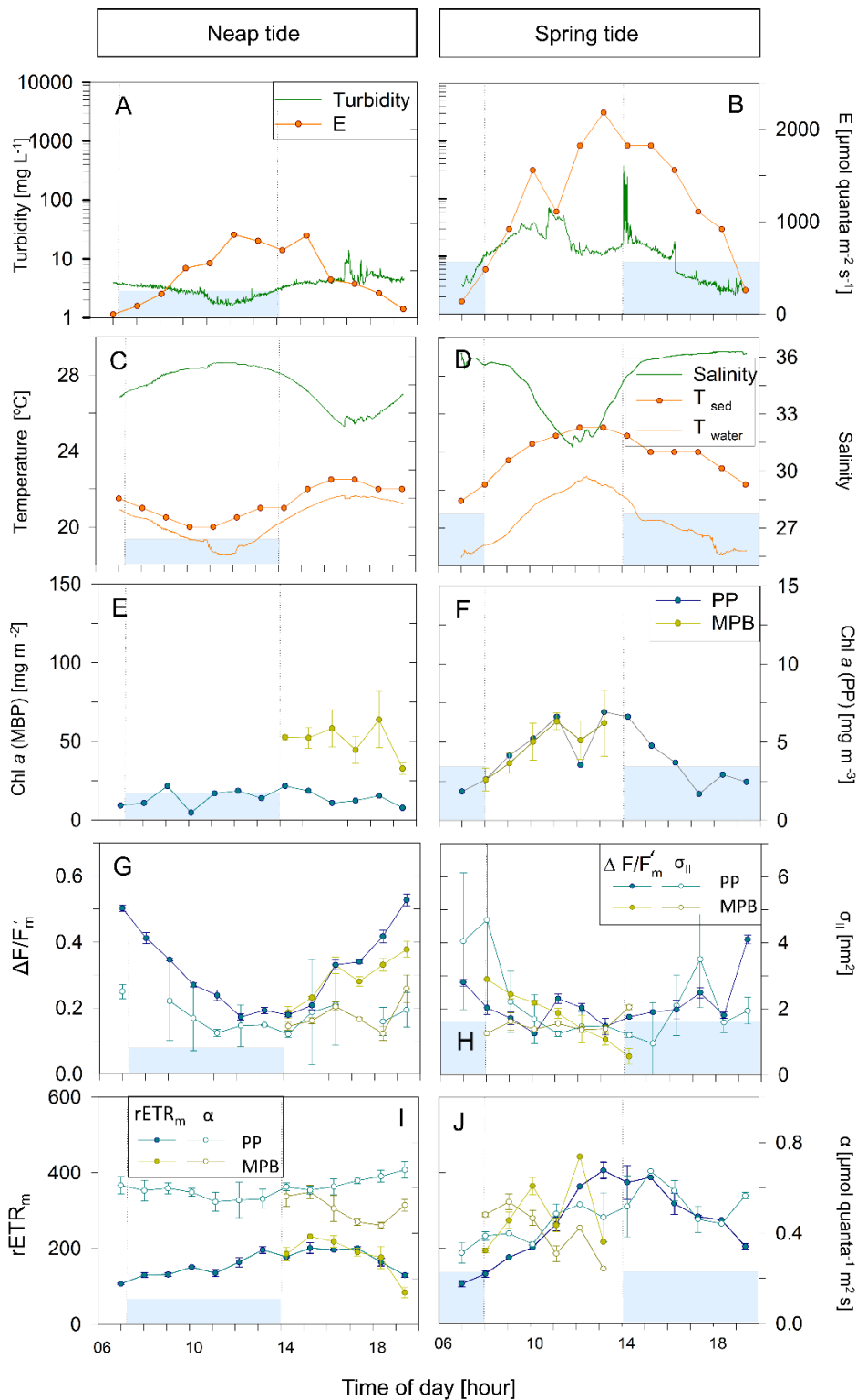


Figure 4. Hourly variation of abiotic (A-D) and photophysiological (E-J) parameters along one day in Gafanha de Encarnação (GE) during neap (A, C, E, G, I) and spring tide (B, D, F, H, J) in July 2013. Blue areas represent high tide; vertical bars demonstrate the beginning/end of the high tide. Mean values of three replicates. Error bars represent one standard error.

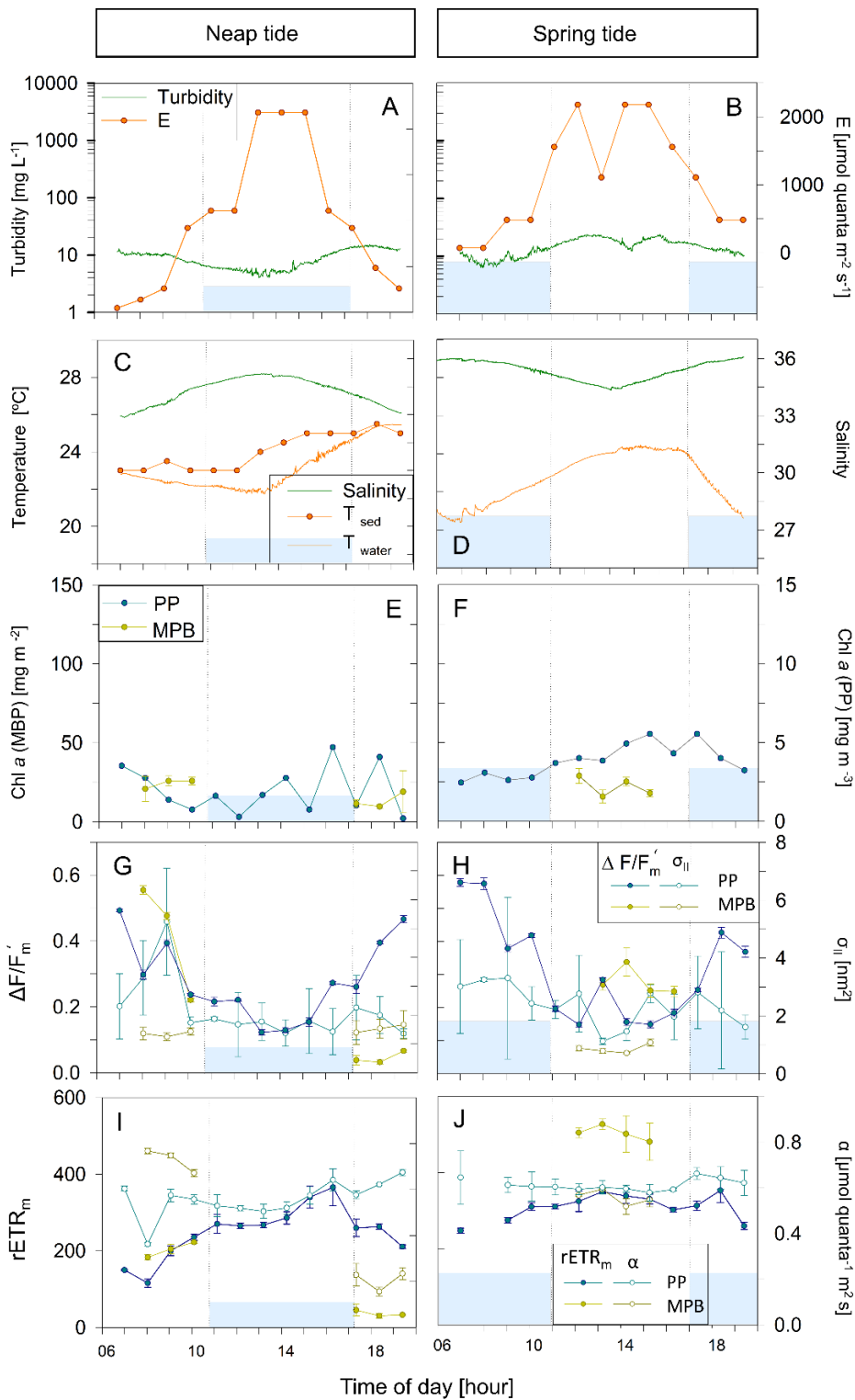


Figure 5. Hourly variation of abiotic (A-D) and photophysiological (E-J) parameters along one day in Vista Alegre (VA) during neap (A, C, E, G, I) and spring tide (B, D, F, H, J) in July 2013. Blue areas represent high tide; vertical bars demonstrate the beginning/end of the high tide. Mean values of three replicates. Error bars represent one standard error.

Water column turbidity varied markedly during the tidal cycle, typically reaching higher values during low tide (Figures 3-5, A,B) and showing short periods of very high values close to ebb (Figures 3 A, B) or flood (Figure 4 B). This oscillation in water turbidity is expected to affect considerably the fraction of incident solar irradiance that is available for phytoplankton and for the microphytobenthos.

Water temperature was often more constant during high tide (deeper water column), typically increasing during low tide periods, especially when occurring at mid-day (neap tides; Figure 3 D; 4 C-D; 5 D). At the site closest to the mouth of the estuary (GE), a sharp inversion of water temperature could be observed at the middle of the low tide period, associated with an equally marked change in salinity, denoting a sudden replacement of water masses at the sampling site, from freshwater-dominated (higher temperature, low salinity) to oceanic (lower temperature, high salinity) (Figure 4 D). Aside from the incident sunlight, the tides had a measurable impact on the water temperature, as the incoming oceanic seawater during high tide was often substantially cooler than the water already inside the estuary. Sediment temperature exhibited the same general pattern as in the water column, with higher values during low tide, when sediment was exposed (Figure 3-5 C, D), and especially during spring tides, when low tide occurred at mid-day (Figures 3-5, D). The sediment was generally warmer than the water column, often reaching values above 26 °C (Figures 3 D).

Salinity of the water column was usually lower during low tides at GE and VA, when the influence of freshwater was greatest, and higher in high tide, reaching values typical of seawater (around 35). This pattern of variation was more marked in site GE, the one closest to the estuary mouth (e.g. Figures 4 C, D). On another site (TO), water salinity remained virtually constant due to reduced inflow of fresh water in that canal (Figures 3 C,D).

Phytoplankton biomass, as measured by chlorophyll *a* concentration in the water column, showed a large hourly variability, particularly in sites TO and GE during spring tides (Figures 3 E, F; 4F). Maximum values tended to occur the low tide periods (Figures 2-4, F). Variations from about 1.5 to 7.7 mg Chl *a* m⁻³ in 4 h were observed in site TO (Figure 3 F). On Site VA, the farthest from the estuary mouth, hourly variations were much smaller (Figures 5 E, F). In contrast with the phytoplankton, the chlorophyll *a* content of the sediment didn't show consistent patterns of variation, although in some instances a clear increase during the low tide period could be observed (Figure 4 F).

The effective quantum yield of PSII, $\Delta F/F_m'$, also varied markedly along the day, both for phytoplankton in general and for microphytobenthos during neap tide. For phytoplankton, the same overall pattern was observed, with values varying from 0.5-0.6

during early morning or late afternoon, and around 0.1, under the highest solar irradiances. The pattern was observed in all days, with $\Delta F/F_m'$ mainly responding (inversely) to PAR, irrespectively of tidal stage. During neap tides, an almost symmetrical pattern was found, with the decrease of $\Delta F/F_m'$ observed during the morning recovering completely during the afternoon (Figures 3-5, G). On spring tide days, the recovery of $\Delta F/F_m'$ seemed incomplete (Figures 3-5, H), likely associated to the shallower water column during the middle of the day, allowing the exposure to higher light levels, higher temperature and lower salinity, possibly causing more slowly-reversible photodamage. For microphytobenthos, $\Delta F/F_m'$ values were generally similar to those of phytoplankton, following the same overall trend of varying inversely with incident solar irradiance (Figures 3-5 G, H).

The data on the absorption cross section of PS II, σ_{II} , was characterized by a large variability between replicates, especially for phytoplankton during neap tides (e.g. Figures 3-5 G). Both for phytoplankton and microphytobenthos, σ_{II} varied similarly to $\Delta F/F_m'$, largely responding inversely to solar irradiance (e.g. Figure 3 G). However, σ_{II} seemed to be more affected by tidal stage, as in some days it did not decrease under high solar irradiance if under high tide (Figure 4 G). In the case of microphytobenthos, σ_{II} values were consistently lower than for phytoplankton, which was possibly associated to the shorter periods of light exposure to which benthic populations are exposed (ca. 4 h). Clear trends of hourly variation were not very evident, yet a tendency to vary inversely with solar irradiance could be identified (e.g. Figures 3-5 H).

Short-term photoacclimation status, as measured by RLC parameters α and $rETR_m$, varied hourly both for phytoplankton and microphytobenthos. On most days, $rETR_m$ varied more and showed a better-defined pattern of variation, increasing towards the middle of the day, and reaching minimum values at beginning and end of the day (Figures 4, 5 I-J). For phytoplankton, light-limited photosynthesis (denoted by α) remained relatively constant along the day, on most days (e.g. Figures 3 J; 4 I; 5 J), but occasionally showed erratic, short-term variations (Figure 3 J). The values of α and $rETR_m$ of microphytobenthos were similar to those measured in the water column, but $rETR$ varied following less defined trends, and more variable in absolute terms: similar (Figure 3 I), significantly lower (Figure 4 I) or significantly higher (Figure 4 J) than the phytoplankton.

Spatio-temporal variability: fortnight and seasonal time scales

As expected, maximum intensities and daily light doses of solar irradiance varied markedly with season, with maximum values being measured in July and in May/June (Figure 6 A-C). However, an appreciable variation was measured regarding incident solar irradiance between spring and neap tides, due to variation in cloud cover during the sampling days (Figure 6 A-C). Considering the high turbidity of the water column, the total daily doses received at the intertidal sites depended substantially on the timing of the low tide period (Figure 6 A-C). Also, due to the delay in tidal propagation inside the estuary, causing the timing of low tide to vary between the sampling sites, a systematic variation in daily solar light dose received in the three sites was observed. Water turbidity was relative constant across sampling sites and seasons, being affected mainly by the tide, but a tendency for higher values during autumn and winter was observed. Occasional peaks in turbidity were measured, causing a large data dispersion (e.g. TO July; Figure 6 A).

Water and sediment temperature showed a clear seasonal variation in all sampling sites, with maximum average values occurring in July (23.3 ± 1.83 °C for water in TO, and 28.3 ± 0.96 °C in sediments at VA) and minimum values (10.3 ± 0.63 , for water TO and 12.3 ± 0.58 for sediments in GE) being observed in February. A virtually identical seasonal pattern was found for all sampling sites (Figure 6 D-F). The seasonal variation in water temperature was closely followed by equally large changes in water salinity, for all sampling sites. Highest average salinities (35.0 ± 0.52) were observed in July, and minimum values (2.0 ± 2.47) in February in VA, directly resulting from the seasonal variation in freshwater input (Figure 6 D-F), as this sampling site is located farthest from the mouth of the estuary (Figure 6 F).

Both the biomass of phytoplankton and microphytobenthos (as expressed per unit area) varied significantly with seasons (ANOVA, $F_{3,817} = 319.54$; $P < 0.001$; and $F_{3,317} = 13.54$; $P < 0.001$, respectively; Figure 5 G-I). However, the two communities differed regarding when the maximum biomass was reached, its variation with spring-neap tidal cycle, and its spatial distribution. In the case of phytoplankton, maximum average values were observed in spring and summer, and the lowest in winter (Figure 6 G-I). In contrast, microphytobenthos biomass reached maximum values later in the year, in summer and autumn. The biomass of phytoplankton was significantly higher in spring than in neap tides (ANOVA, $F_{1,817} = 25.14$; $P < 0.001$), showing higher values during spring tides. The same trend was observed for the microphytobenthos, but the differences between spring and neap tides were not significant (ANOVA, $F_{1,317} = 1.47$; $P = 0.226$).

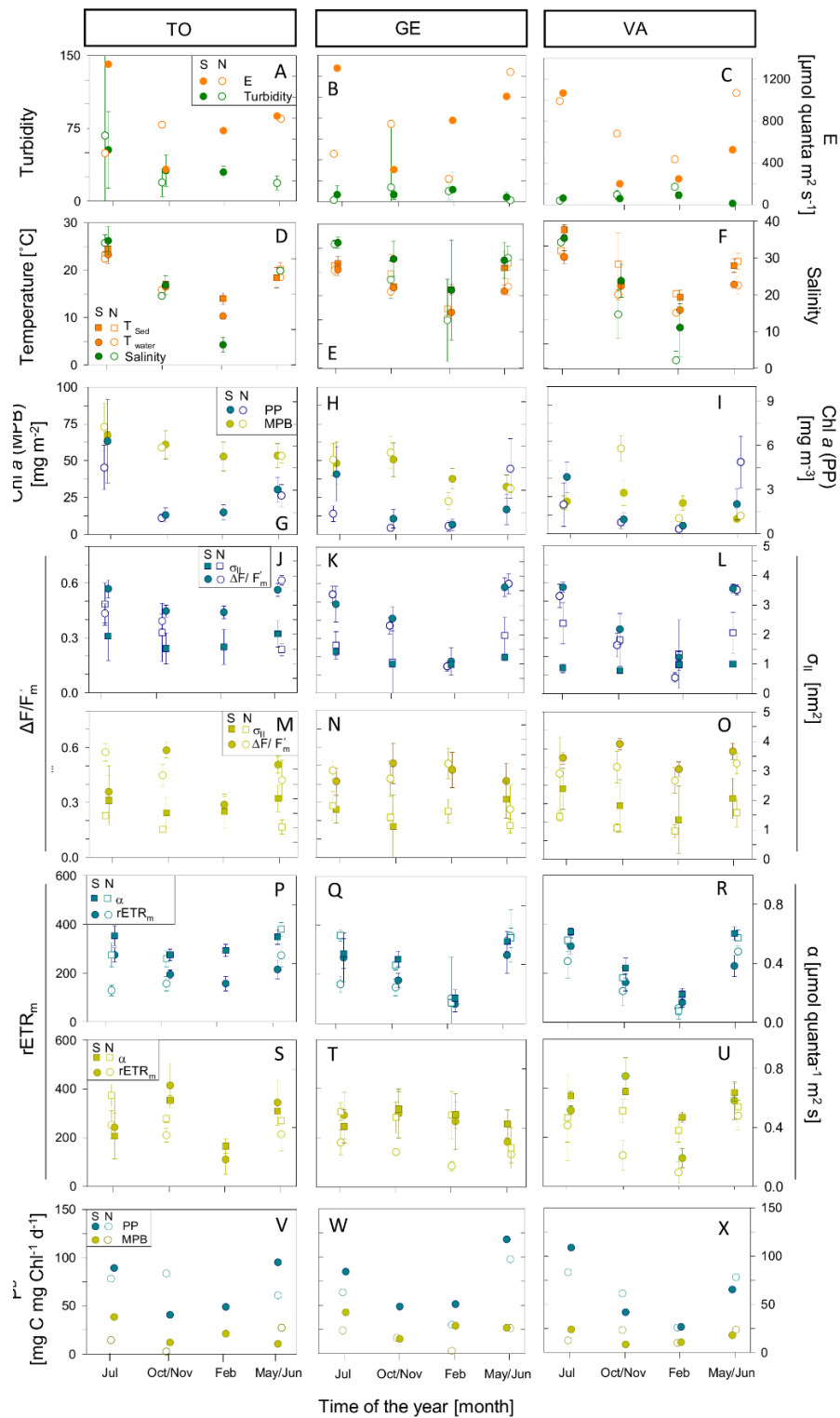


Figure 6. Seasonal variation of abiotic (A-F) and photophysiological (G-X) parameters in sampling sites Torreira (TO; A, D, G, J, M, P, S, V), Gafanha da Encarnação (GE; B, E, H, K, N, Q, T, W) and Vista Alegre (VA; C, F, I, L, O, R, U, X). PP in blue and MPB yellow. Spring tide (full circles) and Neap tide (empty circles). Mean values of three replicates. Error bars represent one standard error.

Both phytoplankton and microphytobenthos biomass varied significantly between sampling sites (ANOVA, $F_{2,817} = 25.14$; $P < 0.001$, and $F_{2,317} = 45.07$; $P < 0.001$, respectively), and in both cases the highest values were measured in site TO. In the case of the phytoplankton, the remaining two sites did not differ significantly (Tukey HSD, $P > 0.05$). Regarding the microphytobenthos, all sampling sites differed from each other (Tukey HSD, $P < 0.001$ for all pairwise comparisons), the lowest biomass values being found for site VA (Figure 6 G-I).

Phytoplankton and microphytobenthos also differed regarding the spatio-temporal variability of photophysiological parameters $\Delta F/F_m'$ and σ_{II} . In the case of the phytoplankton, both $\Delta F/F_m'$ and σ_{II} varied significantly with seasons (ANOVA, $F_{3,820} = 230.74$; $P < 0.001$ and $F_{3,705} = 43.63$; $P < 0.001$, respectively; Figure 6 J-O), the maximum values being measured in summer and the minimum in winter (Figure 6 K-L). Also in the case of the microphytobenthos $\Delta F/F_m'$ and σ_{II} varied significantly with seasons ($F_{3,335} = 48.02$; $P < 0.001$ and $F_{3,335} = 27.44$; $P < 0.001$, respectively). However, maximum values were observed for autumn ($\Delta F/F_m'$) or summer (σ_{II}), while minimum values were measured in spring (for both parameters) (Figure 6 M-O).

For phytoplankton, $\Delta F/F_m'$ varied significantly between spring and neap tides (higher values for spring tides) (ANOVA, $F_{1,820} = 67.01$; $P < 0.001$), while σ_{II} did not show significant differences (ANOVA, $F_{1,705} = 1.78$; $P > 0.1$). The opposite pattern was observed for the microphytobenthos, with σ_{II} varying between spring and neap tides (ANOVA, $F_{1,335} = 10.65$; $P < 0.01$), and $\Delta F/F_m'$ increasing significantly from neap to spring tides (ANOVA, $F_{1,335} = 15.414$; $P < 0.001$). In terms of spatial variation, phytoplankton showed a significant variation in $\Delta F/F_m'$ between sampling sites (ANOVA, $F_{2,820} = 28.04$; $P < 0.001$), with maximum values occurring at TO and minimum ones at VA, while no differences among sites were found regarding σ_{II} (ANOVA, $F_{2,705} = 2.29$; $P > 0.1$). In the case of the microphytobenthos, $\Delta F/F_m'$ also varied significantly between sampling sites (ANOVA, $F_{2,335} = 6.61$; $P < 0.01$), with maximum values being observed for site VA and minimum for site GE. σ_{II} varied significantly between sites (ANOVA, $F_{2,335} = 22.46$; $P < 0.001$), but showed the opposite pattern, with maximum values occurring at site GE and minimum ones at VA (Figure 6 M-O). Still regarding the parameters $\Delta F/F_m'$ and σ_{II} , the phytoplankton and the microphytobenthos differed not only concerning their spatio-temporal variability, but also in terms of their absolute values. While $\Delta F/F_m'$ showed comparable values (0.43 ± 0.16 and 0.47 ± 0.09 for phytoplankton and microphytobenthos (ANOVA, $F_{1,44} = 1.13$; $P > 0.1$), respectively; σ_{II} was significantly higher in the case of the phytoplankton (1.80 ± 1.19 and 1.19 ± 0.03 for phytoplankton and microphytobenthos, respectively; ANOVA, $F_{1,44} = 25.25$,

$P < 0.001$). Regarding the photoacclimation state, phytoplankton samples showed a significant seasonal variability in both light-limited (α) and light-saturated ($rETR_m$) photosynthetic activity (ANOVA, $F_{3,751} = 456.82$; $P < 0.001$ and $F_{3,749} = 307.2$; $P < 0.001$, respectively), with maximum value occurring in spring and minimum values observed in winter (Figure 6 P-R). The two parameters were also significantly higher in spring than in neap tides (ANOVA, $F_{1,751} = 71.44$; $P < 0.001$ and $F_{1,749} = 74.80$; $P < 0.001$, respectively). Spatially, differences were found only regarding α (ANOVA, $F_{2,751} = 41.37$; $P < 0.001$), with maximum values being reached at site TO and minimum ones at site VA (Figure 6 P,R). Regarding the microphytobenthos, also both α and $rETR_m$ varied significantly among seasons (ANOVA, $F_{3,335} = 7.661$; $P < 0.001$ and $F_{3,334} = 46.44$; $P < 0.001$, respectively), but with maximum values observed in autumn and minimum ones in winter (Figure 6 S-U). As observed for the phytoplankton, both parameters showed significantly higher values during spring tides than during neap tides (ANOVA, $F_{1,335} = 5.44$; $P < 0.05$ and $F_{1,334} = 81.94$; $P < 0.001$, for α and $rETR_m$ respectively). Both α and $rETR_m$ varied significantly between sampling sites (ANOVA, $F_{2,335} = 8.654$; $P < 0.001$ and $F_{2,334} = 3.45$; $P < 0.05$ *, respectively), in both cases reaching higher values at site VA and minimum values at site GE (Figure 6 T,U).

This large spatio-temporal variability in α and $rETR_m$ was reflected in substantial variations in the photoacclimation parameter E_k (data not shown). For both phytoplankton and microphytobenthos, E_k varied significantly over seasons (ANOVA, $F_{3,754} = 4.3$; $P < 0.01$ and $F_{3,334} = 39.91$; $P < 0.001$, respectively), reaching maximum values in spring and autumn (phytoplankton) or spring (microphytobenthos). For both types of samples, E_k was significantly higher on spring than on neap tides (ANOVA, $F_{1,754} = 4.6$; $P < 0.05$ and $F_{1,334} = 79.10$; $P < 0.001$, for phytoplankton and microphytobenthos, respectively). Phytoplankton E_k varied significantly between sampling sites (ANOVA, $F_{2,754} = 11.6$; $P < 0.001$), the highest values occurring at site VA and the minimum at site TO. In contrast, no significant differences were found between sampling sites for microphytobenthos ($F_{1,334} = 0.77$; $P = 0.466$).

Overall, the photoacclimation state of phytoplankton and microphytobenthos was very similar, with E_k values averaging 490.8 ± 211.7 and 491.5 ± 175.7 $\mu\text{mol quanta m}^{-2} \text{s}^{-1}$, respectively. However, with the exception of the winter sampling period, E_k was higher for the microphytobenthos (ranging from 490.7 ± 197.5 in summer to 561.9 ± 124.9 $\mu\text{mol quanta m}^{-2} \text{s}^{-1}$ in spring), than for the phytoplankton (ranging from 408.5 ± 28.5 in summer to 473.6 ± 107.7 $\mu\text{mol quanta m}^{-2} \text{s}^{-1}$ in spring).

Biomass-specific productivity

Despite the differences observed in physical conditions in the water column and the intertidal sediments, and the photophysiological and photoacclimation state of phytoplankton and microphytobenthos, the spatio-temporal patterns of variability of daily biomass-specific rates, P^B , of the two communities resulted relatively similar (Figure 6 V-X). For both phytoplankton and microphytobenthos, the daily rates of carbon fixation varied significantly with season (ANOVA, $F_{3,719} = 58.56$; $P < 0.001$ and $F_{3,315} = 17.40$; $P < 0.001$, respectively) and phase of the spring-neap tidal cycle (ANOVA, $F_{1,719} = 4.83$; $P < 0.05$ and $F_{1,315} = 5.19$; $P < 0.05$, respectively). With the exception of autumn, maximum values were observed for summer and spring, during spring tides, and minimum values for winter and neap tides. No significant differences were found between sampling sites. However, the absolute values of P^B were on average much higher for the phytoplankton than for the microphytobenthos, averaging 68.0 ± 26.1 and 19.1 ± 10.3 mg C mg Chla⁻¹ d⁻¹, respectively.

Light attenuation coefficients

The vertical light profiles measured in the sediment samples from the three sampling sites revealed an exponential attenuation of downwelling irradiance, enabling a very good fit of an exponential model (Figure 7). The attenuation coefficient k ranged from 3.9 ± 0.8 mm⁻¹ (TO) to 9.0 ± 0.8 mm⁻¹ (VA), GE reaching the intermediate value of 6.1 ± 0.6 mm⁻¹.

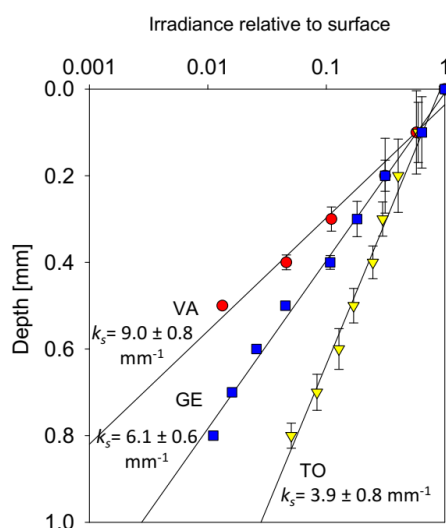


Figure 7. Vertical profile of spectrally-averaged irradiance (percentage of incident irradiance) in intertidal sediments of the three sampling sites Vista Alegre (VA), Gafanha da Encarnação (GE) and Torreira (TO). Number are the downwelling light attenuation coefficients (K_s) for each type of sediment. Mean values of three replicates. Error bars represent one standard error.

Areal production rates

Despite the fact that the hourly rates of biomass-specific production were higher for phytoplankton than for microphytobenthos, the depth-integrated areal rates revealed an opposite tendency. Due to the large differences in the biomass involved in photosynthesis, the depth-integrated hourly production rates of the microphytobenthos were often much higher than the corresponding rates of the phytoplankton (Figure 8 A-D). This difference was particularly large when the periods of low tide occurred at the middle of the day (e.g. Figure 8 B-D). The higher productivity of microphytobenthos was also verified when comparing the daily rates, despite the shorter periods of light exposure, considered for their calculation (264.5 ± 228.8 and 140.4 ± 154.8 mg C m⁻² d⁻¹, respectively; Figure 9 A-C). Maximum daily rates of carbon fixation ranged from 8.1 (winter, NT, GE) to 505.0 (summer, ST, TO) mg C m⁻² d⁻¹ for the phytoplankton, and from 25.6 (winter, ST, GE) to 909.0 (summer, ST, BE) mg C m⁻² d⁻¹, for the microphytobenthos.

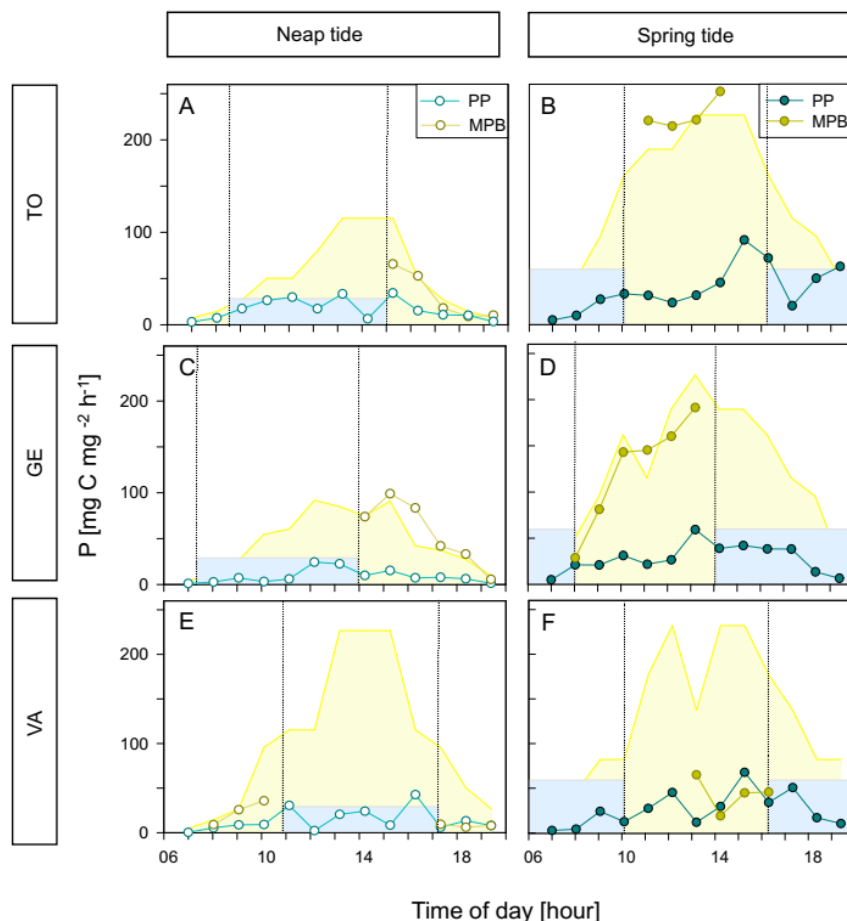


Figure 8. Hourly rates of biomass-specific primary production of phytoplankton (PP) and microphytobenthos (MPB) along two days in July 2013, on neap tides (A, C, E) and spring tides (B, D, F), at the three sampling sites, Torreira (TO; A, B), Gafanha da Encarnação (GE; C, D) and Vista Alegre (VA; E, F).

The marked seasonal and fortnight variability present in the biomass and photosynthetic performance was reflected on a significant variation in daily rates of areal production between seasons and spring-neap tide conditions (Figure 8; 9), of both phytoplankton ($F_{3,309} = 75.26$; $P < 0.001$ and $F_{1,309} = 11.19$; $P < 0.001$, comparing between seasons and spring-neap tides, respectively) and microphytobenthos ($F_{1,106} = 12.87$; $P < 0.001$ and $F_{1,106} = 9.90$; $P < 0.01$, comparing between seasons and spring-neap tides, respectively). In both cases, maximum values were attained in spring and summer, and on spring tides; minimum values occurred on winter and neap tides. Significant differences were also present regarding the spatial distribution. For the phytoplankton, large variations were found ($F_{2,309} = 7.66$; $P < 0.001$), showing maximum daily production for site TO and lower but comparable rates for sites GE and VA. For the microphytobenthos, significant variations between sampling sites were also observed ($F_{2,106} = 12.31$; $P < 0.001$), again with maximum values observed for site TO and minimal for VA.

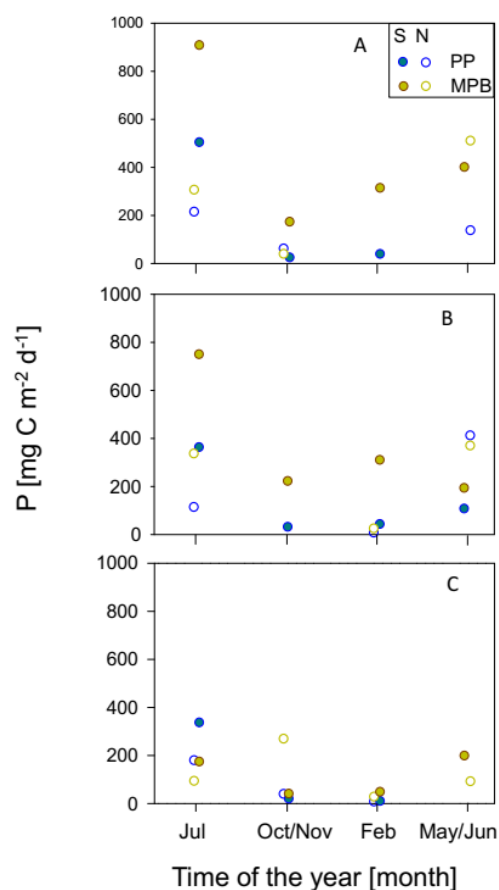


Figure 9. Seasonal variation of daily rates of primary production of phytoplankton (PP) and microphytobenthos (MPB) during spring (S) and neap (N) tide in sampling sites Torreira (A), Gafanha da Encarnação (B) and Vista Alegre (C).

Upscaling to ecosystem-level productivity

The data used to upscale the areal primary production rates to ecosystem-level values are summarized in Table 1. Per unit area, microphytobenthos productivity reached higher values than for the phytoplankton, with exception of the site VA (for which the values were practically identical). Phytoplankton rates averaged $48.9 \text{ g C m}^{-2} \text{ yr}^{-1}$, ranging from 44.7 to $51.8 \text{ g C m}^{-2} \text{ yr}^{-1}$ (for sites VA and GE, respectively). Microphytobenthos productivity rates averaged $105.2 \text{ g C m}^{-2} \text{ yr}^{-1}$, ranging between 43.4 to $164.4 \text{ g C m}^{-2} \text{ yr}^{-1}$ (for sites VA and TO, respectively). This tendency was reinforced when upscaling for the whole estuary, despite the larger area accounted for the phytoplankton: the primary production carried out by microphytobenthos and by phytoplankton were found to attain 7534.0 and 4894.3 t C yr^{-1} , representing 60.6% and 39.4% of the total global rate of primary production of the two communities in the Ria de Aveiro, that reached $12428.3 \text{ t C yr}^{-1}$.

Table 1. Summary of the data used for the upscaling of local areal primary production rates ($\text{g C m}^{-2} \text{ yr}^{-1}$) to ecosystem-level carbon fixation budget (t C yr^{-1}). Percentages refer to the proportion of primary production of phytoplankton or microphytobenthos relatively to the total.

	Site	Area (km^2)	Areal production ($\text{g C m}^{-2} \text{ yr}^{-1}$)	Total production (t C yr^{-1})
Phytoplankton	TO	33.3	50.31	1676.9
	GE	33.3	51.76	1725.3
	VA	33.3	44.76	1492.1
	Total	100.0		4894.3 (39.4%)
Microphytobenthos	TO	34.0	164.40	5589.6
	GE	16.0	107.97	1727.6
	VA	5.0	43.36	216.78
	Total	55.0		7534.0 (60.6%)
			Total	12428.3

Discussion

Abiotic factors

The sampling program carried out in this study allowed to cover and register a large variability in hourly, fortnight and seasonal time scales in all physical parameters measured for three studied sampling sites. Seasonal variability was pronounced for both the water column and the intertidal habitats, namely regarding water temperature, salinity and turbidity. In both habitats, a strong fortnight variability was superimposed on the seasonal cycle. In the intertidal habitat, stronger and faster changes were observed during tidal ebb

and flood, associated to sudden changes between immersion and exposure to sunlight and wind. For the intertidal communities, the experienced environmental variability is known to be characterized by a wider range of conditions than those observed only during low tide periods, due to the contrast between conditions during submersion under high tide (not monitored in this study) and air light exposure during low tide (de Jonge and van Beusekom, 1995; Koh et al., 2007; Pratt et al., 2014). These patterns of temporal variability were essentially the same in all sampling sites, despite the different time delay of the tidal propagation within the estuary, from sites GE to VA. The observed patterns of spatial and temporal environmental variability are typical of tidal estuaries, strongly dominated by the tidal rhythm (Brito et al., 2009; Kwon et al., 2012; Serôdio and Catarino, 1999). This strong periodicity of physical parameters propagated into a large variability in phytoplankton and microphytobenthos biomass and photosynthetic activity, ultimately determining their spatial-temporal patterns of productivity.

Biomass

The concurrent and high temporal resolution sampling of water column and intertidal sediments carried out in this work allowed for a direct comparison of the spatio-temporal variability of the biomass of phytoplankton and microphytobenthos, as well as their photophysiology, photosynthetic performance, and productivity.

In what regards biomass, the direct comparison of absolute values for microphytobenthos and phytoplankton is compromised by well-known difficulties, related to the calculation of values using comparable units. Ecologically-relevant estimates, expressed as areal units [e.g. mg Chl *a* m⁻²] are very dependent on the criteria used for the vertical integration of volumetric measurements (Flemming, 2000; Serôdio et al. 2001; Laviale et al., 2015).

The spatio-temporal variation of phytoplankton and microphytobenthos biomass coincided in several aspects, namely a large variation over seasons and spring-neap tidal cycles, and a large variation over sampling sites, with TO showing the highest values. This overall tendency for the two communities to co-vary spatio-temporally, especially regarding longer (seasonal) time scales, is likely tied to their common control by major abiotic factors, like irradiance and temperature (de Jonge et al., 2012; Haro et al., 2019; Liu et al., 2018) varying markedly over seasons.

Both phytoplankton and microphytobenthos biomass varied seasonally, but maximum values were observed later for the microphytobenthos (summer-autumn) than for the

phytoplankton (spring, summer). The earlier peaking of the phytoplankton biomass may be due to the more pronounced seasonal variation in favorable conditions for growth in the water column than in the benthos. The high nutrient availability in the water column due to upwelling events, or due to terrestrial runoff and fresh water inflow by the end of winter, commonly observed in estuaries and coastal areas (Vajravelu et al., 2018; Vidal et al., 2017) together with the start of favorable light and temperature conditions in spring, may have caused phytoplankton to respond more promptly in terms of growth and accumulation of biomass. The sharp decrease in autumn, also typically observed for estuarine phytoplankton (Pennock and Sharp, 1985; Tian et al., 2009; Vidal et al., 2017), is likely associated to exhaustion of nutrients due to intense uptake during spring and summer. On the other hand, seasonal changes in growth conditions for the microphytobenthos might not be as relevant as for the water column, especially in what regards nutrients, commonly assumed to be not limiting in this habitat all year round (Davis and McIntire, 1983; Brotas et al. 1995). Together with the continuation of favorable light and temperature conditions until autumn months, this may explain the prolonging of high biomass levels into later in the year. The occurrence of a significant fortnight variability in phytoplankton biomass, with maxima during spring tides, may be associated to the fact that during these periods, the shallower water column of low tide coincides with the maximum solar irradiance, allowing a more efficient illumination of the phytoplankton populations (Madariaga, 2002; Mallin and Paerl, 2012; Pennock and Sharp, 1985). Also, the faster water current of spring tides are expected to increase the resuspension of sediment and benthic cells, which may have contributed to the higher chlorophyll *a* content and nutrients in the water column (Delgado et al., 1991a). Naturally, differences in weather conditions between the sampling days may confound the detection of periodic variability associated to the spring-neap tidal cycle (Dring and Luning, 1994; Serôdio et al., 2008). For the microphytobenthos, a tendency for higher value for spring tides was also observed, most likely associated to the fact that the periods of low tide and light exposure during the middle of the day. Moreover, higher concentration of suspended sediment concentration seems to promote higher Chl *a* concentrations (de Jonge and van Beusekom, 1995; Pratt et al., 2014). However, the resulting fortnight variability in growth conditions was not sufficiently important to cause a detectable variation in the accumulation of biomass.

Spatially, the coincidence of higher amounts of both planktonic and benthic biomass may be related to higher rates of resuspension associated to stronger tidal currents at the TO sampling site (Brito et al., 2009; de Jonge and van Beusekom, 1995; Delgado et al., 1991b), that would cause a larger transfer of microalgal biomass from the benthos to the

water column. The reasons for the higher abundance of benthic biomass at this site are uncertain, but maybe related to a larger nutrient availability, caused by the combination of finer sediment granulometry, favoring organic matter remineralization, and of agricultural run-off, originated in the farm fields bordering the canals of the estuary.

Photophysiology and photoacclimation state

The photophysiological parameters $\Delta F/F_m'$ and σ_{II} are mostly controlled by changes in incident irradiance (Andersson et al., 2018; Grégoire et al., 2015; Houliez et al., 2013; Madariaga, 2002; Schreiber et al., 2012) and therefore showed large and rapid (minutes to hours) variations during daytime periods. However, both $\Delta F/F_m'$ and σ_{II} also showed consistent patterns of variation along the year, denoting longer changes in the photophysiological and photoacclimation state of phytoplankton and microphytobenthos. $\Delta F/F_m'$ largely followed the trends observed for the biomass of phytoplankton and microphytobenthos, regarding seasonality (peaking in summer and in autumn, respectively), the variation along the spring-neap tidal cycle (higher during spring tides in the case of the phytoplankton; not varying significantly in the case of the microphytobenthos) and spatial distribution (higher values at site TO, both communities). The similarity between the spatio-temporal variation of $\Delta F/F_m'$ and biomass suggests that the accumulation of biomass is directly related with better conditions enabling a high photosynthetic performance. The higher $\Delta F/F_m'$ values for the phytoplankton observed during spring tides may be associated to the increased availability of nutrients caused by the higher resuspension rates typical of the faster tidal currents occurring during spring tides. The lack of significant variations in $\Delta F/F_m'$ of the microphytobenthos may result from the fact that, in the sedimentary environment, photosynthesis is more limited by light conditions than nutrient availability, which, being present in non-limiting levels, may support a good photophysiological condition along the spring-neap tidal cycle.

Regarding σ_{II} , there was a general tendency to follow the patterns of spatial and temporal variation of $\Delta F/F_m'$ and biomass, namely concerning seasonal and fortnight time scales for phytoplankton. In other cases, the two parameters diverged from each other, indicating the independent short-term regulation of the processes controlling $\Delta F/F_m'$ and σ_{II} . A marked difference between the photophysiology of the phytoplankton and the microphytobenthos was revealed by the consistently higher values of σ_{II} measured for the phytoplankton. Higher values of σ_{II} are indicative of larger PSII antenna sizes, capable of higher light absorption efficiency, beneficial in low light environments and typical of low-light

acclimated organisms (Schreiber et al., 2012). Higher σ_{II} values may be advantageous for the planktonic microalgae living in turbid waters of the Ria de Aveiro estuary, where the experienced light regime calls for the optimization of light absorption. The lower σ_{II} values measured in the microphytobenthos samples are, on the other hand, symptomatic of a smaller PSII antenna, consistent with a high light environment, as the one at the sediment surface when directly exposed to sunlight during low tide.

The results on photoacclimation state obtained from RLCs repeat, in general terms, the overall patterns of spatio-temporal variability in biomass, $\Delta F/F_m'$ and (to a lesser extent) σ_{II} , with α and $rETR_m$ reaching maximum values during spring/summer (phytoplankton) and autumn (microphytobenthos), during spring tides (both communities). The marked seasonal photoacclimation in photophysiological parameters $\Delta F/F_m'$ and σ_{II} described above was confirmed by comparable large changes in the photoacclimation parameter E_k , for both phytoplankton and microphytobenthos. The highest E_k values observed during summer and the lowest values observed during winter denote a variation from a high light-acclimation to a low-light acclimation state following the change in light conditions between the two contrasting seasons. Although not as clear as for σ_{II} , the differences observed between E_k measured in phytoplankton and in microphytobenthos samples, showing a tendency for higher values in the later, supports that the benthic communities appear as high-light acclimated, when compared to their planktonic counterparts. Microphytobenthos showed moreover a fortnightly pattern regarding its photoacclimation state, showing higher values for $\Delta F/F_m'$ α and $rETR_m$ during spring tides when compared to neap tides. A consequence more likely due to the higher light dose received during spring tides rather than an effect of tidal height (Haro et al., 2019). The high light acclimation of estuarine intertidal microphytobenthos has been referred before, supported by relatively high values of E_k (Serodio et al. 2005, Frankenbach et al. 2018). It has been explained by the exposure to high solar irradiance levels during low tide periods, and, especially in the case of assemblages dominated by motile diatoms (epipellic), by the use of vertical migration as a form of control of light exposure within the photic zone of the sediment (Consalvey et al., 2004; Haro et al., 2019; Serôdio et al., 2001). Curiously, the microphytobenthos did not show a significant variation in the photoacclimation state between sampling sites, as opposed to what was previously reported for the sites VA and GE (Frankenbach et al 2018). This discrepancy cannot be explained yet, but might be due to differences in taxonomical composition.

Biomass-specific, areal and ecosystem-level productivity

In this study, the daily biomass-specific rates of productivity, P^B , were derived from the photophysiological parameters related to light usage efficiency ($\Delta F/F_m'$ and σ_{II}), integrated over daylight hours. As such, the patterns of spatio-temporal variation of P^B largely followed the ones observed for those parameters. Probably due to the larger values of σ_{II} measured in the water column, the production rates of the phytoplankton resulted substantially higher than those of the microphytobenthos, for all sampling occasions and sites. The incorporation of photosynthetic biomass and the vertical light attenuation in the water and in the sediment in the calculation of daily areal productivity rates did not alter the overall patterns of spatio-temporal distribution. However, it resulted in the inversion of the relative importance of phytoplankton and microphytobenthos. As expressed by units of area, benthic carbon fixation rates were on average 1.9 times higher than those in the water column. Despite the fact that the productivity rates determined in this study were based on chlorophyll fluorescence measurements, they fitted well within the range published values, based on the direct quantification of carbon fixation or oxygen evolution, for both estuarine phytoplankton and microphytobenthos (Table 2).

Regarding the phytoplankton, the average annual rate of $48.9 \text{ g C m}^{-2} \text{ yr}^{-1}$ appears as relatively low considering the median value of $252 \text{ g C m}^{-2} \text{ yr}^{-1}$ reported by the exhaustive meta-analysis study of Cloern et al. (2014). According to the classification of Nixon (1995), the studied sites from the Ria de Aveiro could be classified as oligotrophic. On the other hand, the average annual rate of $105.3 \text{ g C m}^{-2} \text{ yr}^{-1}$ determined for the microphytobenthos, is remarkably close to the value of $100 \text{ g C m}^{-2} \text{ yr}^{-1}$, taken as the typical value for primary production rate on estuarine intertidal flats (Underwood and Kromkamp, 1999; Daggert et al., 2018).

The relative contribution of the phytoplankton and the microphytobenthos to the ecosystem-level productivity has been discussed for decades (Underwood and Kromkamp, 1999), and some studies have reported that benthic productivity may reach over 50% of total estuarine carbon fixation (Cadée and Hegeman, 1974; Joint, 1978). The results of the present study showed that, despite an area twice as large accounted for the phytoplankton than for the microphytobenthos, the primary production carried out by the microphytobenthos may reach more than 60% of the 12 kt C yr^{-1} annual rate estimated for the whole Ria de Aveiro. This estimate is amongst the highest reported in the literature and similar to the value of 63.5% obtained by Joint (1978).

Table 2. Daily and annual primary productivity rates of phytoplankton and microphytobenthos as measured in this study and in published studies. Average values unless stated otherwise. ^a maximum daily values. ^b range of compiled values.

	Areal production		Reference
Phytoplankton	Daily (mg C m ⁻² d ⁻¹)	134.1	This study
		0.23-1.18	Morelle et al. 2018 ^a
		0.69	Cloern et al. 2014
		2-778	Gameiro et al. 2011
		1.2-4.8	Kromkamp et al. 2008
	Annual (g C m ⁻² yr ⁻¹)	48.9	This study
		252	Cloern et al. 2014
		140-700	Underwood & Kromkamp 1999
		77-92	Gameiro et al. 2011
	64.8	Morelle et al. 2018	
Microphytobenthos	Daily (mg C m ⁻² d ⁻¹)	259.8	This study
		1-2888 ^b	MacIntyre et al. 1996
		50-200	Daggers et al 2018
		5-1900	Underwood & Kromkamp 1999
		427	Serôdio & Catarino 2000
	Annual (g C m ⁻² yr ⁻¹)	105.2	This study
		142	Savelli et al. 2018
		47-178	Brotas et al. 1995
		156	Serôdio & Catarino 2000
	60-300	Underwood & Kromkamp 1999	

Assumptions and limitations of chlorophyll fluorescence-based productivity estimates

With the aim of obtaining an integrated characterization of the spatio-temporal variability of the photosynthetic activity and productivity of benthic and planktonic microalgal communities, this study employed a synoptic sampling plan to measure the activity of microphytobenthos and phytoplankton under *in situ* conditions, on the same sites, same days, and with the same high temporal resolution. Key for the parallel comparison of the two communities was the use of the same chlorophyll fluorescence-based technique for planktonic and benthic samples.

A novelty of this study was the estimation, for the first time, of production rates of microphytobenthos based on measurements of absolute rates of PSII electron transport (ETR). Previous studies have used chlorophyll fluorescence to estimate productivity rates of microphytobenthos, but they were based on determinations of relative ETR, integrated on empirically-derived indices (Barranguet 2000, Serôdio et al., 2007). For the phytoplankton, the use absolute ETR-based indices for the estimation of productivity rates

has been addressed extensively for a long time, mostly based on ‘pump-and-probe’ (e.g. Kolber and Falkowski, 1993; Sakshaug et al., 1997) or ‘fast repetition rate fluorometry’ (FRRF) (e.g. Houliiez et al., 2014) protocols. The protocol used in the present study, developed only recently, and specifically for the MC-PAM, and has been used only a few times, and only for phytoplankton (Morelle et al., 2018a; Morelle and Claquin, 2018). While being also based on single-turnover pulses (Kromkamp et al., 2008; Schreiber et al., 2012), this protocol is somewhat different from the pump-and-probe or FRRF approaches. Although no direct comparison has been carried out between two types of protocols, the results of this study in what regards the absorption cross section, σ_{II} , a parameter crucial for the determination of absolute ETR values, are comparable and well within the range of values obtained with other instruments.

This study is also novel because absolute ETR-based productivity estimates were applied to both phytoplankton and microphytobenthos. This approach presents several well-known significant operational advantages as compared to traditional methods based on the direct determination based on carbon fixation or oxygen evolution. In the context of the present study, it allowed for direct comparison of the two groups regarding the characterization of photoacclimation state, quantification of photosynthetic activity, and estimation of primary productivity. This approach followed in this study is, however, based on several important assumptions. These apply to both phytoplankton and microphytobenthos, and can be categorized as follows:

a) Conversion of fluorescence indices to biomass-specific carbon fixation rates. The method associated to the MC-PAM requires the *a priori* assumption of the values of PSU, $ne(O_2)$ and PQ (Eqs. 4,5) (Schreiber et al., 2012). A compilation of experimental data compiled by Suggett et al. (2010) shows that $ne(O_2)$, the number of electrons required for evolution of 1 molecule of O_2 , varies from below 1 to above 11 $e^- O_2^{-1}$. However, the values measured for diatoms, dinoflagellates and haptophytes, the dominant groups in the phytoplankton and microphytobenthos of the Ria de Aveiro (Frankenbach et al., 2018; Vidal et al., 2017) vary between 3 and 6 $e^- O_2^{-1}$. In this study, $ne(O_2)$ was assumed to reach 5 $e^- O_2^{-1}$, a value similar to those used by other authors (Kromkamp et al., 2008; Morelle et al., 2018; Schreiber et al., 2012). The photosynthetic quotient, PQ, was assumed be 1.1 mol C mol O_2^{-1} , a value commonly accepted, including in studies on estuarine phytoplankton (Kromkamp et al., 2008). PSU, the number of chlorophyll a molecules per photosynthetic unit, is the most variable parameters required to calculate P^B from fluorescence measurements, having a large direct impact on the final carbon fixation rates. For eukaryotes, the values assumed for PSU have varied from 500 (Lawrenz et al., 2013,

Schreiber et al 2011) and 1000 Chl PSII⁻¹ (Morelle and Claquin, 2018; Schreiber et al., 2012). For diatoms, dinoflagellates and haptophytes, PSU varies between ca. 300 and 700 Chl PSII⁻¹, averaging around 620 Chl PSII⁻¹ (Suggett et al., 2010). In the present study, PSU was assumed to be 600 Chl PSII⁻¹, a value considered representative of the main groups that dominate the phytoplankton and the microphytobenthos in the Ria de Aveiro. In the absence of more detailed data, the same value was assumed for both groups although it is conceivable that it may differ between phytoplankton and the microphytobenthos, not only due to different taxonomic composition as to differences in photoacclimation state. All things considered, it seems unlikely that a depart from these assumptions would significantly affect the main conclusions of this study. Even considering the widest range of variation of $n_e(O_2)$, PQ and PSU, the large difference between the areal and ecosystem-based productivity of phytoplankton and microphytobenthos would still hold.

b) Depth-integration of biomass-specific carbon fixation rates to areal productivity. An implicit assumption of the approach used in this study was to consider, for both the phytoplankton and the microphytobenthos, that the photosynthetic activity was constant over depth. That is, that the responses measured for samples collected at a single depth (water column) or at the surface (sediment) represent the ones in the remaining regions of the photic zone. For the phytoplankton, this assumption seems realistic, due to the homogeneity of the water column in the shallow and highly turbulent regions of the estuary. In the case of the microphytobenthos, this approach may be more problematic, especially due to the fact that the measurements were carried out on cells in suspension, under conditions not representative of the vertically heterogeneous physico-chemical environment of the sediment (MacIntyre et al., 1996; Serôdio, 2003).

c) Upscaling of areal to ecosystem-level productivity. Critical for a realistic evaluation of the planktonic and benthic productivity at the estuary-level, both in absolute as in relative terms, is the correct accounting of the area of subtidal and intertidal habitats, associated to phytoplankton and microphytobenthos productivity, respectively. Also important is to consider the time of day, and its variation along the spring-neap tidal cycle, when low or high tides occur, which determine the light incident on exposed tidal flats and the light penetration in the water column. In this study, due to the lack of detailed information, estuarine-level production was calculated from spatially and temporal-averaged productivity rates. The error associated to this approach is hard to quantify and can only be assessed with a much more extensive sampling program. Another assumption of this study was to consider that no benthic productivity occurred during immersion in high tide. However, this

common assumption seems justified by the high turbidity of the water column and vertical migratory behavior of benthic diatoms (Daggers et al., 2018; Serodio and Catarino, 2000).

Acknowledgments

The research was also funded by the Portuguese Foundation for Science and Technology, FCT, through Project BioChangeR (PTDC/AAC-AMB/121191/2010), and the fellowships SFRH/BPD/110615/2015 (N. Vaz), SFRH/BD/86788/2012 (S. Frankenbach), SFRH/BD/103973/2014 (L.Vaz). In addition, this study was supported by a Sapere-Aude Advanced grant from the Danish Council for Independent Research/Natural Sciences (M. Kühl) and an instrument grant from the Carlsberg Foundation (M. Kühl). Thanks are also due to CESAM (UID/AMB/50017 - POCI-01- 0145-FEDER-007638), to FCT/MEC through national funds (PIDDAC), and the co-funding by the FEDER, within the PT2020 Partnership Agreement and Compete 2020.

References

- Andersson, A., Brugel, S., Paczkowska, J., Rowe, O. F., and Figueroa, D. (2018). Influence of allochthonous dissolved organic matter on pelagic basal production in a northerly estuary. *Estuar. Coast. Shelf Sci.* 204, 225–235.
- Barbier, E. B., Hacker, S. D., Kennedy, C., Koch, E. W., Stier, A. C., and Silliman, B. R. (2011). The value of estuarine and coastal ecosystem services. *Ecol. Monogr.* 81, 169–193.
- Barranguet, C., and Kromkamp, J. (2000). Estimating primary production rates from photosynthetic electron transport in estuarine microphytobenthos. *Mar. Ecol. Prog. Ser.* 204, 39–52.
- Brito, A., Newton, A., Tett, P., and Fernandes, T. F. (2009). Temporal and spatial variability of microphytobenthos in a shallow lagoon: Ria Formosa (Portugal). *Estuar. Coast. Shelf Sci.* 83, 67–76.
- Brotas, V.; Cabrita, T.; Portugal, A.; Serôdio, J.; and Catarino, F. Spatio-temporal distribution of the microphytobenthic biomass in intertidal flats of Tagus Estuary (Portugal). *Hydrobiologia*, 300–301, 1 (1995), 93–104.
- Bueno-Pardo, J., García-Seoane, E., Sousa, A. I., Coelho, J. P., Morgado, M., Frankenbach, S., et al. (2018). Trophic web structure and ecosystem attributes of a temperate coastal lagoon (Ria de Aveiro, Portugal). *Ecol. Modell.* 378, 13–25.
- Cadée, G. C., and Hegeman, J. (1974). Primary production of phytoplankton in the Dutch Wadden Sea. *Netherlands J. Sea Res.* 8, 240–259.
- Caffrey, J. M., Murrell, M. C., Amacker, K. S., Harper, J. W., Phipps, S., and Woodrey, M. S. (2014). Seasonal and Inter-annual Patterns in Primary Production, Respiration, and Net Ecosystem Metabolism in Three Estuaries in the Northeast Gulf of Mexico. *Estuaries and Coasts* 37, 222–241.
- Cloern, J. E., Foster, S. Q., and Kleckner, A. E. (2014). Phytoplankton primary production in the world ' s estuarine-coastal ecosystems. 2477–2501.
- Consalvey, M., Paterson, D. M., and Underwood, G. J. C. (2004). The ups and downs of life in a benthic biofilm: migration of benthic diatoms. *Diatom Res.* 19, 181–202.
- Daggers, T. D., Kromkamp, J. C., Herman, P. M. J., and van der Wal, D. (2018). A model to assess microphytobenthic primary production in tidal systems using satellite remote sensing. *Remote Sens. Environ.* 211, 129–145.

- Davis, M. W., and McIntire, C. D. (1983). Effects of physical gradients on the production dynamics of sediment-associated algae. *Mar. Ecol. Prog. Ser.* 13, 103–114.
- de Jonge, V. N., Pinto, R., and Turner, R. K. (2012). Integrating ecological, economic and social aspects to generate useful management information under the EU Directives' "ecosystem approach." *Ocean Coast. Manag.* 68, 169–188.
- de Jonge, V. N., and van Beusekom, J. E. E. (1995). Wind- and tide-induced resuspension of sediment and microphytobenthos from tidal flats in the Ems estuary. *Limnol. Oceanogr.* 40, 776–778.
- Delgado, M., de Jonge, V. N., and Peletier, H. (1991a). Experiments on resuspension of natural microphytobenthos populations. *Mar. Biol.* 108, 321–328.
- Delgado, M., De Jonge, V. N., and Peletier, H. (1991b). Effect of sand movement on the growth of benthic diatoms. *J. Exp. Mar. Bio. Ecol.* 145, 221–231.
- Dias, J. M., Lopes, J. F., and Dekeyser, I. (1999). Hydrological characterisation of Ria de Aveiro, Portugal, in early summer. *Oceanol. Acta* 22, 473–485.
- Dias, J. M., Lopes, J. F., and Dekeyser, I. (2003). A numerical system to study the transport properties in the Ria de Aveiro lagoon. *Ocean Dyn.* 53, 220–231.
- Dring, M. J., and Luning, K. (1994). Influence of spring-neap tidal cycles on the light available for photosynthesis by benthic marine plants. *Mar. Ecol. Prog. Ser.* 104, 131–137.
- Eaton, J. W., and Moss, B. (1966). The estimation of numbers and pigment content in epipelagic algal populations. *Limnol. Oceanogr.* 11, 584–595.
- Eilers, P. H. C. C., and Peeters, J. C. H. H. (1988). A model for the relationship between light intensity and the rate of photosynthesis in phytoplankton. *Ecol. Modell.* 42, 199–215.
- Field, C. B. (1998). Primary Production of the Biosphere: Integrating Terrestrial and Oceanic Components. *Science*, 281, 237–240.
- Flemming, B. W. (2000). A revised textural classification of gravel-free muddy sediments on the basis of ternary diagrams. *Cont. Shelf Res.* 20, 1125–1137.
- Frankenbach, S., Azevedo, A. A., Reis, V., Dias, D., Vaz, L., Dias, J. M., et al. (2019). Functional resilience of PSII, vertical distribution and ecosystem-level estimates of subsurface microphytobenthos in estuarine tidal flats. *Cont. Shelf Res.* 182, 46–56.
- Frankenbach, S., Schmidt, W., Frommlet, J., and Serôdio, J. (2018). Photoinactivation, repair and the motility-physiology trade-off in microphytobenthos. *Mar. Ecol. Prog. Ser.* 601, 41–57.

- Genty, B., Briantais, J.-M. M., and Baker, N. R. (1989). The relationship between the quantum yield of photosynthetic electron transport and quenching of chlorophyll fluorescence. *Biochim. Biophys. Acta - Gen. Subj.* 990, 87–92.
- Grégoire, M., Lévy, M., Marra, J., Borges, A. V., and Brasseur, P. (2015). The variability of primary production in the ocean: From the synoptic to the global scale. *J. Mar. Syst.* 147, 1–2.
- Grippo, M. A., Fleeger, J. W., Rabalais, N. N., Condrey, R., and Carman, K. R. (2010). Contribution of phytoplankton and benthic microalgae to inner shelf sediments of the north-central Gulf of Mexico. *Cont. Shelf Res.* 30, 456–466.
- Haro, S., Bohórquez, J., Lara, M., Garcia-Robledo, E., González, C. J., Crespo, J. M., et al. (2019). Diel patterns of microphytobenthic primary production in intertidal sediments: the role of photoperiod on the vertical migration circadian rhythm. *Sci. Rep.* 9, 1–10.
- Houliet, E., Lizon, F., Artigas, L. F., Lefebvre, S. S., and Schmitt, F. G. F. G. (2013). Spatio-temporal variability of phytoplankton photosynthetic activity in a macrotidal ecosystem (the Strait of Dover, eastern English Channel). *Estuar. Coast. Shelf Sci.* 129, 37–48.
- Houliet, E., Simis, S., Nenonen, S., Ylöstalo, P., and Seppälä, J. (2017). Basin-scale spatio-temporal variability and control of phytoplankton photosynthesis in the Baltic Sea: The first multiwavelength fast repetition rate fluorescence study operated on a ship-of-opportunity. *J. Mar. Syst.* 169, 40–51.
- Joint, I. R. (1978). Microbial production of an estuarine mudflat. *Estuar. Coast. Mar. Sci.* 7, 185–195.
- Koh, C.-H., Khim, J. S., Araki, H., Yamanishi, H., and Koga, K. (2007). Within-day and seasonal patterns of microphytobenthos biomass determined by co-measurement of sediment and water column chlorophylls in the intertidal mudflat of Nanaura, Saga, Ariake Sea, Japan. *Estuar. Coast. Shelf Sci.* 72, 42–52.
- Kolber, Z., and Falkowski, P. G. (1993). Use of active fluorescence to estimate phytoplankton photosynthesis in situ. *Limnol. Oceanogr.* 38, 1646–1665.
- Kromkamp, J., Barranguet, C., and Peene, J. (1998). Determination of microphytobenthos PSII quantum efficiency and photosynthetic activity by means of variable chlorophyll fluorescence. *Mar. Ecol. Prog. Ser.* 162, 45–55.
- Kromkamp, J. C., Dijkman, N. A., Peene, J., Simis, S. G. H., and Gons, H. J. (2008). Estimating phytoplankton primary production in Lake IJsselmeer (The Netherlands)

- using variable fluorescence (PAM-FRRF) and C-uptake techniques. *Eur. J. Phycol.* 43, 327–344
- Kühl, M. (2005). Optical microsensors for analysis of microbial communities. *Methods Enzymol.* 397, 166–99.
- Kwon, B. O., Khim, J. S., Park, J., Ryu, J., Kang, S. G., and Koh, C. H. (2012). Short-term variability of microphytobenthic primary production associated with in situ diel and tidal conditions. *Estuar. Coast. Shelf Sci.* 112, 236–242.
- Laviale, M., Ezequiel, J., Pais, C., Cartaxana, P., and Serôdio, J. (2015). The “crème brûlée” sampler: A new high-resolution method for the fast vertical sampling of intertidal fine sediments. *J. Exp. Mar. Bio. Ecol.* 468, 37–44.
- Lawrenz, E., Silsbe, G. M., Capuzzo, E., Ylöstalo, P., Forster, R. M., Simis, S. G. H., et al. (2013). Predicting the Electron Requirement for Carbon Fixation in Seas and Oceans. *PLoS One* 8.
- Lopes, C. L., Azevedo, A., and Dias, J. M. (2013). Flooding assessment under sea level rise scenarios : Ria de Aveiro case study. *Coast. Res* 65, 766–771.
- Lorenzen, C. J. (1967). Determination of Chlorophyll and Pheo-Pigments: Spectrophotometric Equations. *Limnol. Oceanogr.* 12, 343–346.
- Liu, B., Swart, H. E. De, and Jonge, V. N. De (2018). Phytoplankton bloom dynamics in turbid , well-mixed estuaries : A model study. *Estuar. Coast. Shelf Sci.* 211, 137–151.
- Madariaga, I. (2002). Short-term variations in the physiological state of phytoplankton in a shallow temperate estuary. *Hydrobiologia* 475–476, 345–358.
- MacIntyre, H. L., Geider, R. J., and Miller, D. C. (1996). Microphytobenthos: The Ecological Role of the “Secret Garden” of Unvegetated, Shallow-Water Marine Habitats. I. Distribution, Abundance and Primary Production. *Estuaries* 19, 186.
- Mallin, M. A., and Paerl, H. W. (2012). Effects of variable irradiance on phytoplankton in shallow productivity estuaries. 37, 54–62.
- McLusky, D. S., and Elliott, M. (2007). Transitional waters: A new approach, semantics or just muddying the waters? *Estuar. Coast. Shelf Sci.* 71, 359–363.
- Morelle, J., and Claquin, P. (2018). Electron requirements for carbon incorporation along a diel light cycle in three marine diatom species. *Photosynth. Res.* 0, 0.
- Morelle, J., Orvain, F., and Claquin, P. (2018a). A simple, user friendly tool to readjust raw PAM data from field measurements to avoid over- or underestimating of microphytobenthos photosynthetic parameters. *J. Exp. Mar. Bio. Ecol.* 503, 136–146.

- Morelle, J., Schapira, M., Orvain, F., Riou, P., Lopez, P. J., Pierre-Duplessix, O., et al. (2018b). Annual Phytoplankton Primary Production Estimation in a Temperate Estuary by Coupling PAM and Carbon Incorporation Methods. *Estuaries and Coasts* 41, 1–19.
- Nixon, S. W.: Coastal marine eutrophication – a definition, social causes, and future concerns, *Ophelia*, 41, 199–219, 1995
- Pennock, J. R., and Sharp, J. H. (1985). Phytoplankton production in the Delaware Estuary: temporal and spatial variability.
- Plante-Cuny, M. R. (1974). Evaluation par spectrophotométrie des teneurs en chlorophylle a fonctionnelle et en pheopigments des substrats meubles marins. *Off. la Rech. Sci. Tec. O.-m.*
- Pratt, D. R., Pilditch, C. A., Lohrer, A. M., and Thrush, S. F. (2014). The effects of short-term increases in turbidity on sandflat microphytobenthic productivity and nutrient fluxes. *J. Sea Res.* 92, 170–177.
- Rickelt, L. F., Lichtenberg, M., Trampe, E. C. L., and Kühl, M. (2016). Fiber-optic probes for small-scale measurements of scalar irradiance. *Photochem. Photobiol.* 92, 331–342.
- Sakshaug, E., Bricaud, A., Dandonneau, Y., Falkowski, P. G., Kiefer, D. A., Legendre, L., et al. (1997). Parameters of photosynthesis: definitions, theory and interpretation of results. *J. Plankton Res.* 19, 1637–1670.
- Schreiber, U., Klughammer, C., and Kolbowski, J. (2012). Assessment of wavelength-dependent parameters of photosynthetic electron transport with a new type of multi-color PAM chlorophyll fluorometer. *Photosynth. Res.* 113, 127–144.
- Schreiber, U., Klughammer, C., and Kolbowski, J. (2011). High-end chlorophyll fluorescence analysis with the MULTI-COLOR-PAM . I . Various light qualities and their applications . *PAM Appl. Notes* 1, 1–21. Available at: <http://www.walz.com/>.
- Serôdio, J. (2003). A chlorophyll fluorescence index to estimate short-term rates of photosynthesis by intertidal microphytobenthos. *J. Phycol.* 39, 33–46. doi:10.1046/j.1529-8817.2003.02043.x.
- Serôdio, J., and Catarino, F. (2000). Modelling the primary productivity of intertidal microphytobenthos: time scales of variability and effects of migratory rhythms. *Mar. Ecol. Prog. Ser.* 192, 13–30.

- Serôdio, J., and Catarino, F. (1999). Fortnightly light and temperature variability in estuarine intertidal sediments and implications for microphytobenthos primary productivity. *Aquat. Ecol.* 33, 235–241. doi:10.1023/A:1009989229098.
- Serôdio, J., Da Silva, J. M., and Catarino, F. (2001). Use of in vivo chlorophyll a fluorescence to quantify short-term variations in the productive biomass of intertidal microphytobenthos. *Mar. Ecol. Prog. Ser.* 218, 45–61. doi:10.3354/meps218045.
- Serôdio, J., Vieira, S. S., and Barroso, F. (2007). Relationship of variable chlorophyll fluorescence indices to photosynthetic rates in microphytobenthos. *Aquat. Microb. Ecol.* 49, 71–85. doi:10.3354/ame01129.
- Serôdio, J., Vieira, S., and Cruz, S. (2008). Photosynthetic activity, photoprotection and photoinhibition in intertidal microphytobenthos as studied in situ using variable chlorophyll fluorescence. *Cont. Shelf Res.* 28, 1363–1375. doi:10.1016/j.csr.2008.03.019.
- Suggett, D. J., Moore, C. M., and Geider, R. J. (2010). “Estimating aquatic productivity from active fluorescence measurements,” in *Chlorophyll a Fluorescence in Aquatic Sciences: Methods and Applications, Developments in Applied Phycology 4*, eds. D. J. Suggett, O. Prasil, and M. A. Borowitzka (Springer), 103–127.
- Tagliarolo, M., and Scharler, U. M. (2018). Spatial and temporal variability of carbon budgets of shallow South African subtropical estuaries. *Sci. Total Environ.* 626, 915–926. doi:10.1016/j.scitotenv.2018.01.166.
- Tian, T., Merico, A., Su, J., Staneva, J., Wiltshire, K., and Wirtz, K. (2009). Importance of resuspended sediment dynamics for the phytoplankton spring bloom in a coastal marine ecosystem. *J. Sea Res.* 62, 214–228. doi:10.1016/j.seares.2009.04.001.
- Tomás, L. M., Rodrigues, M., Fortunato, A. B., Azevedo, A., Leitão, P. C., Oliveira, A., et al. (2014). Salinity modelling accuracy of a coastal lagoon: a comparative river flow analysis of basin model vs. traditional approaches. *J. Coast. Res.* 70, 586–591. doi:10.2112/SI70-099.1.
- Underwood, G. J. C., and Kromkamp, J. (1999). Primary production by phytoplankton and microphytobenthos in estuaries. *Adv. Ecol. Res.* 29, 93–153. doi:10.1016/S0065-2504(08)60192-0.
- Vajravelu, M., Martin, Y., and Ayyappan, S. (2018). Seasonal influence of physico-chemical parameters on phytoplankton diversity, community structure and abundance at Parangipettai coastal waters, Bay of Bengal, South East Coast of India. *Oceanologia* 60, 114–127. doi:10.1016/j.oceano.2017.08.003.

- Van Colen, C., Underwood, G. J. C., Serôdio, J., and Paterson, D. M., (2014). Ecology of intertidal microbial biofilms: Mechanisms, patterns and future research needs. *J. Sea Res.* 92, 2–5. doi:10.1016/j.seares.2014.07.003.
- Vaz, N., and Dias, J. M. (2008). Hydrographic characterization of an estuarine tidal channel. *J. Mar. Syst.* 70, 168–181. doi:10.1016/j.jmarsys.2007.05.002.
- Vaz, N., Vaz, L., Serôdio, J., and Dias, J. M. (2019). A modeling study of light extinction due to cohesive sediments in a shallow coastal lagoon under well mixed conditions. *Sci. Total Environ.* 694, 133707. doi:10.1016/j.scitotenv.2019.133707.
- Vidal, T. T., Calado, A. J., Moita, M. T., and Cunha, M. R. (2017). Phytoplankton dynamics in relation to seasonal variability and upwelling and relaxation patterns at the mouth of Ria de Aveiro (West Iberian Margin) over a four-year Period. *PLoS One* 12, 1–25. doi:10.1371/journal.pone.0177237

Chapter 6

FINAL REMARKS AND FUTURE PERSPECTIVES

A main achievement of this study was the establishment of novel methodological approaches for the study of the photophysiology and productivity of microphytobenthos. On one hand, the validation and optimization of imaging fluorometry based on multi-actinic illumination to be applied to microphytobenthos samples paved the way to study their photophysiology with unprecedented detail (Chapters 2, 3). Their application to two different natural microphytobenthic communities of the Ria de Aveiro allowed a deeper understanding of the relative importance of photoprotective mechanism against photoinhibition, through the comparative assessment of their effective impact in preventing PSII photoinactivation (Chapter 3). On the other hand, the application of novel chlorophyll fluorescence protocols allowed to measure the absolute rates of PSII electron transport and enabled the estimation of primary production rates. This approach resulted in a comparative evaluation of the phytoplankton and microphytobenthos productivity of in a same estuary, the Ria de Aveiro, along the same spatial and temporal scales (Chapter 5).

The study of microphytobenthos photophysiology is often based on the characterization of light-response curves of PSII relative electron transport rate (rETR), measured using Pulse Amplitude Modulation (PAM) fluorometry (e.g. Kromkamp et al., 1998; Laviale et al., 2015; Perkins et al., 2010; Serôdio et al., 2008). The traditional approach of generating light response based on sequential protocols (Chevalier et al., 2010; Lefebvre et al., 2011; Serôdio et al., 2005; Ubertini et al., 2015; Waring et al., 2007) has major drawbacks, namely the lack of independency between measurements (Herlory et al., 2007; Ihnken et al., 2010; Jesus et al., 2006; Perkins et al., 2006), and, in the case of microphytobenthic biofilms, the confounding influence of vertical migration (Herlory et al., 2007; Jesus et al., 2006; Perkins et al. 2006). Light-induced vertical movements of motile diatoms during the construction of the light curve unavoidably affect the characterization of the inherent physiological response of the cells forming the biofilm. This work (Chapter 2) showed that these limitations may be overcome by the adaptation of a recently-proposed method, based on the generation of non-sequential light-response curves using multi-actinic light sources ('single-pulse light curves', SPLC; Serôdio et al., 2013). The method was optimized for the study of microphytobenthos biofilms, in order to allow to measure steady-state light responses, while minimizing the effects of vertical migration.

This approach was shown to be an advantageous alternative in relation to conventionally used protocols and is particularly promising for the case of biofilms dominated by motile species. It is foreseen that it may be used to study with unprecedented resolution the light-response of benthic microalgal communities, for example detecting

short-term changes in their photoacclimation state under the rapidly changeable abiotic conditions typical of the intertidal environment.

Photoinhibition has been considered a major potential limiting factor of microphytobenthos productivity (Admiraal, 1984; Kromkamp et al., 1998b; Serôdio et al., 2001). The high photosynthetic rates often observed in spite of the harsh conditions of the intertidal habitat have been attributed to the operation of particularly effective photoprotective mechanisms: photo-regulated vertical migration, allowing motile cells to safely optimize the balance between light exposure and dissipation of excess absorbed light energy (the 'behavioral photoprotection' hypothesis), and energy-dissipation mechanism, collectively named as non-photochemical quenching (NPQ) (Admiraal, 1984; Consalvey et al., 2004; Laviale et al., 2015; Serôdio et al., 2012; Underwood and Kromkamp, 1999). The relative importance of behavioral and physiological protection has attracted considerable interest in recent years (Barnett et al., 2015; Blommaert et al., 2017; Mouget et al., 2008; Pniewski et al., 2015; Serôdio et al., 2001; Van Leeuwe et al., 2008). However, the evaluation of the photoprotective role of vertical migration and NPQ has been based on indirect evidence, namely on the magnitude of NPQ or net photoinactivation, and not on the actual effects in terms of induced decrease of the susceptibility to photodamage.

The recently-developed multi-actinic approach of Serôdio et al. (2017) allowed to measure rates of PSII photoinactivation and repair, by assessing the efficiency of physiological photoprotection in terms of photosystem II (PSII) photoinactivation caused by light stress. The results reported in Chapter 3 brought new light to the understanding of the interplay between photoprotection and photoinhibitory stress. The comparison of the inherent physiological photoprotection capacity of epipelagic (dominated by motile species) and epipsammic (dominated by non-motile species) diatom communities, point to a trade-off between motility-based and physiological photoprotective mechanisms, a corollary of the 'behavioral photoprotection' hypothesis (Juneau et al., 2015; Laviale et al., 2016; Serôdio et al., 2001): epipelagic species, having the possibility to adjust light exposure behaviorally, have a reduced physiological capacity for preventing photodamage and are more susceptible to photoinactivation; non-motile forms are less susceptible to photoinactivation, and more dependent on physiological mechanisms to optimize their photoprotection capacity.

Due to its high-throughput capacity, the approach used in this study opens the way to the measurement of PSII photoinactivation and repair and may easily be applied to systematically test the 'new paradigm' hypothesis in different photoautotrophs. In the case of microphytobenthos, a natural follow-up of this work would be the study of the

photoinactivation versus repair balance in populations from habitats of contrasting light regimes (e.g. different tidal height) and taxonomic composition.

The existence of substantial amounts of chlorophyll *a* buried in sediment layers below the surface is well known (Brotas and Serodio, 1995; De Jonge and Colijn, 1994; Fenchel and Straarup, 1971; Mundree et al., 2003; Steele and Baird, 1968). This subsurface biomass has been hypothesized to play an important ecological role in intertidal estuarine areas, as a source of photosynthetically competent cells capable of 're-inoculating' the surface and contributing to the maintenance of high levels of productivity (Delgado et al., 1991; Easley et al., 2005). However, the importance of this subsurface stock of microalgae, as well as their potential viability, has attracted limited attention (Wasmund, 1989).

The study described in Chapter 4 allowed to quantitatively evaluate the relative importance of subsurface microalgal biomass, for different sediments of the Ria de Aveiro. It was found that surface biomass (0.0-0.5 cm) only accounted for one fifth to one third of the total biomass present below the surface (0.5-10 cm), and that the amount of subsurface viable biomass reached 2-3 times the biomass present at the surface layers. The study also confirmed the role of subsurface microalgal biomass as a potential source of photosynthetically active cells for the biofilm on the surface. Buried cells were found to withstand prolonged periods in continuous darkness and to regain photosynthetic activity within a short period (1.5 to 3 hours, depending on sediment type) of exposure to surface conditions.

The findings of this study call the attention for the importance of subsurface functional microalgal biomass, paving the way for similar approaches in other estuarine ecosystems. An interesting aspect that deserves a more in-depth analysis is the detailed taxonomic characterization of the subsurface microalgal populations, and of the viability variability amongst species or higher taxonomic groups. A natural follow up of this study would be the direct quantification of vertical distribution of sediment carbon content, which here was only inferred from chlorophyll *a* content.

The phytoplankton and the microphytobenthos have been considered as the main groups of primary producers in the estuarine environment (Cloern et al., 2014; Underwood and Kromkamp, 1999). Likely, due to methodological difficulties, most studies on estuarine primary productivity have focused only on one of these groups, resulting in the fact that directly comparable carbon fixation budgets are still relatively scarce. By taking advantage of a novel chlorophyll fluorescence-based method, the study of Chapter 5 allowed the detailed characterization of the spatio-temporal variability of the primary productivity of phytoplankton and microphytobenthos in the tidal estuarine system of the Ria de Aveiro.

Being based on synoptic high temporal resolution measurements, this study further enabled to estimate directly comparable rates of primary productivity for the two groups. While biomass-specific productivity rates were found to reach higher levels for the phytoplankton than for the microphytobenthos (averaging 68.0 and 19.1 mg C mg Chl a⁻¹ d⁻¹, respectively), areal production rates were generally higher for the microphytobenthos, with annual rates reaching 105.2 g C m⁻² yr⁻¹, as opposed to 49.9 g C m⁻² yr⁻¹ for the phytoplankton. When upscaling for the whole estuarine area of the Ria de Aveiro, the results reinforce the importance of the intertidal areas, found to contribute with more than 60% of the total ecosystem-level budget 12428.3 t C yr⁻¹.

Together with the results of Chapter 4, these results reinforce the importance of the intertidal areas as the main sites of primary production, acting as significant carbon sinks and reservoirs of active 'blue carbon'. In terms of primary productivity, the importance of the intertidal areas is likely higher than the estimated in this study, as other communities of primary producers, such as seagrass and macroalgae, will also contribute to annual carbon fixation budgets.

The fluorescence protocol used in this study for the estimation of primary productivity was introduced with the MC-PAM in 2012 and has only been used a few times for this purpose (Morelle and Claquin, 2018). The results here shown, especially considering that they cover a wide range of spatial and temporal scales of *in situ* variability, indicate that this method represents a valid approach for the study of primary productivity of microalgae communities. Considering the operational advantages of fluorescence-based methods, this approach may in the future be used for a more rapid and comprehensive characterization of the primary productivity of phytoplankton and microphytobenthos in other aquatic ecosystems. The full validation of this approach would benefit from the systematic comparison with other methods, either fluorescence-based methods that were established longer ago (e.g. FRRF), or methods relying on the direct measurement of carbon uptake.

References

- Admiraal, W. (1984). The ecology of estuarine sediment-inhabiting diatoms. *Prog. Phycol. Res.* 3, 269–322.
- Barnett, A., Méléder, V., Blommaert, L., Lepetit, B., Gaudin, P., and Vyverman, W., Sabbe, K., Dupuy, C., and Lavaud J. (2014). Growth form defines physiological photoprotective capacity in intertidal benthic diatoms. *ISME J.* 9, 32–45.
- Blommaert, L., Huysman, M. J. J., Vyverman, W., Lavaud, J., and Sabbe, K. (2017). Contrasting NPQ dynamics and xanthophyll cycling in a motile and a non-motile intertidal benthic diatom. *Limnol. Oceanogr.* 62, 1466–1479.
- Brotas, V., and Serodio, J. (1995). A mathematical model for the vertical distribution of Chlorophyll a in estuarine intertidal sediments. *Netherlands J. Aquat. Ecol.* 29, 315–321.
- Chevalier, E. M., Gévaert, F., and Créach, A. (2010). In situ photosynthetic activity and xanthophylls cycle development of undisturbed microphytobenthos in an intertidal mudflat. *J. Exp. Mar. Bio. Ecol.* 385, 44–49.
- Cloern, J. E., Foster, S. Q., and Kleckner, A. E. (2014). Phytoplankton primary production in the world ' s estuarine-coastal ecosystems. *Biogeosciences* 11, 2477–2501.
- Consalvey, M., Paterson, D. M., and Underwood, G. J. C. (2004). The ups and downs of life in a benthic biofilm: migration of benthic diatoms. *Diatom Res.* 19, 181–202.
- De Jonge, V. N., and Colijn, F. (1994). Dynamics of microphytobenthos biomass in the Ems Estuary. *Mar. Ecol. Prog. Ser.* 104, 185–196.
- Delgado, M., de Jonge, V. N., and Peletier, H. (1991). Experiments on resuspension of natural microphytobenthos populations. *Mar. Biol.* 108, 321–328.
- Easley, J. T., Hymel, S. N., and Plante, C. J. (2005). Temporal patterns of benthic microalgal migration on a semi-protected beach. *Estuar. Coast. Shelf Sci.* 64, 486–496.
- Fenchel, T., and Straarup, B. J. (1971). Vertical Distribution of Photosynthetic Pigments and the Penetration of Light in Marine Sediments. *Oikos* 22, 172–182.
- Herlory, O., Richard, P., and Blanchard, G. F. (2007). Methodology of light response curves: application of chlorophyll fluorescence to microphytobenthic biofilms. *Mar. Biol.* 153, 91–101.
- Ihnken, S., Eggert, A., and Beardall, J. (2010). Exposure times in rapid light curves affect photosynthetic parameters in algae. *Aquat. Bot.* 93, 185–194.

- Jesus, B., Perkins, R. G., Consalvey, M., Brotas, V., and Paterson, D. M. (2006). Effects of vertical migrations by benthic microalgae on fluorescence measurements of photophysiology. *Mar. Ecol. Prog. Ser.* 315, 55–66. doi:10.3354/meps315055.
- Juneau, P., Barnett, A., Méléder, V., Dupuy, C., and Lavaud, J. (2015). Combined effect of high light and high salinity on the regulation of photosynthesis in three diatom species belonging to the main growth forms of intertidal flat inhabiting microphytobenthos. *J. Exp. Mar. Bio. Ecol.* 463, 95–104.
- Kromkamp, J., Barranguet, C., and Peene, J. (1998). Determination of microphytobenthos PSII quantum efficiency and photosynthetic activity by means of variable chlorophyll fluorescence. *Mar. Ecol. Prog. Ser.* 162, 45–55.
- Laviale, M., Ezequiel, J., Pais, C., Cartaxana, P., and Serôdio, J. (2015). The “crème brûlée” sampler: A new high-resolution method for the fast vertical sampling of intertidal fine sediments. *J. Exp. Mar. Bio. Ecol.* 468, 37–44.
- Laviale, M., Frankenbach, S., and Serôdio, J. (2016). The importance of being fast: comparative kinetics of vertical migration and non-photochemical quenching of benthic diatoms under light stress. *Mar. Biol.* 163, 1–12.
- Lefebvre, S., Mouget, J.-L., and Lavaud, J. (2011). Duration of rapid light curves for determining the photosynthetic activity of microphytobenthos biofilm in situ. *Aquat. Bot.* 95, 1–8.
- Morelle, J., and Claquin, P. (2018). Electron requirements for carbon incorporation along a diel light cycle in three marine diatom species. *Photosynth. Res.* 137 (2) 201-214.
- Mouget, J. L., Perkins, R., Consalvey, M., and Lefebvre, S. (2008). Migration or photoacclimation to prevent high irradiance and UV-B damage in marine microphytobenthic communities. *Aquat. Microb. Ecol.* 52, 223–232.
- Mundree, S., Perissinotto, R., and Nozais, C. (2003). Seasonal variations in the vertical distribution of benthic microalgae in the upper sediment of the Mdloti Estuary, South Africa. *Bot. Mar.* 46, 323–331.
- Perkins, R. G., Mouget, J.-L., Lefebvre, S., and Lavaud, J. (2006). Light response curve methodology and possible implications in the application of chlorophyll fluorescence to benthic diatoms. *Mar. Biol.* 149, 703–712.
- Perkins, R. G., Lavaud, J., Serôdio, J., Mouget, J. L., Cartaxana, P., Rosa, P., Barille, L., Brotas, V., and Jesus, B.M. (2010). Vertical cell movement is a primary response of intertidal benthic biofilms to increasing light dose. *Mar. Ecol. Prog. Ser.* 416, 93–103.

- Pniewski, F. F., Biskup, P., Bubak, I., Richard, P., Latała, A., and Blanchard, G., (2015). Photo-regulation in microphytobenthos from intertidal mudflats and non-tidal coastal shallows. *Estuar. Coast. Shelf Sci.* 152, 153–161.
- Serôdio, J., Ezequiel, J., Barnett, A., Mouget, J. L., Méléder, V., Laviale, M. and Lavaud, J., (2012). Efficiency of photoprotection in microphytobenthos: Role of vertical migration and the xanthophyll cycle against photoinhibition. *Aquat. Microb. Ecol.* 67, 161–175.
- Serôdio, J., Da Silva, J. M., and Catarino, F. (2001). Use of *in vivo* chlorophyll a fluorescence to quantify short-term variations in the productive biomass of intertidal microphytobenthos. *Mar. Ecol. Prog. Ser.* 218, 45–61.
- Serôdio, J., Ezequiel, J., Frommlet, J., Laviale, M. and Lavaud, J., (2013). A method for the rapid generation of nonsequential light-response curves of chlorophyll fluorescence. *Plant Physiol.* 163, 1089–102.
- Serôdio, J., Vieira, S., Cruz, S. and Barroso, F. (2005). Short-term variability in the photosynthetic activity of microphytobenthos as detected by measuring rapid light curves using variable fluorescence. *Mar. Biol.* 146, 903–914.
- Serôdio, J., Vieira, S., and Cruz, S. (2008). Photosynthetic activity, photoprotection and photoinhibition in intertidal microphytobenthos as studied *in situ* using variable chlorophyll fluorescence. *Cont. Shelf Res.* 28, 1363–1375.
- Steele, J. H., and Baird, I. E. (1968). Production ecology of a sandy beach. *Limnol. Oceanogr.* 13, 14–25.
- Ubertini, M., Lefebvre, S., Rakotomalala, C., and Orvain, F. (2015). Impact of sediment grain-size and biofilm age on epipelagic microphytobenthos resuspension. *J. Exp. Mar. Bio. Ecol.* 467, 52–64.
- Underwood, G. J. C., and Kromkamp, J. (1999). Primary production by phytoplankton and microphytobenthos in estuaries. *Adv. Ecol. Res.* 29, 93–153. doi:10.1016/S0065-2504(08)60192-0.
- Van Leeuwe, M. A., Brotas, V., Consalvey, M., Forster, R. M., Gillespie, D., Jesus, B., Roggeveld, J., and Gieskes W.W.C. (2008). Photoacclimation in microphytobenthos and the role of xanthophyll pigments. *Eur. J. Phycol.* 43, 123–132. doi:10.1080/09670260701726119.
- Waring, J., Baker, N. R., and Underwood, G. J. C. (2007). Responses of estuarine intertidal microphytobenthic algal assemblages to enhanced ultraviolet B radiation. *Glob. Chang. Biol.* 13, 1398–1413. doi:10.1111/j.1365-2486.2007.01378.x.

Wasmund, N. (1989). Micro-autoradiographic determination of the viability of algae inhabiting deep sediment layers. *Estuar. Coast. Shelf Sci.* 28, 651–656. doi:10.1016/0272-7714(89)90052-8.